



THE HONG KONG  
POLYTECHNIC UNIVERSITY

香港理工大學

Pao Yue-kong Library

包玉剛圖書館

---

## Copyright Undertaking

This thesis is protected by copyright, with all rights reserved.

**By reading and using the thesis, the reader understands and agrees to the following terms:**

1. The reader will abide by the rules and legal ordinances governing copyright regarding the use of the thesis.
2. The reader will use the thesis for the purpose of research or private study only and not for distribution or further reproduction or any other purpose.
3. The reader agrees to indemnify and hold the University harmless from and against any loss, damage, cost, liability or expenses arising from copyright infringement or unauthorized usage.

### IMPORTANT

If you have reasons to believe that any materials in this thesis are deemed not suitable to be distributed in this form, or a copyright owner having difficulty with the material being included in our database, please contact [lbsys@polyu.edu.hk](mailto:lbsys@polyu.edu.hk) providing details. The Library will look into your claim and consider taking remedial action upon receipt of the written requests.

UNDERSTANDING THE ROLES OF ZN1 ION IN NEW  
DELHI METALLO-BETA-LACTAMASE 1 BY  
KINETIC ASSAYS AND MOLECULAR DYNAMICS  
SIMULATIONS OF PROTEIN MUTANTS

FUNG YIK HONG

PhD

The Hong Kong Polytechnic University

2018

The Hong Kong Polytechnic University

Department of Applied Biology and Chemical Technology

Understanding the Roles of Zn<sup>2+</sup> Ion in New Delhi Metallo-β-  
Lactamase 1 by Kinetic Assays and Molecular Dynamics  
Simulations of Protein Mutants

Fung Yik Hong

A Thesis Submitted in Partial Fulfilment of the Requirements  
for the Degree of Doctor of Philosophy

August 2018

## **Certificate of Originality**

I hereby declare that this thesis is my own work and that, to the best of my knowledge and belief, it reproduces no material previously published or written, nor material that has been accepted for the award of any other degree or diploma, except where due acknowledgement has been made in the text.

---

Fung Yik Hong

August 2018

## **Abstract**

New Delhi metallo-beta-lactamase 1 (NDM-1) was first detected in 2008 in India. NDM-1 is an enzyme that can hydrolyze a broad range of beta-lactam antibiotics, including the carbapenem family which is known as the antibiotics of last resort. As infections involving NDM-1 have great resistance to antibiotics, they are usually very difficult to treat. Therefore, bacteria carrying NDM-1 are referred as “super bugs”. NDM-1 uses six amino-acid residues to bind two zinc ions in its active-site: H120, H122, H189 (Zn1 site) and D124, C208, H250 (Zn2 site). Multiple studies had shown that the Zn2 ion and the residues in the Zn2 site, such as D124 and C208, are very important in the hydrolysis reaction. On the other hand, the role of the Zn1 ion in NDM-1 is less studied. In this project, the roles of Zn1 ion were explored and its functions in NDM-1 were determined.

Residue H120 of NDM-1 was mutated to alanine (A), asparagine (N) and glutamine (Q) in order to knock out the binding of the Zn1 ion. Interestingly, the Zn1 ion was found to remain in the enzyme after the mutations. The mutants were tested for their hydrolytic activities to six different beta-lactam antibiotics: ampicillin, penicillin G, cefotaxime, ceftazidime, imipenem and meropenem. The activities of the mutants were reduced from 6 to 810 folds for different antibiotics. Molecular dynamics simulations suggested that the Zn1

ion moved away from its original position due to mutations. This consequently moved the hydroxide ion and Zn<sup>2+</sup> ion away from the beta-lactam ring of the antibiotics and reduced the hydrolytic activities. For the H120A and H120N mutants, the bridging hydroxide ion moved 1.3 Å away from its original position. This movement broke its hydrogen bond with the D124 residue and resulted in an unfavorable conformation for nucleophilic attack. For the H120Q mutant, the Zn<sup>2+</sup> ion was moved 2.13 Å from its original location and this resulting position was not suitable for stabilizing the hydrolysis intermediate.

My studies suggested that the exact location of the Zn<sup>1+</sup> ion is critical to the activity of NDM-1. The relative location of the Zn<sup>1+</sup> ion is important for the formation of the Zn<sup>1+</sup>-OH-Zn<sup>2+</sup> bridge during hydrolysis. A specific location of the Zn<sup>1+</sup> ion is required to hold the hydroxide ion and the Zn<sup>2+</sup> ion in the correct positions to perform nucleophilic attack for the hydrolysis reaction and to stabilize the negatively charged intermediate.

## **Acknowledgements**

I would like to express my immense gratitude to my chief supervisor, Prof. K. Y. Wong for his support, encouragement, supervision and invaluable suggestion on this project. In addition, I would like to express my sincere gratitude to Prof. Thomas Y. C. Leung for his valuable comments.

Moreover, I would like to thank Dr. L. Y. So for teaching me molecular biology technique, Dr. M. W. Tsang for teaching me the beta-lactamase activity assay, and Dr. Y. W. Chen for teaching me the molecular dynamics simulations. I would also like to thank Dr. J. Chiou for her technical suggestions about the zinc content measurement, Ms. Zoe Chan for providing the His-tagged BlaC tuberculosis (TB) beta-lactamase T216C enzyme, and Mr. P. K. So for his generous assistance in mass spectrometry.

In addition, I am also greatly indebted to my groupmates, Dr. W. L. Cheong, Dr. Warrick K. C. Lo, Dr. N. Sun, Ms. K.C. Cheung, Ms. R. L. Du, Dr. Y. Wang, Dr. E. Ha, Mr. H. W. Man, Mr. W. P. Kong and all my friends who have given me valuable suggestion and encouragement.

Furthermore, I would like to acknowledge the Research Committee of the Hong Kong Polytechnic University for the award of a postgraduate studentship and the University Grants Committee for the award of the Hong Kong PhD Fellowship to support my study from 2014 to 2016.

Last, but not least, I would like to give my special thanks to my family for their persistent love and support.



# Table of Contents

<b>Certificate of Originality .....</b>	<b>i</b>
<b>Abstract .....</b>	<b>ii</b>
<b>Acknowledgements .....</b>	<b>iv</b>
<b>Table of Contents .....</b>	<b>vi</b>
<b>List of Figures and Tables .....</b>	<b>ix</b>
<b>Abbreviations .....</b>	<b>xvii</b>
<b>Chapter 1. Introduction .....</b>	<b>1</b>
1.1. Beta-lactam antibiotics.....	2
1.2. Worldwide antibiotics resistance and “super bugs” carrying NDM-1.	7
1.3. Classification of beta-lactamases .....	9
1.4. Class B beta-lactamses.....	12
1.5. New Delhi Metallo-beta-lactamase 1 (NDM-1) .....	22
1.6. Aims and objectives of this project.....	28
<b>Chapter 2. Protein Expressions and Zinc Content Measurements.....</b>	<b>30</b>
2.1. Introduction.....	31

2.2.	Experiment .....	35
2.2.1.	Materials .....	35
2.2.2.	Experimental Methods .....	39
2.3.	Results and Discussion .....	47
2.3.1.	Preparation of the NDM-1 proteins .....	47
2.3.2.	Zinc content of NDM-1 proteins measured by ICP-OES .....	53
2.3.3.	Zinc ions binding analysis of NDM-1 proteins by MS .....	55
2.3.4.	Experimental control of the zinc binding His-tag .....	62
2.3.5.	Cleavage of His-tag and the zinc content measured by ICP-OES .....	64
2.4.	Concluding Remarks .....	69
 <b>Chapter 3. Beta-Lactamase Activity Assays with Different Antibiotics.</b>		<b>71</b>
3.1.	Introduction .....	72
3.2.	Experiment .....	77
3.2.1.	Materials .....	77
3.2.2.	Experimental Methods .....	79
3.3.	Results and Discussions .....	81
3.3.1.	Optimization of Zn concentration condition for the Beta- lactamase activity assay .....	81

3.3.2. The Beta-lactamase activity assays of NDM-1 WT and mutants ...	83
3.4. Concluding Remarks .....	105
<b>Chapter 4. Molecular Dynamics Simulations .....</b>	<b>106</b>
4.1. Introduction .....	107
4.2. Experiment .....	110
4.2.1. Software .....	110
4.2.2. Experimental Methods .....	111
4.3. Results and Discussions .....	114
4.3.1. MD simulation of NDM-1 WT (Control) .....	114
4.3.2. MD simulation of NDM-1 H120A.....	121
4.3.3. MD simulation of NDM-1 H120N.....	128
4.3.4. MD simulation of NDM-1 H120Q.....	135
4.4. Concluding Remarks .....	142
<b>Chapter 5. Conclusions .....</b>	<b>145</b>
<b>References .....</b>	<b>149</b>

# List of Figures and Tables

## Figures

Figure 1.1. The beta-lactam ring structure in all beta-lactam antibiotics.....	3
Figure 1.2 The core beta-lactam ring structure of a) Penicillins, b) Cephalosporins, c) Monobactams and d) Carbapenems .....	6
Figure 1.3 a) Serine-beta-lactamase uses the serine residue to perform the hydrolysis reaction. b) Metallo-beta-lactamase requires zinc ions in the active-site to perform hydrolysis reaction.....	10
Figure 1.4 The current ambler classification scheme of beta-lactamases. ....	11
Figure 1.5 The binding sites of the three subclasses (B1, B2 and B3) are different in depth and width. ....	14
Figure 1.6 The metal coordination of different metallo-beta-lactamases subclasses. ....	17
Figure 1.7 The proposed di-zinc mechanism (B1/B3) .....	19
Figure 1.8 The proposed mono-zinc mechanism (B1/B3) .....	20
Figure 1.9 The proposed mono-zinc mechanism (B2) .....	21
Figure 1.10 The crystal structures of hydrolyzed antibiotics with NDM-1. ...	23

Figure 1.11 A proposed mechanism of meropenem hydrolysis by NDM-1 using QM/MD simulations. ....	25
Figure 2.1 The plasmid map of pET28a from Novagen.....	36
Figure 2.2 The elution profile of NDM-1 WT from cell lysate.....	48
Figure 2.3 The elution profile of NDM-1 H120A from cell lysate. ....	49
Figure 2.4 The elution profile of NDM-1 H120N from cell lysate. ....	50
Figure 2.5 The elution profile of NDM-1 H120Q from cell lysate. ....	51
Figure 2.6 The SDS-PAGE of NDM-1 proteins after buffer exchange. ....	52
Figure 2.7 The native mass spectrometry of NDM-1 WT without addition of zinc sulfate. ....	57
Figure 2.8 The native mass spectrometry of NDM-1 WT with the addition of 50 $\mu$ M zinc sulfate. ....	58
Figure 2.9 The native mass spectrometry of NDM-1 H120A with the addition of 50 $\mu$ M zinc sulfate. ....	59
Figure 2.10 The native mass spectrometry of NDM-1 H120N with the addition of 50 $\mu$ M zinc sulfate. ....	60
Figure 2.11 The native mass spectrometry of NDM-1 H120Q with the addition of 50 $\mu$ M zinc sulfate. ....	61

Figure 2.12 The native mass spectrometry data of the His-tagged BlaC TB beta-lactamase T216C.....	63
Figure 2.13 The SDS-PAGE of His-tag cleavage of NDM-1 WT by Thrombin enzyme with different incubation time. ....	66
Figure 2.14 The SDS-PAGE of the NDM-1 WT and mutants after purified by the size-exclusion chromatography.....	67
Figure 3.1 The crystal structure of NDM-1 WT binding with Ampicillin....	72
Figure 3.2 The beta-lactam ring changes in UV absorption after being hydrolyzed.....	73
Figure 3.3 a) the Michaelis-Menten plot and b) the Lineweaver–Burk plot.	74
Figure 3.4 The reaction rate of NDM-1 WT (20 nM) vs. increasing concentration of zinc with fixed amount of Ampicillin (700 μM). .	82
Figure 3.5 The reaction rate of NDM-1 WT vs. a) Ampicillin, b) Penicillin G, c) Cefotaxime, d) Ceftazidime, e) Imipenem, and f) Meropenem...	88
Figure 3.6 The reaction rate of NDM-1 H120A vs. a) Ampicillin, b) Penicillin G, c) Cefotaxime, d) Ceftazidime, e) Imipenem, and f) Meropenem .....	91

Figure 3.7 The reaction rate of NDM-1 H120N vs. a) Penicillin G, b) Cefotaxime, c) Ceftazidime, d) Imipenem, and e) Meropenem...	94
Figure 3.8 The reaction rate of NDM-1 H120Q vs. a) Ampicillin, b) Penicillin G, c) Cefotaxime, d) Ceftazidime, e) Imipenem, and f) Meropenem .....	97
Figure 3.9 The lineweaver-burk plots of a) H120A vs Ceftazidime, b) H120A vs. Imipenem, c) H120N vs. Ceftazidime, d) H120N vs. Imipenem, e) H120N vs. Meropenem, and f) H120Q vs. Ceftazidime.....	100
Figure 3.10 The comparison of reaction rates between all NDM-1 mutants vs. Ampicillin. ....	101
Figure 3.11 The comparison of reaction rates between all NDM-1 mutants vs. Penicillin G. ....	101
Figure 3.12 The comparison of reaction rates between all NDM-1 mutants vs. Cefotaxime. ....	102
Figure 3.13 The comparison of reaction rates between all NDM-1 mutants vs. Ceftazidime. ....	102
Figure 3.14 The comparison of reaction rates between all NDM-1 mutants vs. Imipenem. ....	103
Figure 3.15 The comparison of reaction rates between all NDM-1 mutants vs. Meropenem. ....	103

Figure 4.1	The coordination geometries of the two zinc ions of NDM-1 ...	109
Figure 4.2	The workflow of the preparation of MM force field .....	112
Figure 4.3	The RMSD analysis of the backbone atoms in the NDM-1 WT simulation comparing to the MD starting model structure over the simulation time.....	116
Figure 4.4	The active-site of the lowest potential energy structure of the MD simulation NDM-1 WT.....	117
Figure 4.5	The bond distance between the hydrogen of the hydroxide ion and the oxygen of the Asp 124 residue of NDM-1 WT over the simulation time.....	118
Figure 4.6	The superimposition of the lowest energy structure of the NDM-1 WT simulation with the NDM-1 M67V mutant/hydrolyzed Penicillin G complex.....	119
Figure 4.7	The active-site comparison between the NDM-1 WT simulation and the NDM-1 M67V mutant complexed with hydrolyzed Penicillin G .....	120
Figure 4.8	The RMSD analysis of the backbone atoms in the NDM-1 H120A simulation comparing to the MD starting model structure over the simulation time.....	123
Figure 4.9	Comparison between the lowest potential energy structures of the NDM-1 WT (yellow) and H120A (cyan) simulations. ....	124



Figure 4.10 Comparison between the active-sites of the lowest potential energy structures of NDM-1 WT (yellow) and H120A (cyan) simulations. ....	125
Figure 4.11 The bond distance between the hydrogen of the hydroxide ion and the oxygen of the Asp 124 residue of NDM-1 H120A over the simulation time.....	126
Figure 4.12 The active-site comparison between the NDM-1 H120A simulation and the NDM-1 M67V mutant complexed with hydrolyzed Penicillin G .....	127
Figure 4.13 The RMSD analysis of the backbone atoms in the NDM-1 H120N simulation comparing to the MD starting model structure over the simulation time.....	130
Figure 4.14 Comparison between the protein structures of the NDM-1 WT (yellow) and H120N (cyan) simulations.....	131
Figure 4.15 Comparison between the active-sites of NDM-1 WT (yellow) and H120N (cyan) simulations. a) Time = 4.90 ns, b) Time = 8.26 ns. . .....	132
Figure 4.16 The bond distance between the hydrogen of the hydroxide ion and the oxygen of the Asp 124 residue of NDM-1 H120N over the simulation time.....	133

Figure 4.17 The active-sites comparison between the NDM-1 H120N simulation and the NDM-1 M67V mutant complexed with hydrolyzed Penicillin G .....	134
Figure 4.18 The RMSD analysis of the backbone atoms in the NDM-1 H120Q simulation comparing to the MD starting model structure over the simulation time.....	137
Figure 4.19 Comparison between the lowest potential energy structures of the NDM-1 WT (yellow) and H120Q (cyan) simulations. ....	138
Figure 4.20 Comparison between the active-sites of the lowest potential energy structures of NDM-1 WT (yellow) and H120Q (cyan) simulations. ....	139
Figure 4.21 The bond distance between the hydrogen of the hydroxide ion and the oxygen of the Asp 124 residue of NDM-1 H120Q over the simulation time.....	140
Figure 4.22 The active-site comparison between the NDM-1 H120Q simulation and the NDM-1 M67V mutant complexed with hydrolyzed Penicillin G .....	141

## Tables

Table 2.1	Comparison between beta-lactamase NDM-1, CphA and GOB-18. .....	33
Table 2.2	Primers used for constructing NDM-1 mutants .....	37
Table 2.3	Reagents for PCR cloning and site-directed mutagenesis .....	40
Table 2.4	The ICP-OES data and the calculations of zinc content of each His-tagged NDM-1 samples.. .....	54
Table 2.5	The ICP-OES data and the calculations of zinc content of each His- tag cleaved NDM-1 samples.....	68
Table 3.1	The list of testing compounds and their extinction coefficients ....	78
Table 3.2	The kinetic parameters of NDM-1 mutants vs. different beta- lactam antibiotics .....	104

## Abbreviations

[E] <sub>T</sub>	Total enzyme concentration
[S]	Substrate concentration
μ	Micro
μL	Microliter
Å	Ångström
Arg	Arginine
Asn	Asparagine
Asp	Aspartic acid
BBL numbering	Class B Beta-Lactamase numbering
CaCl <sub>2</sub>	Calcium Chloride
CaCl <sub>2</sub>	Calcium Chloride
Cd <sup>2+</sup>	Cadmium (II) ion
Co <sup>2+</sup>	Cobalt (II) ion
Coot	Crystallographic Object-Oriented Toolkit
Coul	Coulomb's law
Cu <sup>2+</sup>	Copper (II) ion
Cys	Cysteine
Da	Dalton
DNA	Deoxyribonucleic acid
dNTPs	deoxy-ribonucleoside triphosphates

<i>E.coli</i>	<i>Escherichia coli</i>
EM	Energy Minimization
ESI-MS	Electrospray Ionization Mass Spectrometry
Fplc	Fast Protein Liquid Chromatography
g	Gram
Gly	Glycine
GOB	Goblet Cell Protein
His	Histidine
His-tag	Polyhistidine-tag
hr	Hour
IPTG	Isopropylthiogalactoside
K	Kelvin
$k_{cat}$	Specificity constant
$k_{cat}/K_m$	Catalytic efficiency
kDa	kilodalton
kJ	Kilojoules
$K_m$	Michaelis constant
kV	kilovolt
L	Liter
LJ	Lennard-Jones potential
M	Molar
MD	Molecular Dynamics
$MgCl_2$	Magnesium Chloride

min	Minute
mL	Milliliter
mM	Millimolar
MM	Molecular Mechanics
Mn <sup>2+</sup>	Manganese (II) ion
mol	mole
MS	Mass Spectrometry
MW	Molecular Weight
NaCl	Sodium Chloride
NDM-1	New Delhi Metallo-beta-lactamase 1
ng	Nanogram
Ni <sup>2+</sup>	Nickel (II) cation
Ni-NTA	Nickel-Nitrilotriacetic acid
nm	Nanometer
nM	Nanomolar
NMR	Nuclear Magnetic Resonance
NPT	constant Number of particles, Pressure, and Temperature
ns	Nanosecond
NVT	constant Number of particles, Volume, and Temperature
°C	Degree Celsius
OD <sub>600</sub>	Optical Density at wavelength 600 nm

OH	Hydroxide
PBP	Penicillin-Binding Protein
PCR	Polymerase Chain Reaction
PDB ID	Protein Data Bank ID
ps	picosecond
QM	Quantum Mechanics
RESP	Restrained Electrostatic Potential
RMSD	Root-Mean-Square Deviation
rpm	Rotation Per Minute
SDS-PAGE	Sodium Dodecyl Sulfate Polyacrylamide Gel Electrophoresis
sec	Second
Ser	Serine
TB	Tuberculosis
Tris-HCl	Tris(hydroxymethyl)aminomethane- Hydrochloride
UV	Ultraviolet
V (unit)	Volt
v/v	Volume/Volume
Vis	Visiable
$V_{\max}$	Maxium rate of reaction
VMD	Visual Molecular Dynamics
WT	Wild-Type

Zn	Zinc
Zn1	Zinc 1
Zn2	Zinc 2
$\Delta\varepsilon$	Molar extinction coefficient



# **Chapter 1. Introduction**

## 1.1. Beta-lactam antibiotics

The original meaning of “antibiotic” was an organic compound produced by an organism which is toxic to another microorganism.<sup>1-2</sup> Today, antibiotics are the most common drugs used for the treatment of bacterial infections. They can either kill or inhibit the growth of bacteria.<sup>3</sup> Since more and more bacteria become resistant to common antibiotics, there is an urgent need to develop new antibiotics for the treatment of bacterial infections. There are many classes of antibiotics including beta-Lactams, macrolides, tetracyclines, quinolones, aminoglycosides, sulphonamides, glycopeptides and oxazolidinones.<sup>4-6</sup> Different ways are used to classify these antibiotics, but the most common way is based on their molecular structure.<sup>7</sup> In this project, I shall focus on the beta-lactam antibiotics. All beta-lactam antibiotics contain a structure called the beta-lactam ring (Figure 1.1).<sup>8</sup> This 3-carbon and 1-nitrogen ring is highly reactive. During the synthesis of bacterial cell wall, an enzyme called Penicillin-Binding Protein (PBP) is used to cross-link peptide units to form peptidoglycan. Beta-lactam antibiotics interfere with cell wall synthesis by binding to this PBP and the beta-lactam ring reacts with the PBP active-site in order to permanently inactivate it. The absence of PBP activities results in the failure of peptidoglycan synthesis and leads to cell lysis thus cell death.<sup>9</sup> There are four classes of beta-lactam antibiotics: penicillins, cephalosporins, monobactams, and carbapenems.

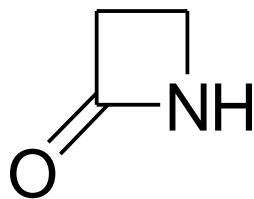


Figure 1.1. The beta-lactam ring structure in all beta-lactam antibiotics

Penicillin was first reported by Alexander Fleming in 1929 and it was the first antibiotic grouped into the class called “penicillins”.<sup>10</sup> All penicillins contain a core structure of 6-aminopenicillanic acid ring (Figure 1.2a).<sup>11-12</sup> The diverse compounds in this class mostly end up with a suffix –cillin in their name. The members of the penicillins include penicillin G, ampicillin, carbenicillin, oxacillin, methicillin, nafcillin, piperacillin and ticarcillin.<sup>13</sup> Among all of these antibiotics, penicillin G was the first released antibiotic drug. Although penicillin G was discovered in the 1920’s, it took more than 20 years of studies before it was released.<sup>14</sup> Unfortunately, penicillin G only has a very narrow target spectrum. It is only effective to Gram positive bacteria and a few Gram negative bacteria (e.g. *Treponema pallidum*).<sup>14</sup> Therefore, some other antibiotics have been developed with different side groups (the groups surrounding the beta-lactam ring core structure), e.g. ampicillin and carbenicillin. These side groups protect them from being degraded and help them to pass through the outer membrane of bacterial cell walls.<sup>15</sup> These extend the target spectrum of the penicillin antibiotics towards Gram negative bacteria.

The class of cephalosporins has a very similar core structure comparing to the penicillins. Figure 1.2b showed the core structure of cephalosporins.<sup>11, 16</sup> The compounds of cephalosporins have a large variety of side groups to enable them to bind to different Penicillin-Binding Proteins (PBPs), resist degradation by bacteria strains or ionize to improve the entrance to Gram-negative bacteria<sup>17</sup>, these increase their ability to target Gram-negative bacteria. Cephalosporins are subdivided into 1<sup>st</sup>-5<sup>th</sup> generations. The later the generation, the more effective they are against Gram-negative bacteria.<sup>17</sup> Members of the cephalosporins class include cefacetile, cefaclor, cefotaxime, ceftazidime, cefclidine, and ceftobiprole. The cephalosporins class is the most commonly prescribed antibiotics, which covers one-third of antibiotics administered by the National Health Scheme in the United Kingdom.<sup>14</sup>

Monobactam is a very special class of beta-lactam antibiotics. Comparing to the other three classes of beta-lactam antibiotics, the beta-lactam ring of monobactam is standing alone without fusing to any other ring structure (Figure 1.2c).<sup>18-19</sup> The most commonly known monobactam antibiotic is aztreonam. Aztreonam has a very narrow target spectrum which is only effective against aerobic Gram-negative bacteria, such as *Neisseria* and *Pseudomonas*. The monobactams are most likely not effective to any other anaerobes or Gram-positive bacteria.<sup>20</sup>

The last class of beta-lactam antibiotics is the carbapenems. All members in the carbapenem family contain a core structure as shown in Figure 1.2d.<sup>21</sup> The carbapenems are one of the most important classes of beta-lactam antibiotics. In the late 1960's, the penicillins antibiotics became very ineffective to treat bacterial infections due to the resistance by an enzyme called beta-lactamase.<sup>21</sup> During that time, it was urgent to discover new antibiotics for this type of bacterial infections. That was when the first "carbapenem" was found. Thienamycin was the first reported carbapenem antibiotic and it was isolated from *Streptomyces cattleya*.<sup>22</sup> Thienamycin was the standard for all the other carbapenem antibiotics and several other carbapenems were also identified after the thienamycin.<sup>21, 23-24</sup> The carbapenems are very important because they can resist the hydrolysis reaction of most beta-lactamases. Among almost all known beta-lactam antibiotics, carbapenems have the broadest target spectrum which are effective against both Gram-positive and Gram-negative bacteria. The carbapenem antibiotics are also called the "antibiotics of last resort".<sup>25</sup> They are mainly used when the patients are gravely ill or they are infected by resistant bacteria. Members of the carbapenems class include imipenem, meropenem, and ertapenem.<sup>26</sup> Unfortunately, today, bacteria with carbapenems resistance are increasing globally.<sup>27-28</sup>

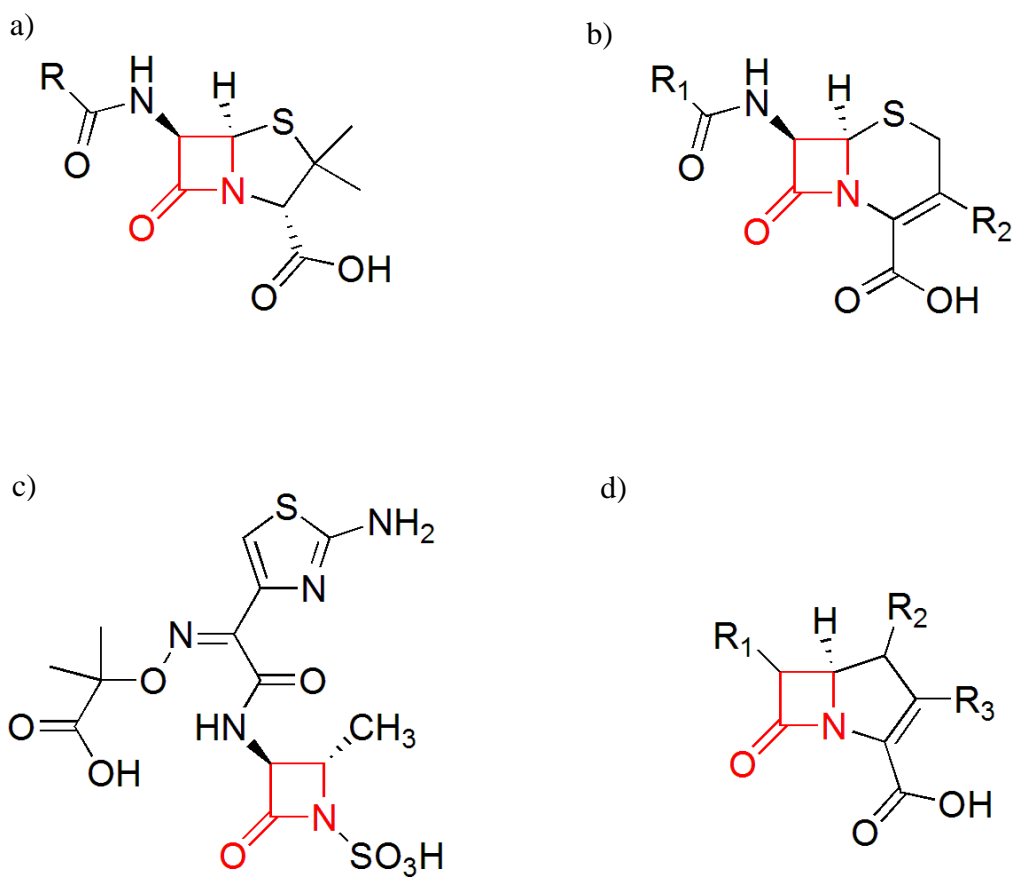


Figure 1.2 The core beta-lactam ring structure of a) Penicillins, b) Cephalosporins, c) Monobactams and d) Carbapenems

## 1.2. Worldwide antibiotics resistance and “super bugs” carrying NDM-1

Although antibiotics are very effective tools in treating bacterial infections, the more the use of antibiotics, the more resistance will be built in bacteria.<sup>29</sup> Antibiotic resistance is mainly created by natural selection processes.<sup>30-31</sup> The resistance effects will start showing up within a short time after introduction of new antibiotic compounds and the level of the antibiotic resistance is strongly correlated to the amount of antibiotic consumption.<sup>29, 32</sup> Over decades, lots of antibiotics are not only used for therapeutic treatments but also used in agricultural and animal industries. Antibiotics used in these industries are usually the same antibiotics used clinically, and this further drives the increase of resistance effects.<sup>33</sup> In some countries, animals take in antibiotics from their food or drinking water. Through the food chain, antibiotics resistant bacteria are transferred to the human populations.<sup>34</sup> Furthermore, in developed countries, most of the antibiotics are available for purchase without medical prescriptions and this is another cause of antibiotic resistance development.<sup>35</sup>

Today, many infections become difficult or impossible to treat due to antibiotic resistance of bacteria.<sup>36</sup> The main approach to fight against antibiotic resistant bacteria is by modification of the structure of current antibiotics or developing new types of drug compounds.<sup>37-38</sup> However, the development of new beta-lactam antibiotics based on existing compounds is not catching up with the rate

of resistance development by the beta-lactamases.<sup>38</sup> Moreover, the development of resistance might not be only restricted to one particular antibiotic compound. The resistance can be developed based on the structure of the antibiotics, so related antibiotic compounds in the same class might also become ineffective.<sup>39</sup> Additionally, bacteria can be resistant to multiple classes of antibiotics at the same time too.<sup>40</sup> Bacteria resistant to multiple antibiotics are called multi-resistant bacteria or “super bugs”. Infections caused by super bugs are very difficult to treat.<sup>41</sup>

Recently, one of the most alarming enzymes expressed by super bugs is called New Delhi Metallo-Beta-Lactamase 1 (NDM-1). NDM-1 is a beta-lactamase that can hydrolyze almost all beta-lactam antibiotics, including Carbapenems, the last resort antibiotics.<sup>42</sup> NDM-1 was first found in a *Klebsiella pneumoniae* strain from a patient in India in 2008.<sup>43</sup> Subsequently, 17 newly evolved NDM-1 enzymes were identified in the last few years.<sup>44-47</sup> Bacterial infection involving NDM-1 can resist almost all beta-lactam antibiotics and it is still a big challenge for therapeutic treatments.<sup>42</sup> The research of new inhibitors for NDM-1 is still one of the hottest topics in the field.



### 1.3. Classification of beta-lactamases

Beta-lactamases are enzymes that can hydrolyze beta-lactam antibiotics.<sup>48</sup> Up to now, there are two ways to classify beta-lactamases: the functional classification and the ambler classification. The most updated one is the functional classification.<sup>49</sup> The functional classification is based on the proposal written by Bush *et al.* in 1995.<sup>50</sup> This classification mainly depends on the phenotypes of using different types of substrates and inhibitors under clinical aspects. Although the functional classification is the newest one, the most commonly known classification actually is the ambler classification<sup>51-52</sup> and this thesis will be based on the ambler classification.

In the ambler classification, beta-lactamases are divided into four classes based on the amino acid sequences: A, B, C and D.<sup>51</sup> In this classification, the Classes A, C and D are grouped into the serine-beta-lactamases, in which the enzymes use the serine residue in their active-sites to perform hydrolysis of the beta-lactam antibiotics. Different from the other classes, Class B is a metalloenzyme and this class is also called the metallo-beta-lactamases. In Class B, there are one or two zinc ions in the active-site to perform hydrolysis. Figure 1.3 showed the mechanistic difference between these two types of beta-lactamases.<sup>53</sup> NDM-1 is a metallo-beta-lactamase, so it is grouped into Class B.<sup>54</sup>

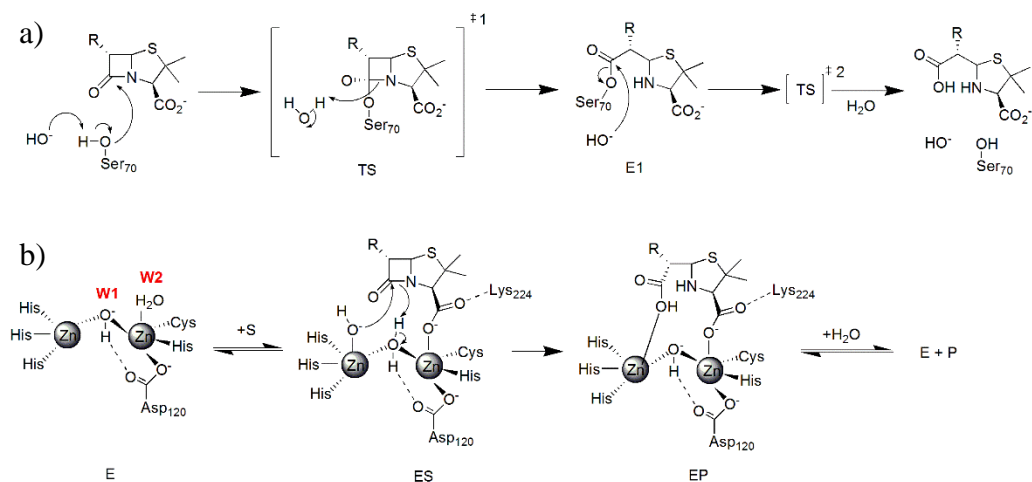


Figure 1.3 a) Serine-beta-lactamase uses the serine residue to perform the hydrolysis reaction. b) Metallo-beta-lactamase requires zinc ions in the active-site to perform hydrolysis reaction.

The ambler classification was originally only designed for two classes: Classes A and B.<sup>51</sup> However, as time goes on, a new type of beta-lactamases was found, which only had little sequence similarity to Class A enzymes. This type of beta-lactamases is grouped and called Class C; also known as AmpC beta-lactamases.<sup>55</sup> And later on, another type of beta-lactamases was found. This time, the beta-lactamases had sequence similarities between Class A and C. This type of beta-lactamases is grouped to form a new class called Class D.<sup>56</sup> On the other hand, a similar situation happened to the Class B too. New types of metallo-beta-lactamases were found and showed distinct differences. Therefore, the Class B beta-lactamases are further divided into three subclasses:

B1, B2 and B3.<sup>57</sup> Further details of classifications of Class B subclasses will be discussed in the next section. Figure 1.4 shows the overall ambler classification scheme.<sup>51</sup>

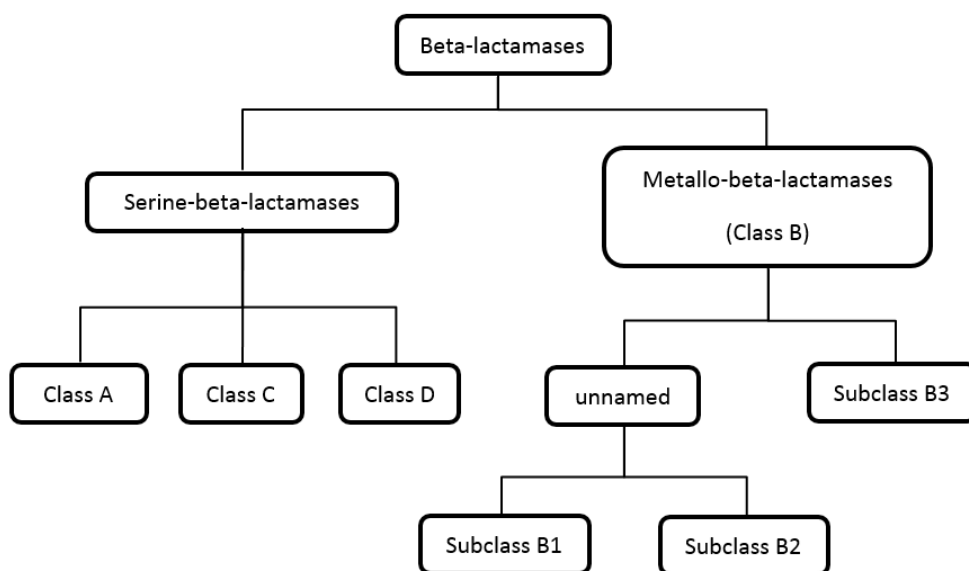


Figure 1.4 The current ambler classification scheme of beta-lactamases.

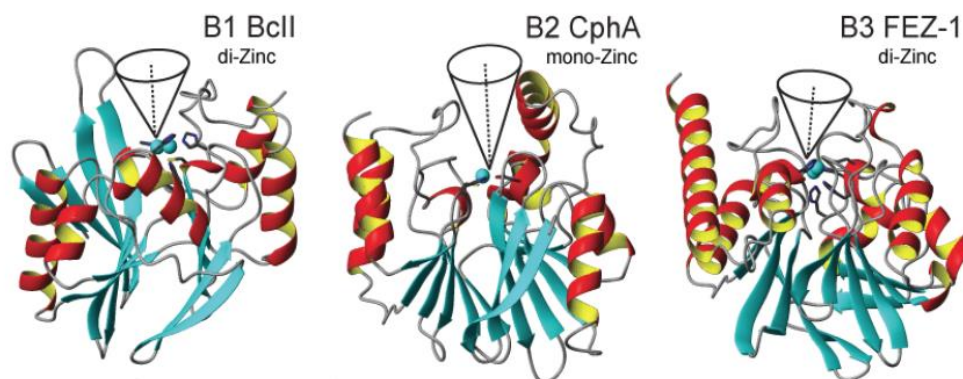
#### 1.4. Class B beta-lactamases

As mentioned before, Class B metallo-beta-lactamase is further subdivided into three subclasses: B1, B2, and B3.<sup>57</sup> The subclasses of Class B are classified based on the overall structure, substrate specificity, metal coordination and catalytic mechanism.<sup>58</sup> Importantly, NDM-1 is grouped into the B1 subclass of metallo-beta-lactamases.<sup>54</sup>

When aligning the subclasses together, the sequence similarities are actually very small.<sup>57, 59-60</sup> The sequence identity between B1 and B2 is 14~24%, and it is only 2~14% when compared to B3. Based on phylogenetic analysis, there are actually only two subclasses, B1/B2 and B3.<sup>61-62</sup> Subclasses B1 and B2 are evolutionary related to each other and they have a certain amount of sequence and structural similarities. However, the substrate specificities and catalytic mechanism are clearly different between B1 and B2, so they are separated into two subclasses. On the other hand, B3 is more evolutionarily distinct from the other two, but it has a very similar catalytic mechanism to B1.<sup>61-62</sup> When looking at the overall structure, all class B beta-lactamases have a common structure, a four-layer  $\alpha\beta\beta\alpha$  structure called metallo-beta-lactamase fold (Figure 1.5). This folding structure was first identified in the metallo-beta-lactamase, but it was also found in different types of proteins other than beta-lactamases.<sup>63</sup> Although all subclasses share the same metallo-beta-lactamase fold, the size

and shape of the binding site in the three subclasses are significantly different. In Figure 1.5, the cones show the substrate binding site of each subclass.<sup>58</sup> The binding sites are different in depth and width. The B2 subclass does not have a mobile loop structure that is present in B1, which lowers its substrate binding specificity.<sup>64</sup> In the case of B3 subclass, there is an intermolecular disulphide bridge connecting the elongated  $\beta$ 12- $\alpha$ 5 loop.<sup>65-68</sup> This disulphide bridge is present in almost all B3 subclass proteins, except GOB-18. GOB-18 is a special B3 beta-lactamase which only contains one cysteine.<sup>69</sup>

Since the size and shape of the binding sites between the three subclasses are different, the substrates specificities of them are different too. The bottom of Figure 1.5 shows the target spectrum of each subclass.<sup>58</sup> Subclass B1 has the broadest target spectrum among all subclasses. B1 beta-lactamases are effective on penicillins, cephalosporins and carbapenems.<sup>70-71</sup> In comparison, B2 beta-lactamases can only hydrolyze carbapenems and almost do not work on penicillins and cephalosporins.<sup>71-73</sup> On the opposite, B3 beta-lactamases can hydrolyze penicillins and cephalosporins but are not really effective on carbapenems.<sup>71</sup> Finally, all three subclasses do not hydrolyze the monobactams, such as aztreonam.<sup>74</sup> Class B beta-lactamases are also resistant to classic serine-beta-lactamase inhibitors, e.g. clavulanic acid, sulbactam, and tazobactam.<sup>71, 74</sup> Importantly, the zinc ions are required for binding substrates in all these metallo-beta-lactamases.<sup>75</sup>



+	Penicillins	Carbapenems	Penicillins
	Cephalosporins		Cephalosporins
-	Carbapenems	Monobactams	Monobactams
-	Monobactams		Monobactams

Figure 1.5 The binding sites of the three subclasses (B1, B2 and B3) are different in depth and width. Therefore, the substrate specificities are also different among the three subclasses. (Figure was adopted from reference 58)

Zinc ion is the cofactor of Class B beta-lactamases.<sup>76</sup> There are two zinc binding sites in the Class B beta-lactamase: Zn1 and Zn2 sites. The Zn1 site refers to the three histidine residues site and the Zn2 site refers to the aspartate-cysteine-histidine residues site. Although the residues of Zn2 site might be different between subclasses, in general, most of the Zn2 sites are composed of these three residues. In living cells, Class B beta-lactamases only bind to zinc ion. However, *in vitro* experiments showed that other metal ions can be exchanged and the enzymes still retained significant activities; these ions

included  $\text{Cd}^{2+}$ ,  $\text{Co}^{2+}$ ,  $\text{Ni}^{2+}$ ,  $\text{Cu}^{2+}$ , and  $\text{Mn}^{2+}$ .<sup>77-81</sup> From here on, Zn1 site or Zn2 site represents the site including the zinc ion and the coordinating residues. Zn1 ion or Zn2 ion refers to only the zinc ion itself.

In the B1 subclass, two zinc ions are usually bound in the active site (Figure 1.6, top right). The Zn1 site is composed of H116, H118 and H196 (based on the standard numbering scheme for class B beta-lactamases, BBL numbering<sup>57, 82</sup>) and the Zn2 site is composed of D120, C221, and H263. A water molecule or a hydroxide ion is acting as a ligand bridging the two zinc ions.<sup>83</sup> The distance between the 2 zinc ions can be quite different when comparing different crystal structures of the same enzyme; it can range from 3.5 to 4.6 Å.<sup>84</sup> Moreover, crystal structures of enzymes having only a single zinc ion have also been recorded, where the single zinc ion was binding to the Zn1 site and a water molecule was binding to the Zn2 site (Figure 1.6, top left).<sup>85-87</sup> Because of these single zinc ion structures, there was a concern about the number of zinc ions required for the catalytic activity of the B1 subclass enzymes. Studies have shown that the B1 enzymes were catalytically active under the condition of 1: 1 ratio of zinc: enzyme, and the activity became slower as more zinc was added.<sup>88</sup> Based on this finding, the single zinc ion mechanism was proposed.<sup>86</sup> Later on, more studies have shown that the enzymes were under a mixture of di-zinc and mono-zinc conditions, where the Zn1 ion is binding more tightly and the Zn2 ion is weaker in binding.<sup>87, 89-91</sup> Based on the zinc titration studies with mass

spectrometry (MS) and nuclear magnetic resonance (NMR), it was suggested that only the di-zinc enzyme is relevant for catalytic activity.<sup>92</sup>

The B3 subclass beta-lactamases are also shown to be di-zinc enzymes based on crystallography studies (Figure 1.6, bottom right).<sup>65-68</sup> The Zn1 site has the same metal coordination as the B1 subclass, where the H116, H118 and H196 residues bind to the Zn1 ion. On the other hand, the Zn2 site is different to that of B1, which composes of D120, H263 and H121. The aspartate (D120) and histidine (H263) are equivalent to those in the B1 subclass, but the histidine (H121) is not. Same as B1, a water molecule or a hydroxide ion is bridging the two zinc ions. The GOB family is an exception of the B3 subclass. The GOB family has a different metal coordination comparing to the other B3 enzymes, where the histidine residue (His116) is replaced by a glutamine residue (Gln116) at the Zn1 site.<sup>93</sup> Moreover, the enzyme GOB-18 of the GOB family has also shown evidence of significant activities under mono-zinc form, where the mono-zinc ion is bound to the Zn1 site only.<sup>94</sup>

The B2 subclass beta-lactamases have a distinct metal coordination to the B1 and B3 subclasses. Based on the crystal structures of Sfh1 and CphA, the Zn1 site is composed of N116, H118 and H196 and the Zn2 site is composed of D120, C221 and H263 (Figure 1.6, bottom left).<sup>64, 95</sup> The B2 subclass beta-lactamases are mono-zinc enzymes. Contrary to B1 and B3, the mono-zinc ion binds to the Zn2 site and the water molecule binds to the Zn1 site. The B2



subclass enzymes do bind a second zinc ion at the Zn1 site when excess amount of zinc is added. However, the B2 subclass enzymes are inhibited by the addition of the second zinc ion at Zn1 site in a noncompetitive manner, which is an opposite effect comparing to the B1 and B3 subclasses.<sup>96</sup>

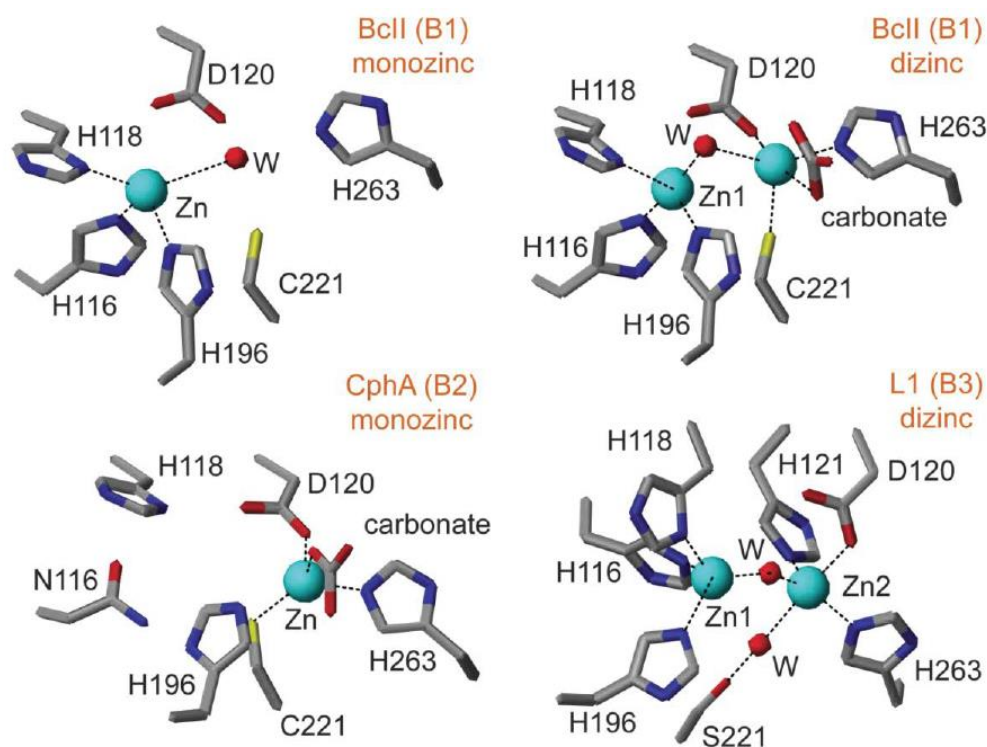


Figure 1.6 The metal coordination of different metallo-beta-lactamase subclasses. For B1 subclass, both mono-zinc and di-zinc forms were identified. For the B2 subclass, only mono-zinc form was identified and the zinc ion is at the Zn2 site. For B3 subclass, most of the enzymes are di-zinc forms and the coordinate residues are different from the B1 subclass. Protein Data Bank ID (PDB ID): Di-zinc BcII (1BVT), mono-zinc BcII(1BMC), mono-zinc CphA (1X8G) and di-zinc L1 (1SML) (Figure was taken from reference 58)

The catalytic mechanisms of Class B beta-lactamases were studied extensively.<sup>97-104</sup> Two possible roles of zinc ions were suggested: 1) the zinc ions act as Lewis acids and facilitate the bridging hydroxide ion to attack the carbonyl carbon nucleophilically at the beta-lactam ring of the substrate and/or 2) the zinc ions are used to stabilize the negatively charged anion intermediate. However, the exact roles of the zinc ions are very difficult to determine. Three mechanistic models were proposed: the di-zinc model, the mono-zinc model (B1/B3) and the mono-zinc model (B2).

Based on structural and mechanistic data, the di-zinc model was proposed (Figure 1.7), and it is almost identical for both B1 and B3.<sup>98, 105-108</sup> In this di-zinc mechanism, the hydroxide ion between the two zinc ions performs a nucleophilic attack to the carbonyl carbon of the beta-lactam ring and breaks the C-N bond of the antibiotic. It is possible that the Zn1 ion polarizes the carbonyl group of the beta-lactam ring to facilitate the nucleophilic attack. However, most of the simulation models suggest that the interaction between the Zn1 ion and the carbonyl oxygen occurs after the nucleophilic attack.<sup>109-112</sup> Therefore, it is most likely that the Zn1 ion is just forming an “anion hole” to stabilize the tetrahedral intermediate. For most of the antibiotic substrates, the breaking of C-N bond is the rate-limiting step.<sup>75, 113</sup> Finally, the anionic intermediate is protonated and the hydrolyzed product is released. In this final protonation step, there are two possible proton sources: 1) from another water

molecule binding to the Zn<sup>2+</sup> ion or 2) a bulk water molecule oriented by the D120 residue. There is no direct evidence showing which case is correct.<sup>114</sup>

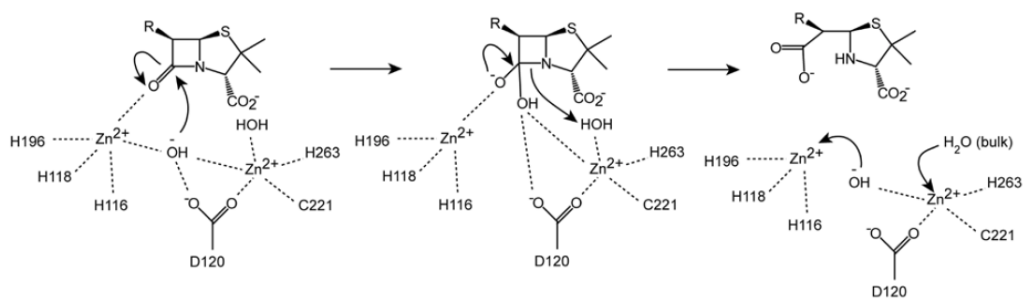


Figure 1.7 The proposed di-zinc mechanism (B1/B3) (Figure was taken from reference 58)

There are two types of mono-zinc mechanisms: 1) the B1/B3 subclasses and 2) the B2 subclass. Figure 1.8 shows the mono-zinc mechanism for the B1/B3 subclass. Although B1 subclass is included, experiments results have suggested that only the di-zinc enzyme is relevant for catalytic activity for most of the B1 subclass, except the SPM enzyme.<sup>85</sup> Therefore, this mono-zinc mechanism is mainly applying to the GOB family in the B3 subclass.<sup>93-94</sup> At the start of this mono-zinc mechanism, a water molecule binds at the Zn2 site. The water molecule is deprotonated by the D120 residue and initiates a nucleophilic attack to the carbonyl carbon of the beta-lactam ring. The tetrahedral intermediate is stabilized by the Zn1 ion. Then, the intermediate is protonated by the hydrogen from the D120 residue and the hydrolyzed product is released.<sup>86</sup>

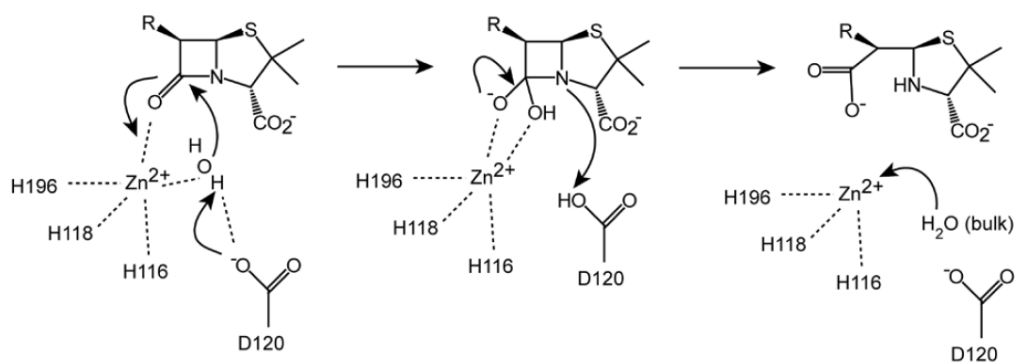


Figure 1.8 The proposed mono-zinc mechanism (B1/B3) (Figure was taken from reference 58)

The last proposed mechanism is the mono-zinc mechanism (B2). The B2 subclass has a very distinct mechanism comparing to the B1 and B3 subclasses, because they only have one zinc ion at the Zn2 site (no Zn1 ion). This proposed mechanism is based on the simulation model calculated on the CphA enzyme with the binding of hydrolyzed biapenem product (Figure 1.9).<sup>115-117</sup> Contrary to the two mechanisms above, a non-zinc binding water molecule performs the nucleophilic attack. This water molecule is located at the Zn1 site and deprotonated by the D120 or/both H118 residues. After the nucleophilic attack, the intermediate is stabilized by the Zn2 ion. Finally, the intermediate is protonated by the D120 residue and the hydrolyzed product is released.

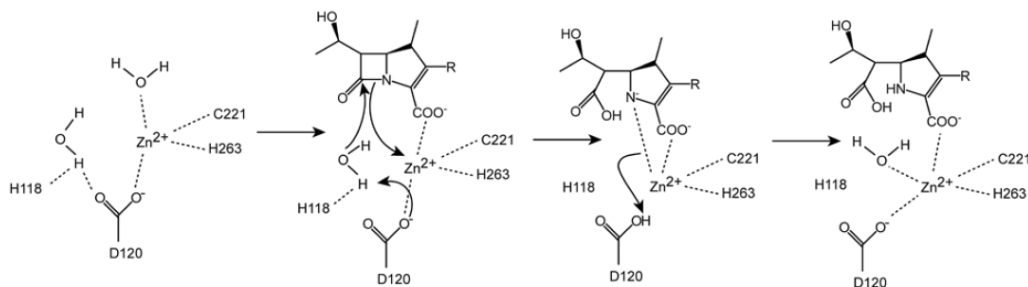


Figure 1.9 The proposed mono-zinc mechanism (B2) (Figure was taken from reference 58)

### 1.5. New Delhi Metallo-beta-lactamase 1 (NDM-1)

NDM-1 has a sequence identity of 32.4% to VIM-1/VIM-2.<sup>118</sup> The metal coordination is same as the other B1 enzymes, where Zn1 site is composed of three histidine residues and Zn2 site is composed of aspartate-cysteine-histidine residues.<sup>114, 119</sup> Also, NDM-1 is a di-zinc enzyme and has a very board range of target spectrum, which hydrolyzes penicillins, cephalosporins, and carbapenems.<sup>42</sup> Although many studies are targeting to develop inhibitors for treating bacteria carrying NDM-1, they have not been very successful. Most of these inhibitors are only effective *in vitro* but not clinically approved.<sup>120-122</sup> Development of new inhibitors for NDM-1 is still one of the hottest topics in the field. Understanding of the mechanism of NDM-1 is a very important factor in developing new inhibitors for treatments.<sup>123</sup>

Several crystal structures of product compounds binding to the NDM-1 were reported, and they gave important information about the catalytic mechanism of NDM-1 (Figure 1.10).<sup>114, 119</sup> In all of these structures, the beta-lactam ring of the antibiotics binds in the same way to the NDM-1 active-site whereas the aromatic side groups vary in their binding location depending on the substrate structure. All of these crystal structures have a water or hydroxide ion bridging between the two zinc ions. Also, the carboxylate group of the beta-lactam product produced by the hydrolysis reaction is shown to be coordinating with

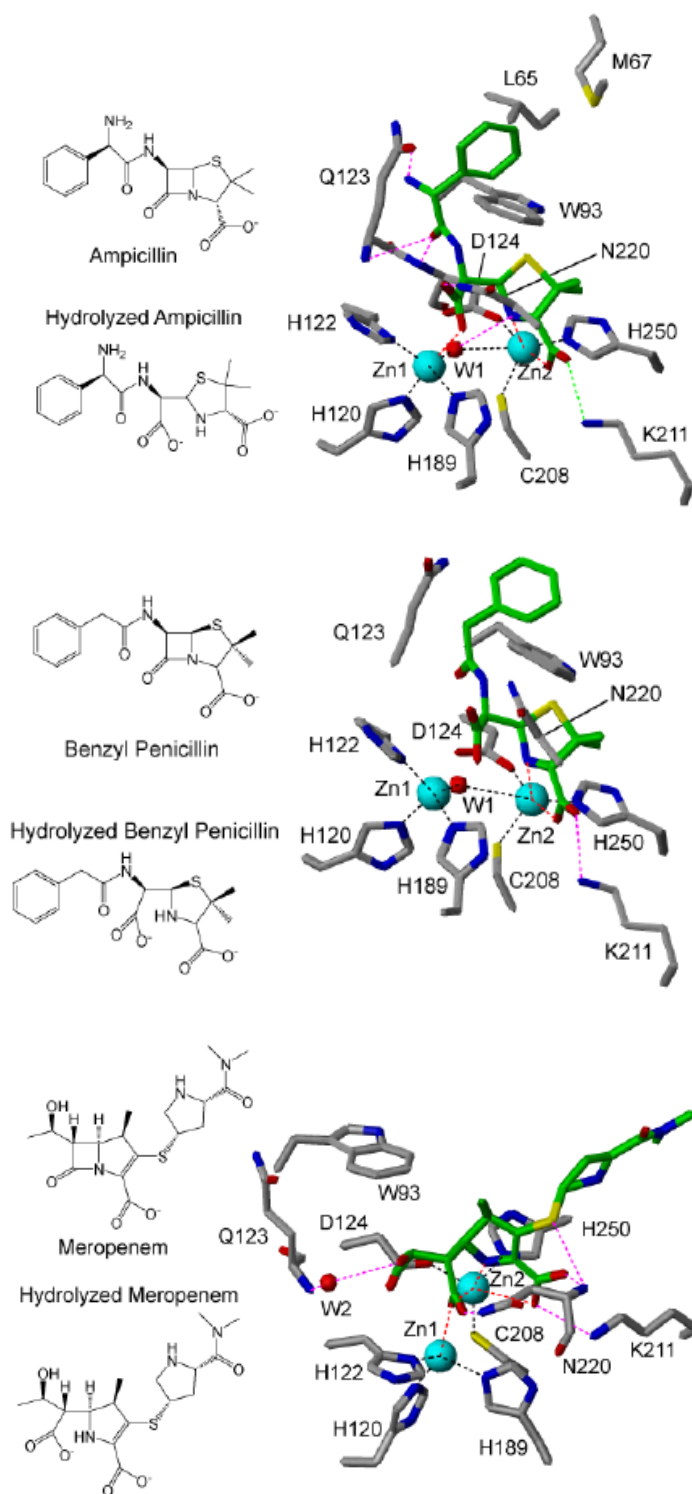


Figure 1.10 The crystal structures of hydrolyzed antibiotics with NDM-1. (PDB ID: Ampicillin - 3Q6X, Benzyl Penicillin - 4EYF, and Meropenem - 4EYL) (Figure was taken from reference 58)

the Zn1 ion in all of the crystal structures. Same as all the other metallo-beta-lactamases, NDM-1 cannot hydrolyze monobactams such as aztreonam. The reason is that their beta-lactam ring lacks a fused ring and the linked carboxylate group. Without this group the monobactams cannot interact with the Zn2 ion, so that they are not a substrate of NDM-1.<sup>114</sup>

The catalytic mechanism of NDM-1 was studied in depth too. Figure 1.11 is a recently reported mechanism of meropenem hydrolysis by NDM-1. This mechanism is produced by Quantum Mechanics/Molecular Dynamics (QM/MD) simulations.<sup>124</sup>



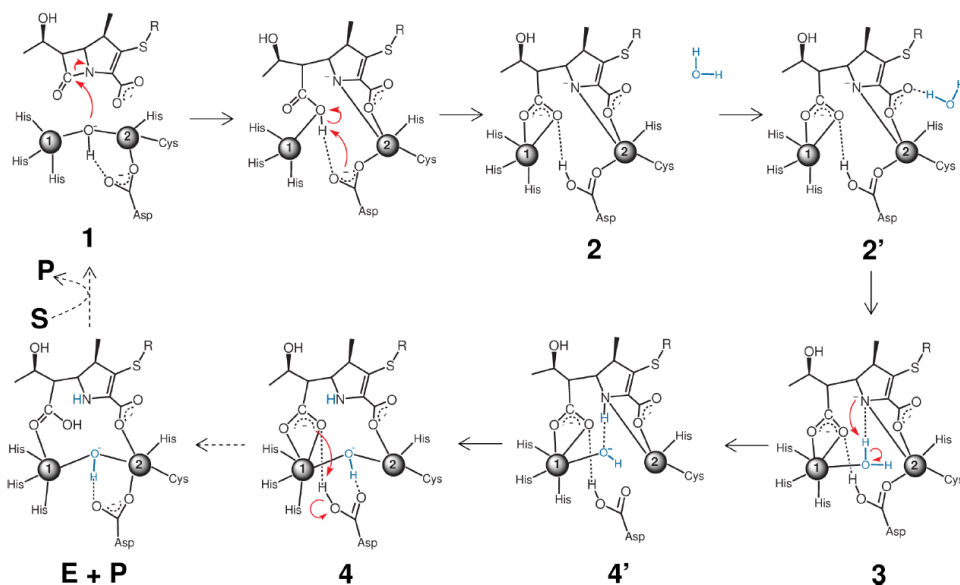


Figure 1.11 A proposed mechanism of meropenem hydrolysis by NDM-1 using QM/MD simulations. (Figure was taken from reference 124)

In this proposed mechanism, the two zinc ions are acting as Lewis acids to facilitate the nucleophilic attack to break the beta-lactam ring of meropenem. After breaking the C-N bond, the Zn1 ion interacts with the carboxylate group produced by hydrolysis and the Zn2 ion interacts with the negatively charged nitrogen anion to further stabilize the intermediate. Then a water molecule from the bulk solvent is oriented into the middle between the two zinc ions and acts as a proton source for the intermediate protonation. Finally, the hydrolyzed meropenem is released after the protonation. Overall, the mechanism is very similar to the di-zinc mechanism (B1/B3) mentioned before.

Several studies have shown the importance of the Zn<sup>2+</sup> ion and the residues at the Zn<sup>2+</sup> site of NDM-1. Fast's group has mutated the Cys 208 residue of the Zn<sup>2+</sup> site to Asp, Ser and His.<sup>125</sup> Among these mutations, the C208H mutant has completely knocked out the binding of Zn<sup>2+</sup> ion and significantly impaired the activities of NDM-1. Chen's group has also reported Ebselen as an NDM-1 inhibitor.<sup>122</sup> Ebselen can interact and covalently bind to the C208 residue at the Zn<sup>2+</sup> site. The binding of Ebselen blocks the binding of Zn<sup>2+</sup> ion and results in an inhibition effect to NDM-1. These studies have shown that the existence of Zn<sup>2+</sup> ion is very important in NDM-1 which requires two zinc ions to be active. Another study done by the Zheng's group has demonstrated the important function of the Asp 124 residue at the Zn<sup>2+</sup> site.<sup>126</sup> Zheng's group mutated the Asp 124 residue to Asn, which only reduced the point charge of the residue without other major change to the Zn<sup>2+</sup> site. However, this mutation has impaired the activities of NDM-1 greatly. This was because the reduction of point charge has weakened the interaction with the Zn<sup>2+</sup> ion and resulted in a position change of the Zn<sup>2+</sup> ion. Since the Zn<sup>2+</sup> ion is involved in stabilizing the negatively charged nitrogen intermediate, this study showed that the position of the Zn<sup>2+</sup> ion is very important. Moreover, the aspartate residue also forms hydrogen bond with the bridging hydroxide ion and orients the hydroxide ion to perform the nucleophilic attack. The Asn mutant lost the ability to do this, which was another reason of impairment in activities.

On the other hand, there were not many studies on the Zn1 site compared to the Zn2 site. Several Zn1 site mutations were studied on the other subclasses of metallo-beta-lactamases. Galleni's group has mutated the CphA (a B2 beta-lactamase) at N116H/N220G, where the N116 of CphA is equivalent to the H120 of NDM-1 at the Zn1 site.<sup>127</sup> This mutation has restored the binding of Zn1 ion at the Zn1 site and the enzyme became effective in hydrolyzing the penicillins and cephalosporins, which the CphA WT is completely inactive. This mutated CphA has shown a similar target spectrum as the B1 subclass. Bebrone's group has also mutated the GOB-1 enzyme (a B3 beta-lactamase) at Q120A and Q120N, where the Q120 of GOB-1 is equivalent to the H120 of NDM-1 at the Zn1 site.<sup>93</sup> Both of these mutations led to the knockout of Zn1 ion from the Zn1 site. The activities of the mutated GOB-1 have been impaired significantly to all types of antibiotics because of the missing of Zn1 ion. Based on these studies, there is a possibility that the Zn1 ion is greatly involved in the substrates selection, which generates the target substrate spectrum of NDM-1 and all other B1 beta-lactamases.

## 1.6. Aims and objectives of this project

Until now, there are two main proposed functions of the Zn1 ion: 1) to act as a Lewis acid to facilitate the nucleophilic attack for breaking the C-N bond and 2) to stabilize the intermediate for the protonation step. However, there is a high possibility that the Zn1 ion is also involved in other roles in NDM-1, such as binding of substrates or selection of substrates. For example, the CphA N116H/N220G mutant has restored the Zn1 ion binding to the Zn1 site and produced a broad target spectrum similar to the B1 subclass. This mutation has resulted in no change to the shape of the binding site but the target spectrum was broadened just by the recovery of Zn1 ion binding. This implies the importance of Zn1 ion in all the metallo-beta-lactamases. In this project, our goal is to gain a deeper understanding of the role of the Zn1 ion in the NDM-1 enzyme. Better understanding of the Zn1 site of NDM-1 might possibly lead to the development of new types of inhibitors or even new drug candidates.

The experiments are separated into three parts and they will be discussed in chapters 2, 3 and 4 respectively. In chapter 2, the Zn1 site residues will be mutated by site-directed mutagenesis and the zinc content of the mutants will be measured. Since the existence of the Zn1 ion is very important in our study, the zinc content measurement will be the critical step of this project. Then in chapter 3, the NDM-1 mutants will be tested on their hydrolytic activities

towards three different types of beta-lactam antibiotics, including the representatives of penicillins, cephalosporins and carbapenems. This chapter is mainly used to test the effects caused by the mutations at Zn1 site. Finally, in chapter 4, Molecular Dynamics (MD) simulations will be used to explain the observations in chapters 2 and 3.

# **Chapter 2. Protein Expressions and Zinc Content Measurements**

## 2.1. Introduction

There are two objectives in this chapter: 1) select a suitable position to mutate the NDM-1 to knock out the binding of the Zn1 ion, 2) measure the zinc content of the mutants to confirm the effects of the mutations.

NDM-1 is a Class B beta-lactamase, which binds to two zinc ions in its active-site.<sup>119, 128-129</sup> Six key residues are involved in binding of the two zinc ions: H120, H122, D124, H189, C208 and H250. The H120, H122 and H189 residues bind to the Zn1 ion and the D124, C208 and H250 residues bind to the Zn2 ion. Table 2.1 compares NDM-1 with two different Class B beta-lactamases: CphA and GOB-18 (both have no Zn1 ion binding).<sup>64, 94, 130</sup> The classification of the Class B beta-lactamase subclass mainly depends on their structure, metal coordination and substrate specificity.<sup>58</sup> NDM-1 has a broad range of substrate specificities and binds to two zinc ions in its active-site, which is grouped into the B1 subclass. CphA is a B2 subclass beta-lactamase. B2 subclass is a class of carbapenemases, which almost only hydrolyzes carbapenems, and it only binds to one zinc ion in its active-site (Zn2 site). GOB-18 is a special B3 subclass beta-lactamase. Comparing to the other B3 subclass beta-lactamases, GOB-18 can bind only to one zinc ion at the Zn2 site and remains active, while the other B3 subclass beta-lactamases all bind two zinc ions.<sup>65-69</sup> GOB-18 also hydrolyzes penicillins, carbapenems, and

cephalosporins like the B1 subclass beta-lactamases. When comparing the metal coordinating residues, residue 120 has the highest variety among the three enzymes. Especially when comparing between the NDM-1 and CphA, the only difference in key zinc binding residue is H120 to N120 and the zinc content has dropped from 2 to 1. Previous studies from different groups have worked on the position 120 of CphA and GOB-1, which showed position 120 does have a significant effect on the binding of Zn<sup>1</sup> ion. Galleni's group has mutated the CphA to give N116H/N220G (residue 116 of CphA is equivalent to residue 120 of NDM-1) and successfully recovered the binding of Zn<sup>1</sup> ion, which showed a similar target spectrum as the B1 subclass.<sup>127</sup> Bebrone's group has also mutated GOB-1 to obtain Q120A and Q120N, and they also successfully knocked out the Zn<sup>1</sup> ion binding from the GOB-1 enzyme.<sup>93</sup> It is very likely that position H120 plays a very important role in binding of Zn<sup>1</sup> ion in the Class B beta-lactamase. Therefore, our study will mainly focus on this H120 position in NDM-1. Three mutants will be tested in this project: 1) H120A – deletion of the histidine side chain in order to reduce the binding affinity to the Zn<sup>1</sup> ion, 2) H120N – mimics the active-site of the CphA enzyme in order to reduce the binding of Zn<sup>1</sup> ion, 3) H120Q – mimics the Zn<sup>1</sup> site of GOB-18 enzyme in order to form a mono-zinc protein like GOB-18. After these mutations, the zinc contents of the mutants were measured to confirm the effects on Zn<sup>1</sup> ion binding caused by the mutations.



Table 2.1 Comparison between beta-lactamase NDM-1, CphA and GOB-18.<sup>64, 94, 119, 128-130</sup>

Enzyme	Subclass	Number of zinc binding in active-site	Metal Coordination	Substrate Specificity
NDM-1	B1	2	H120, H122, H189 (Zn1 site) D124, C208, H250 (Zn2 site)	Penicillins Cephalosporins Carbapenems
CphA	B2	1	N120, H122, H189 (No zinc binding) D124, C208, H250 (Zn2 site)	Carbapenems
GOB-18	B3	1	Q120, H122, H189 (No zinc binding) D124, H125, H250 (Zn2 site)	Penicillins Cephalosporins Carbapenems

The zinc content of the mutants will be determined by Inductively Coupled Plasma Optical Emission Spectrometry (ICP-OES).

In ICP-OES, argon gas is ionized and generates a plasma.<sup>131</sup> The protein sample is then vaporized and introduced into the plasma to excite the zinc atom in the sample. When the zinc atom returned to the low energy position, an emission at 202.5 nm will be released. By measuring the intensity of this light emission, the zinc concentration in the sample can be measured. Since ICP-OES can only determine the overall zinc concentration in the sample, this measured zinc concentration needs to be divided by the NDM-1 protein concentration in the sample to calculate the zinc content per protein molecule. The detailed calculations are showed in Section 2.2.2.5. Although this is an indirect measuring method, it can measure the average zinc content of the protein under an equilibrium environment.

## 2.2. Experiment

### 2.2.1. Materials

#### 2.2.1.1. Bacterial strain

The *E.coli* TOP10F' competent cells (Thermo Fisher Scientific) were used in the site-directed mutagenesis experiment to construct the NDM-1 mutants. BL21(DE3) chemical competent cells (Sigma-Aldrich) were used for over-expression of the NDM-1 wild-type (WT) and mutants.

#### 2.2.1.2. Plasmids

Plasmid pET28a (Novagen) was used to clone and express the NDM-1 WT and mutants.<sup>132</sup> This vector has a kanamycin resistant marker and the map of this plasmid is shown in Figure 2.1. NDM-1 WT was cloned in between the *BamHI* and *XhoI* restriction sites. An N-terminal polyhistidine-tag (His-tag) was added on to the protein for purification by nickel affinity chromatography.

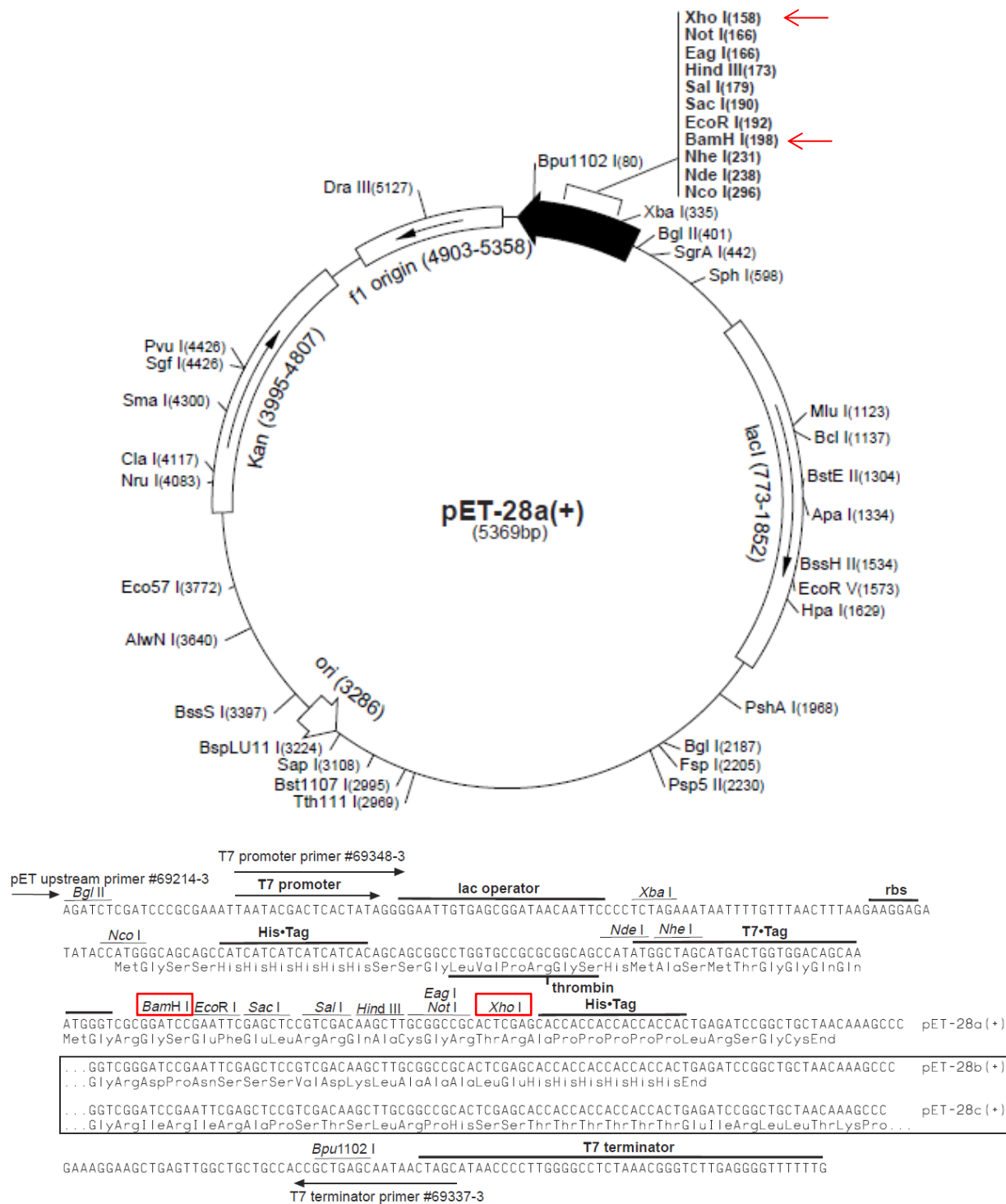


Figure 2.1 The plasmid map of pET28a from Novagen. The NDM-1 mutants were cloned between the BamHI and XhoI sites.

### 2.2.1.3. DNA manipulation reagents

The cloning and site-directed mutagenesis experiments were performed by using the PfuUltra High-Fidelity DNA polymerase (Stratagene). The primers used for the experiment were ordered from Life technologies. Table 2.2 shows the list of primers used for the cloning of NDM-1 WT and the mutations of NDM-1 mutants. Restriction enzymes (*BamHI* and *XhoI*) and the deoxy-ribonucleoside triphosphates (dNTPs) were purchased from Promega. The PCR purification kit and miniprep kit were purchased from QIAGEN.

Table 2.2 Primers used for constructing NDM-1 mutants

<b>Primers</b>	<b>DNA sequence (5'-3')</b>	<b>T<sub>m</sub> (°C)</b>
NDM1-F	AATTGGATCCGGCCAGCAAATGGAAACTGGCGACCAACG	66.9
NDM1-R	ATATCTCGAGTCAGCGCAGCTTGTCGGCCATGC	66.9
H120A-F	GGTGGTGACTGCCGCGCATCAG	57.2
H120A-R	CTGATGCGCGGCAGTCACCACC	57.2
H120N-F	CGGTGGTGACTAACGCGCATCAGGA	57.5
H120N-R	TCCTGATGCGCGTTAGTCACCACCG	57.5
H120Q-F	GGTGGTGACTCAGGCGCATCAGG	57.3
H120Q-R	CCTGATGCGCCTGAGTCACCACC	57.3

#### 2.2.1.4. Media

Luria-Bertani (LB) medium was used for transformation of TOP10 cells. 2xTY medium was used for growing BL21(DE3) cells for expression of proteins. 2xTY medium was prepared by addition of 16 g tryptone, 10 g yeast extract and 5 g sodium chloride into 1 L deionized water. Both LB and 2xTY media were sterilized by autoclave before use. The LB agar plates used for the transformation were prepared by addition of 15 g/L agar powder to the LB medium before autoclave. All the nutrient media were added with 50 µg/mL kanamycin before the addition of bacteria cells. The LB broth, sodium chloride and kanamycin were purchased from Sigma-Aldrich. Tryptone, yeast extract and agar powder were purchased from Oxoid Ltd.

## 2.2.2. Experimental Methods

### 2.2.2.1. Preparation of *E.coli* competent cells

The *E. coli* strain (TOP10 or BL21(DE3)) starter culture was grown in 5 mL sterilized LB medium at 37 °C overnight with 250 rpm shaking. Then the starter culture was diluted 1:100 fold to inoculate a 100 mL sterilized LB culture. The culture was incubated at 37 °C with 250 rpm shaking until the optical density at wavelength 600 nm ( $OD_{600}$ ) reached 0.4. The cells were harvested by centrifugation at 4500 rpm for 30 min at 4 °C. The pellet was re-suspended in 10 mL of sterilized 0.1 M  $CaCl_2$  and incubated at 4 °C with gentle rotation for 1 hr. The cells were pelleted again by centrifugation and re-suspended in 700 mL of 0.1 M  $CaCl_2$ . Afterward, 300 mL of 50% (v/v) sterilized glycerol was added and the final glycerol concentration was 15%. The competent cells were then aliquoted into 100  $\mu$ L per eppendorf tube and quickly frozen by liquid nitrogen and stored at -80 °C.

#### 2.2.2.2. Cloning and site-directed mutagenesis of NDM-1 mutants

The cloning and site-directed mutagenesis were performed by the QuikChange II Site-Directed Mutagenesis Kit (Stratagene). The NDM-1 WT gene was cloned from the genomic DNA of the *E. coli* Castellani and Chalmers strain (ATCC BAA-2469). Primers NDM1-F and NDM1-R (Table 2.2) were used in this cloning experiment. Reagents in Table 2.3 were mixed into the PCR tube. The PCR cycling condition for this cloning was 95 °C for 30 sec, 35 cycles of 95 °C for 30 sec, 65 °C for 1 min, 68 °C for 2 min 30 sec, and finishing with 68 °C 10 min. The amplified NDM-1 WT gene was ligated into the pET28a plasmid between the *Bam*HI and *Xho*I sites (Figure 2.1). After the cloning of WT, site-directed mutagenesis experiments were performed on this plasmid. The site H120 of NDM-1 was mutated into alanine (A), asparagine (N) and glutamine (Q). Table 2.2 listed the primers used for these mutations. Reagents in Table 2.3 were mixed into the PCR tube. The PCR cycling condition for these mutations were 95 °C for 1 min, 20 cycles of 95 °C for 1 min, 60 °C for 1 min, 68 °C for 10 min, and finishing with 68 °C 11 min.

Table 2.3 Reagents for PCR cloning and site-directed mutagenesis

1.25 µL	Forward Primer (100 ng/µL)
1.25 µL	Reverse Primer (100 ng/µL)
1 µL	dNTP
5 µL	Reaction Buffer 10x
3 µL	MgCl <sub>2</sub>
1 µL	Template DNA (5-50ng)
36.5 µL	Water
1 µL	DNA Polymerase
50 µL	Total Volume



#### 2.2.2.3. Transformation of competent cells by heat shock

The plasmid pET28a containing the NDM-1 WT and mutants were transformed into *E. coli* competent cells (TOP10 for DNA manipulation and BL21(DE3) for protein expression). The plasmid DNA was gently mixed with 100  $\mu$ L of competent cell. The transformation mixture was incubated on ice for 30 min. Then the mixture was heat shocked at 42 °C for 45 sec and allowed to recover on ice for 2 min. 1 mL of LB medium was added to the mixture and incubated at 37 °C with 250 rpm shaking for 1 hr. After the incubation, the transformation mixture was spread on the LB agar plate with kanamycin for selection. The plate was incubated at 37 °C overnight. Single colony on the transformed plate was picked and inoculated into a 5 mL LB culture with kanamycin for selection. The plasmid was extracted by the QIAprep Spin Miniprep Kit and the NDM-1 DNA sequences were confirmed by DNA sequencing services provided by BGI Co. Ltd.

#### 2.2.2.4. Protein Expressions of NDM-1 WT and mutants

A single colony of NDM-1 transformed BL21(DE3) cell was inoculated into a 5 mL LB starter culture with kanamycin selection. The starter culture was grown at 37 °C with 250 rpm shaking overnight. Next day, the starter culture was diluted 1:100 fold to inoculate a 400 mL sterilized 2xTY culture. The resulting culture was incubated at 37 °C with 250 rpm shaking until the OD<sub>600</sub> reached to 0.8-1.0. A final concentration of 1 mM isopropylthiogalactoside (IPTG) was added to the culture to induce the expression of NDM-1. Then, the culture was grown at 16 °C with 250 rpm shaking overnight. The cells were collected by centrifugation at 5000 rpm at 4 °C for 30 min and stored at -80 °C.

The 400 mL cell culture pellet was resuspended in 20 mL of solubilization buffer (20 mM sodium phosphate and 0.5 M sodium chloride, pH 7.4) with addition of one protease inhibitor cocktail tablet (Roche Diagnostic GmbH). The resuspended cells were lysed using sonication by a Soniprep 150 ultrasonic disintegrator (10 min, with 10 sec on and 20 sec off pulses, 50 % power). The cell lysate was subjected to centrifugation at 18000 rpm for 30 min at 4 °C. The supernatant was collected and purified by affinity chromatography.

Since the NDM-1 proteins were expressed with a N-terminal His-tag, the proteins were purified by nickel affinity chromatography. A 5 mL HiTrap chelating column (GE Healthcare) was connected to an AKTA FPLC system.

The column was first pre-equilibrated with three column volumes of solubilization buffer. The cell lysate was filtered through a 0.2  $\mu\text{m}$  sterile filter (PALL) and then loaded onto the column. The NDM-1 protein was eluted by slowly increasing the concentration gradient of the elution buffer (solubilization buffer with 0.5 M imidazole). The fractions showing a UV absorbance peak (at 280 nm) were collected and analyzed by SDS-PAGE. The fractions that had the correct NDM-1 molecular mass were buffer exchanged with 15 mM sodium cacodylate buffer, pH 6.5, and stored at 4  $^{\circ}\text{C}$ .

#### 2.2.2.5. Zinc content measurement by ICP-OES

The zinc contents of the NDM-1 mutants were measured by Inductively Coupled Plasma Optical Emission Spectrometry (ICP-OES). For sample preparation, 2 mL of 30  $\mu$ M NDM-1 protein was pipetted into a 12 kDa membrane (Spectrum) and dialyzed in 15 mM sodium cacodylate buffer, pH 6.5, with 200  $\mu$ M zinc sulfate overnight at 4 °C. The protein concentration after dialysis was measured by Bradford assay (Bio-Rad). Then the protein sample was digested by adding 1:1 ratio of 69% concentrated nitric acid and heated up to 95 °C for 30 min. The digested protein sample was filtered by 0.2  $\mu$ m sterile filter (PALL) and then diluted 1:5 with 15 mM sodium cacodylate buffer. The dialysis buffer was also collected and treated with the same preparation as the protein sample. Both the protein sample and the buffer sample were submitted for ICP-OES analysis. The ICP-OES machine was first calibrated with zinc standards (2% nitric acid added) and a standard curve was constructed. The zinc concentrations of the protein sample and the buffer sample were measured in triplicate with reference to the standard curve. Finally, the zinc content per protein molecule of the NDM-1 sample was calculated by the following formula:

$$\text{Zn content per protein} = \frac{(\text{Zn conc. of protein sample}) - (\text{Zn conc. of buffer sample})}{\text{Protein conc. by Bradford assay}}$$

#### 2.2.2.6. Zinc ions binding analysis by Mass Spectrometry

Electrospray Ionization Mass Spectrometry (ESI-MS) analysis was performed on a Waters Synapt G2-Si Quadrupole-Ion Mobility-Time-of-flight Mass Spectrometer. Before ESI-MS analysis, all proteins were buffer exchanged into 50 mM of ammonium acetate buffer, pH 7.0. For denaturing protein analysis, the protein samples were mixed with equal volumes of acetonitrile containing 0.2 % formic acid. The mixtures were then directly infused into the ESI source with a syringe pump. For native protein analysis, the protein samples were directly loaded into metal-coated glass capillaries, which was subsequently mounted onto the nano-ESI source. The nano-ESI capillary voltage and cone voltage were set at 1.5 kV and 30 V, respectively, and the nanoflow gas pressure was set at 0.2 bar.

#### 2.2.2.7. Other experimental control of the zinc-binding ability of His-tag

A purified His-tagged BlaC tuberculosis (TB) beta-lactamase T216C enzyme was obtained from Prof. Thomas Leung's group. It was used to perform a further control experiment. The T216C enzyme was buffer exchanged into 50  $\mu$ M of ammonium acetate buffer (pH 7.0) and followed the same protocol as experimental method 2.2.2.6 mentioned above to determine the zinc-binding ability of the His-Tag itself. Further details will be described in Section 2.3.4.

#### 2.2.2.8. Cleavage of His-tag from the NDM-1 proteins

Thrombin enzyme (Sigma-Aldrich) was used to cleave the His-tag on the NDM-1 WT and mutants (the Thrombin cleavage site is showed in Figure 2.1). The purified NDM-1 proteins were buffer exchanged into cleavage buffer (50 mM Tris-HCl, 150 mM NaCl and 2.5 mM CaCl<sub>2</sub>, pH 8.0). The protein samples were then incubated with the Thrombin enzyme (5 units) for 3 hr at room temperature. The supernatant was collected and then incubated with the Ni-NTA agarose resin (QIAGEN) for 15 min at room temperature. The Ni-NTA resin will bind the non-cleaved His-tag protein and the supernatant will only contain the purified cleaved protein. The supernatant was collected and further purified by HiPrep™ 16/60 Sephacryl™ S-200 HR (GE Healthcare) gel filtration column. The final His-tag cleaved NDM-1 proteins were buffer exchanged into 15 mM sodium cacodylate buffer, pH 6.5, and stored at 4 °C. The zinc contents of the proteins were measured by ICP-OES as described as experimental method 2.2.2.5.

## 2.3. Results and Discussion

### 2.3.1. Preparation of the NDM-1 proteins

The NDM-1 WT, H120A, H120N and H120Q were successfully expressed and purified by the HiTrap chelating column. The elution profiles of the four proteins are showed in Figure 2.2-2.5. The purity of the proteins is shown by SDS-PAGE analysis in Figure 2.6. As the elution profiles showed, the yields of all four NDM-1 proteins were very high. The SDS-PAGE showed all proteins were higher than 95% purity. The proteins are pure enough to perform zinc content experiments and the following assays.

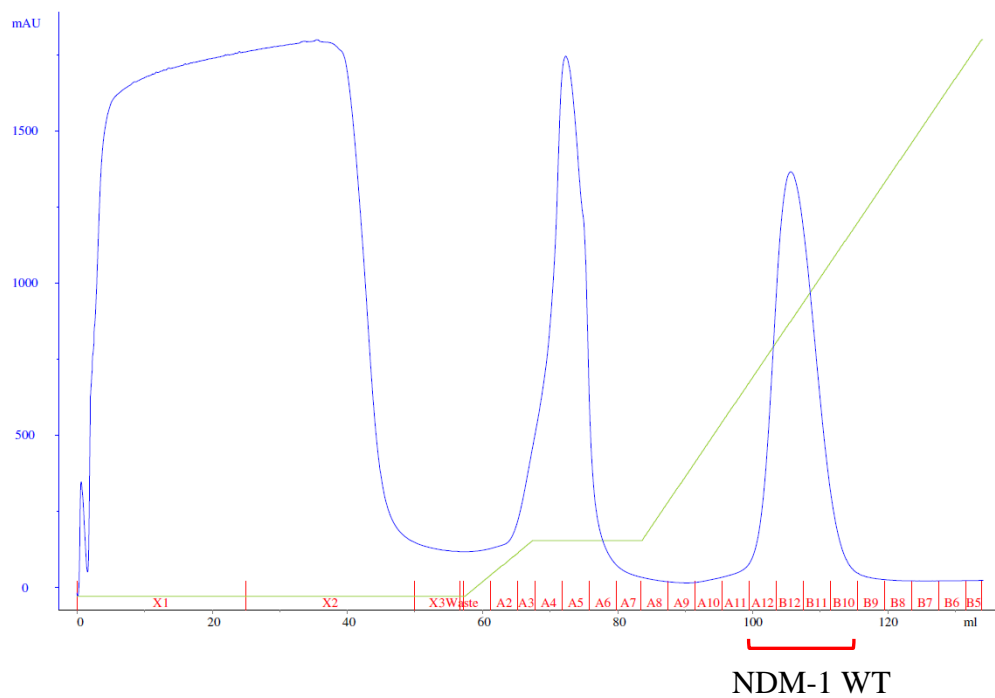


Figure 2.2 The elution profile of NDM-1 WT from cell lysate. The blue line indicates the UV absorbance at 280 nm and the green line indicates the concentration of the elution buffer. The Fractions A12-B10 were collected and buffer exchanged.



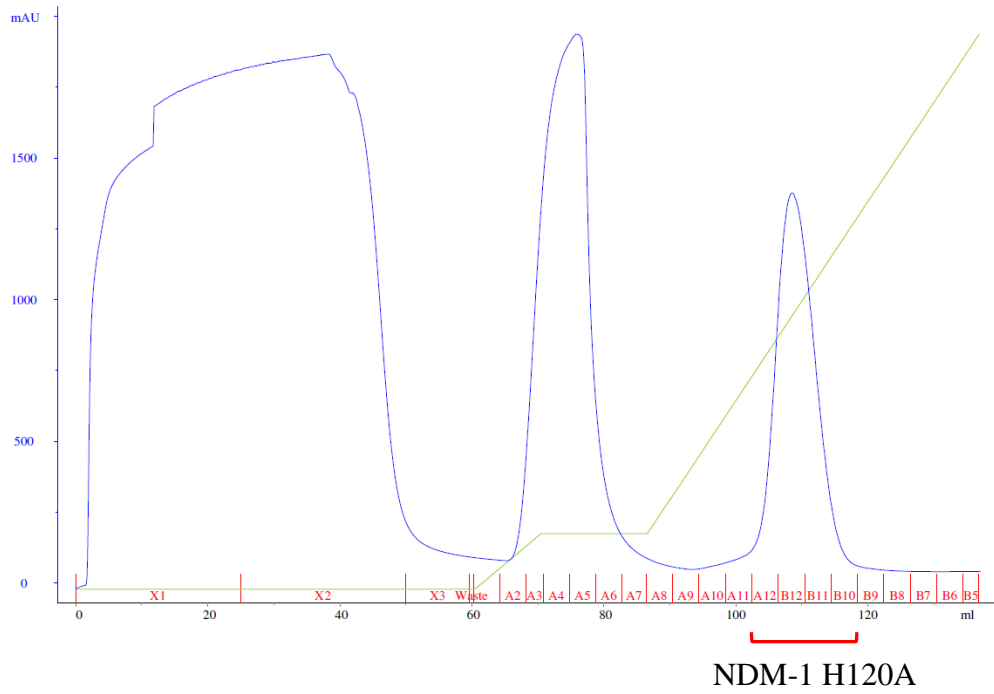


Figure 2.3 The elution profile of NDM-1 H120A from cell lysate. The blue line indicates the UV absorbance at 280 nm and the green line indicates the concentration of the elution buffer. Fractions A12-B10 were collected and buffer exchanged.

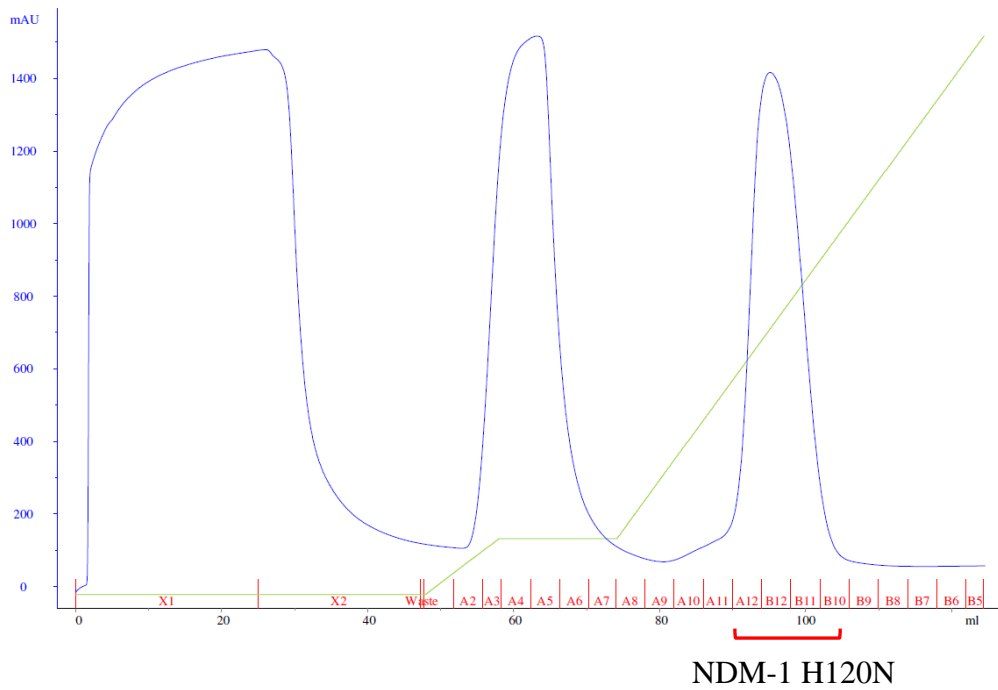


Figure 2.4 The elution profile of NDM-1 H120N from cell lysate. The blue line indicates the UV absorbance at 280 nm and the green line indicates the concentration of the elution buffer. Fractions A12-B10 were collected and buffer exchanged.

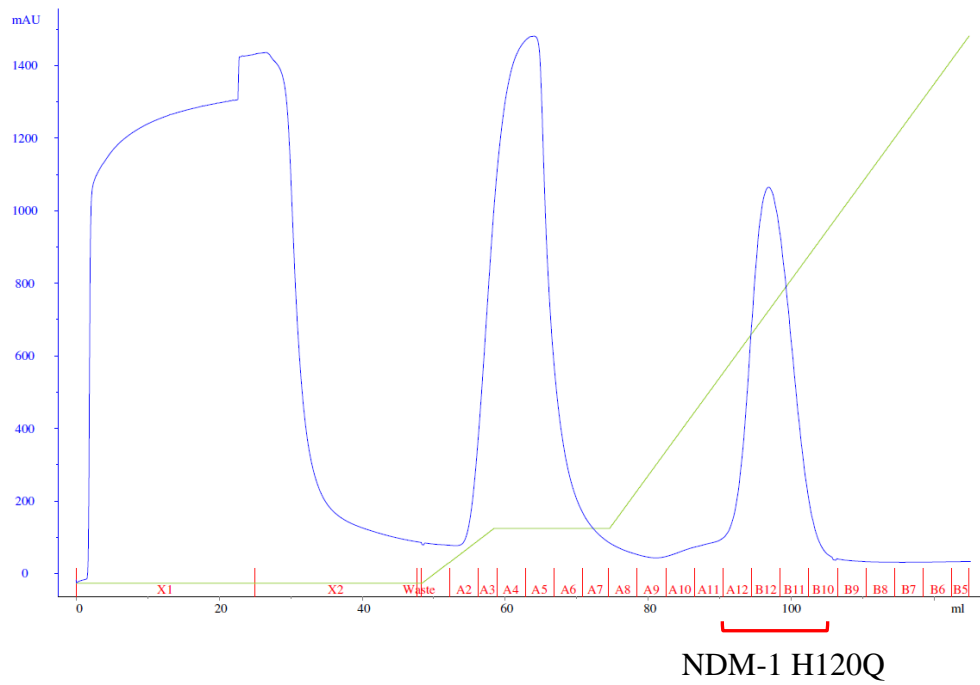


Figure 2.5 The elution profile of NDM-1 H120Q from cell lysate. The blue line indicates the UV absorbance at 280 nm and the green line indicates the concentration of the elution buffer. Fractions A12-B10 were collected and buffer exchanged.

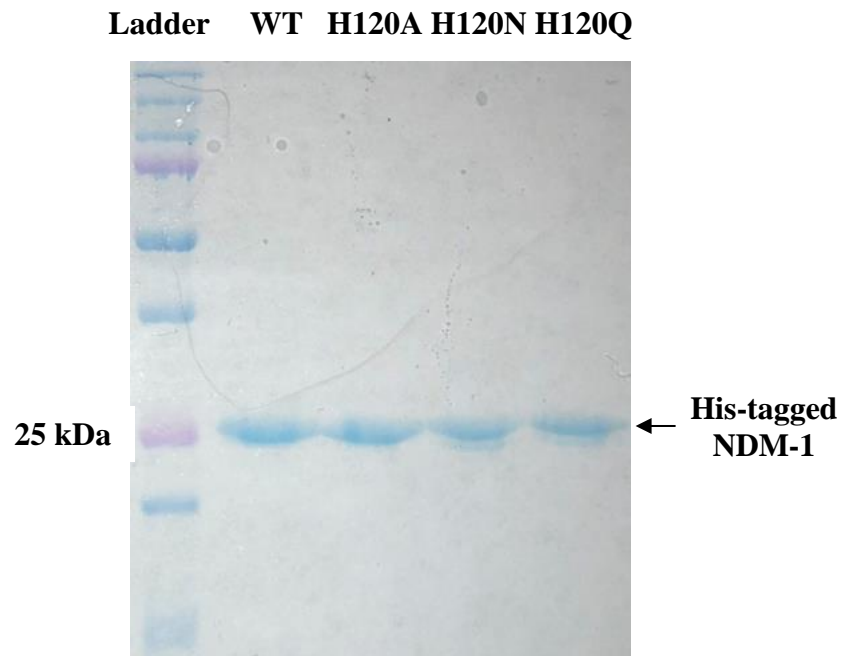


Figure 2.6 The SDS-PAGE of NDM-1 proteins after buffer exchange. Precision Plus Protein Dual Xtra Standards Ladder (Bio-RAD) was used. The expected molecular weight (MW): NDM-1 WT (28.39 kDa), H120A (28.32 kDa), H120N (28.37 kDa) and H120Q (28.38 kDa)

### 2.3.2. Zinc content of NDM-1 proteins measured by ICP-OES

The NDM-1 WT and mutants were analyzed by ICP-OES to determine the zinc concentration in the samples. Table 2.4 shows the zinc concentration data from the ICP-OES and the protein concentration data from the Bradford assays. The data were measured in triplicate and the average values were shown in the table. Zinc content per protein was calculated by the formula showed in Experimental method 2.2.2.5. As the results showed, all four proteins including the mutants have zinc contents above 2.0 (zinc content of WT is 2.2 and the mutants are ranged from 2.1 to 2.5). It is known that NDM-1 binds two zinc ions in their active-site<sup>119, 128-129</sup>. The zinc contents above 2.0 are higher than the maximum number that the NDM-1 proteins can bind. It is possible that the His-tag on the NDM-1 proteins is binding those extra zinc ions, so the overall zinc contents of the samples were above 2.0. Mass spectrometry analysis was therefore further used to confirm this finding. Ignoring the fact that the zinc contents were above 2.0, overall, the data showed none of the mutants have a significant decrease in zinc content comparing to the WT. Therefore, in conclusion, the mutations at position H120 did not really affect the binding of Zn<sup>1</sup> ion in NDM-1.

Table 2.4 The ICP-OES data and the calculations of zinc content of each His-tagged NDM-1 samples. Each zinc concentration data was the average value of a triplicate measurement.

Proteins	Zinc Conc. (protein sample) $\mu\text{M}$	Zinc Conc. (buffer sample) $\mu\text{M}$	Protein Conc. $\mu\text{M}$	Zinc content per protein
WT	$26.1 \pm 0.5$	$20.1 \pm 0.4$	$2.7 \pm 0.1$	$2.2 \pm 0.3$
H120A	$27.0 \pm 0.5$	$20.1 \pm 0.4$	$2.8 \pm 0.1$	$2.5 \pm 0.2$
H120N	$25.2 \pm 0.4$	$19.4 \pm 0.4$	$2.6 \pm 0.1$	$2.2 \pm 0.3$
H120Q	$24.3 \pm 0.4$	$19.4 \pm 0.4$	$2.4 \pm 0.1$	$2.1 \pm 0.3$

### 2.3.3. Zinc ions binding analysis of NDM-1 proteins by MS

The NDM-1 protein samples were further analyzed by MS. As shown in Figure 2.7, when no zinc sulfate is added to the buffer, only 1 Zn was bound to the NDM-1 WT protein. This means that the NDM-1 protein requires extra zinc in the buffer in order to bind two zinc ions in its active site. Therefore, 50  $\mu$ M of zinc sulfate is added to the 50 mM ammonium acetate buffer for the following MS analyses.

Figure 2.8-2.11 show the native MS results of the NDM-1 WT, H120A, H120N and H120Q. As shown by the results, all four proteins displayed major peaks of 3 Zn and 4 Zn binding on. It is known that NDM-1 only binds 2 zinc ions in its active-site to activate the hydrolysis reaction.<sup>119, 128-129</sup> Therefore, binding of 3 Zn or 4 Zn were not expected. Since all these protein samples are a mixture with 2 Zn, 3 Zn and 4 Zn bound, the overall average zinc contents will be above 2.0, which is consistent with the ICP-OES results in Section 2.3.2. It is highly possible that these extra zinc ions are binding on the His-tag. The His-tag does have the ability to bind zinc ions and our NDM-1 proteins did not have their His-tag cleaved. This might be the main reason of forming the 3 Zn and 4 Zn peaks.

Ignoring the fact that extra zinc ions were binding on the proteins, comparing the results between the WT and mutants, the zinc binding complexes pattern of all four proteins were about the same. None of the mutants have a significant reduction of zinc binding when comparing to the WT. Therefore, it further confirmed that the mutations at position H120 did not affect the binding of Zn<sup>2+</sup> ion in NDM-1.



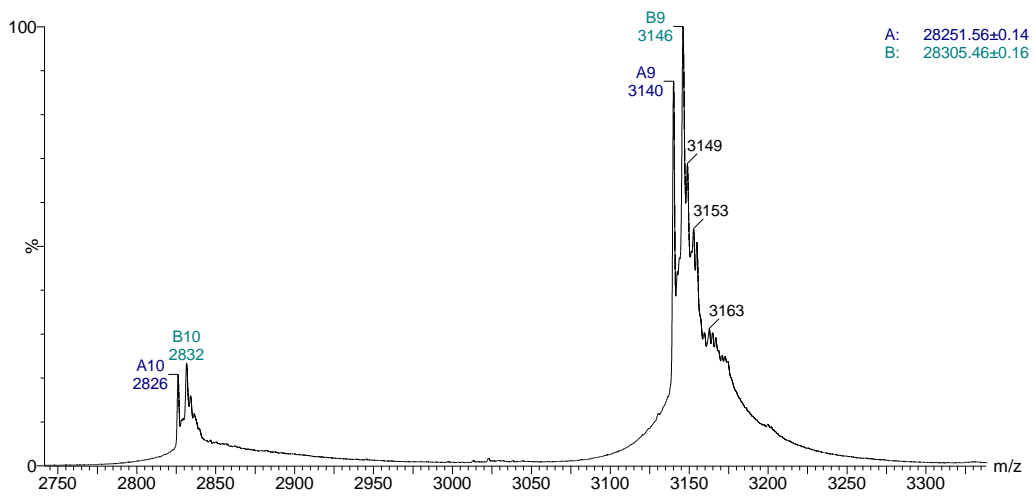


Figure 2.7 The native mass spectrometry of NDM-1 WT without addition of zinc sulfate. The multiple charge ion peaks of complexes A and B are shown. The relative masses of these complexes are listed at the top right. The expected MW: NDM-1 WT (A) = 28240 Da and WT + 1 Zn (B) = 28305 Da.

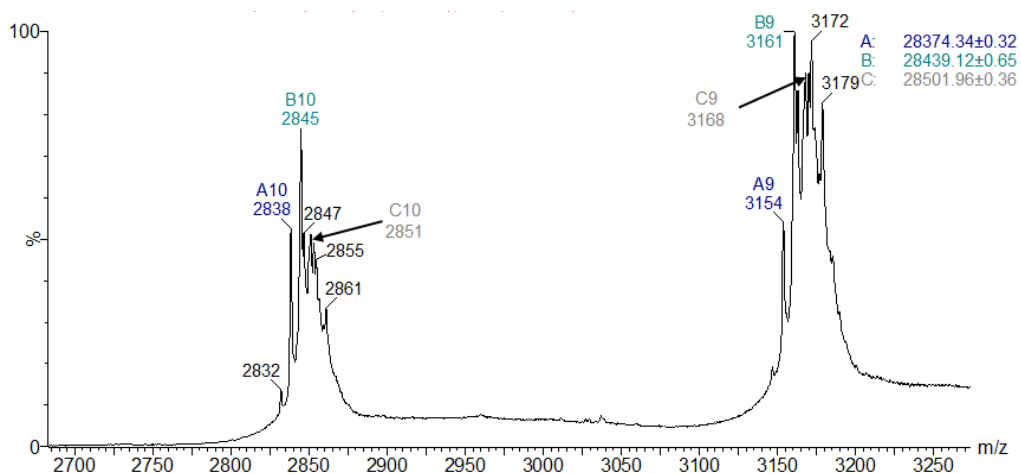


Figure 2.8 The native mass spectrometry of NDM-1 WT with the addition of 50  $\mu$ M zinc sulfate. The multiple charge ion peaks of complexes A, B and C are shown. The relative masses of these complexes are listed at the top right. The expected MW: WT + 2 Zn (A) = 28370 Da, WT + 3 Zn (B) = 28435 Da and WT + 4 Zn (C) = 28500 Da.

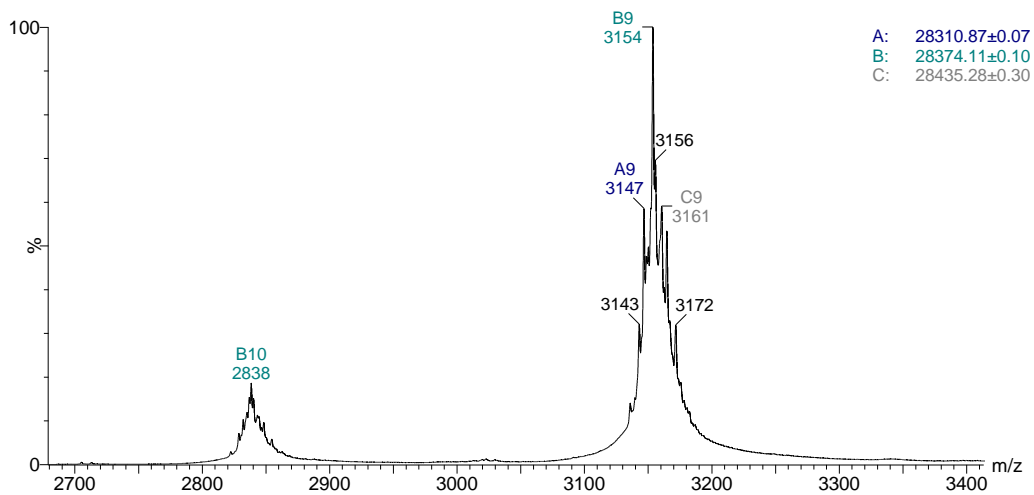


Figure 2.9 The native mass spectrometry of NDM-1 H120A with the addition of 50  $\mu$ M zinc sulfate. The multiple charge ion peaks of complexes A, B and C are shown. The relative masses of these complexes are listed at the top right. The expected MW: H120A + 2 Zn (A) = 28310 Da, H120A + 3 Zn (B) = 28375 Da and H120A + 4 Zn (C) = 28440 Da.

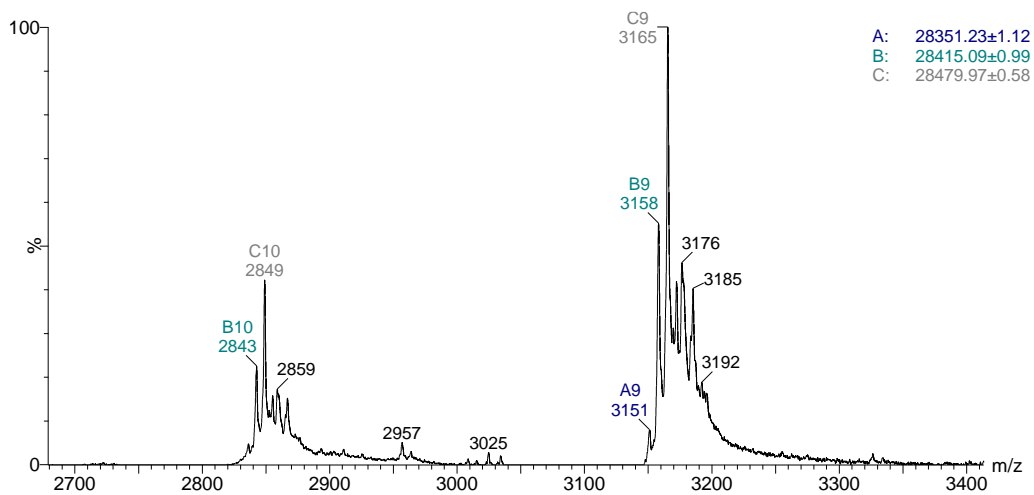


Figure 2.10 The native mass spectrometry of NDM-1 H120N with the addition of 50  $\mu$ M zinc sulfate. The multiple charge ion peaks of complexes A, B and C are shown. The relative masses of these complexes are listed at the top right. The expected MW: H120N + 2 Zn (A) = 28350 Da, H120N + 3 Zn (B) = 28415 Da and H120N + 4 Zn (C) = 28480 Da.

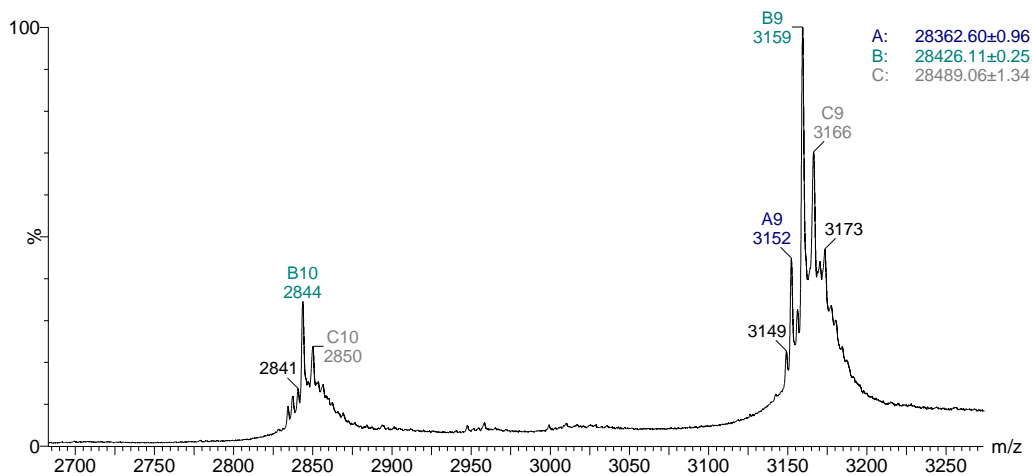


Figure 2.11 The native mass spectrometry of NDM-1 H120Q with the addition of 50  $\mu$ M zinc sulfate. The multiple charge ion peaks of complexes A, B and C are shown. The relative masses of these complexes are listed at the top right. The expected MW: H120Q + 2 Zn (A) = 28360 Da, H120Q + 3 Zn (B) = 28425 Da and H120Q + 4 Zn (C) = 28490 Da.

#### 2.3.4. Experimental control of the zinc binding His-tag

Since the His-tag might affect the zinc content measurement, a different control experiment was performed. The idea is to use a related His-tagged protein which does not bind zinc ions, so that only the zinc ions bound to the His-tag will be measured. For this purpose, the zinc binding of the N-terminal His-tagged BlaC TB beta-lactamase T216C enzyme was analyzed by mass spectrometry. Figure 2.12 shows that His-tagged T216C binds one or two  $Zn^{2+}$  after the addition of 50  $\mu M$  zinc into the buffer. BlaC TB beta-lactamase is a class A beta-lactamase which does not bind zinc ion.<sup>133</sup> Therefore, the binding of zinc ions was mainly due to the His-tag itself. This control experiment showed that the His-tag does affect the measurement of zinc content of the protein. Referring back to the MS results from 2.3.3, the His-tagged NDM-1 WT and mutants all contain a mixture of 2 Zn to 4 Zn complexes. By subtracting the extra zinc ions binding on the His-tag (1-2 zinc ions), the actual zinc ions binding on the NDM-1 WT and mutants were only 1-2. These results were consistent with the literatures reported by the B1 subclass beta-lactamases, where the Zn1 site has a stronger binding affinity with zinc ion and Zn2 site is weaker.<sup>87, 89-91</sup>

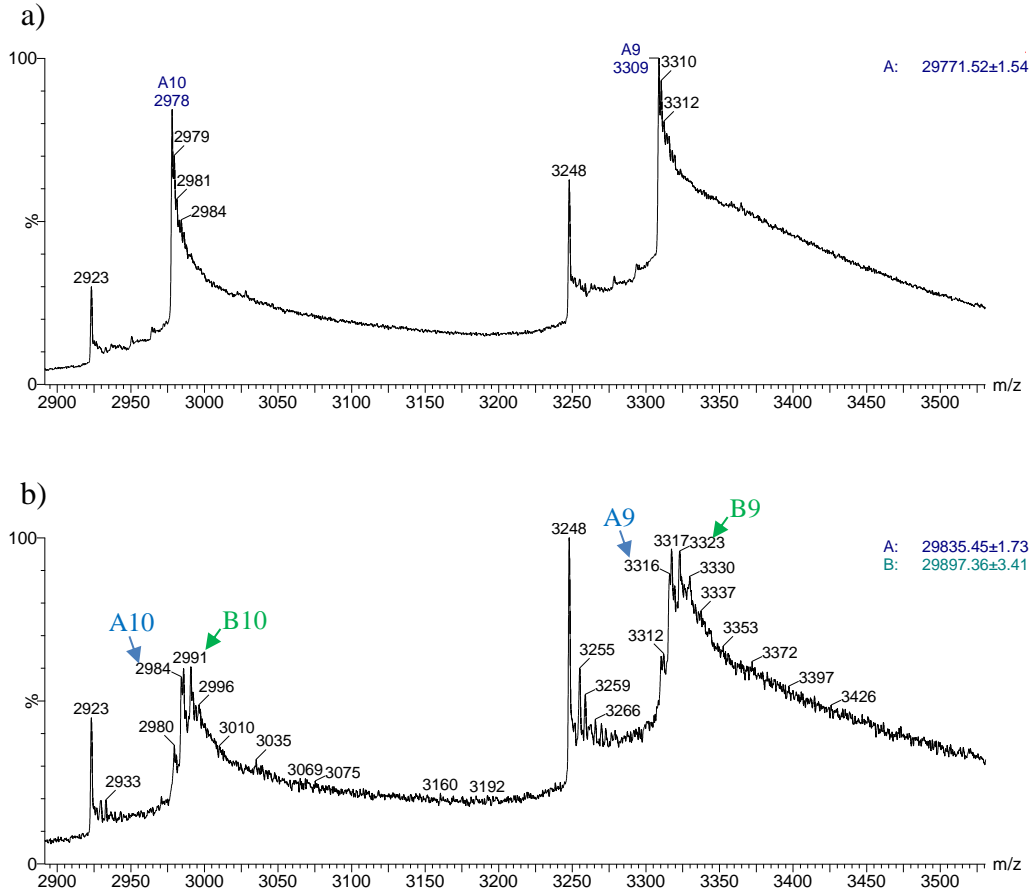


Figure 2.12 The native mass spectrometry data of the His-tagged BlaC TB beta-lactamase T216C. a) Native MS without addition of zinc sulfate. The multiple charge ion peaks of T216C (A) is shown. The relative mass is listed at the top right. The expected MW of T216C is 29770 Da. b) Native MS with addition of 50  $\mu$ M zinc sulfate. The multiple charge ion peaks of complexes A and B are shown. The relative masses of these complexes are listed at the top right. The expected MW: T216C + 1 Zn (A) = 29835 Da and T216C + 2 Zn (B) = 29900 Da.

### 2.3.5. Cleavage of His-tag and the zinc content measured by ICP-OES

Since the His-tag is obviously affecting the zinc content measurement of the NDM-1 samples, it is necessary to cleave this tag to get accurate measurements. Therefore, the His-tag of the NDM-1 proteins were cleaved by the Thrombin enzyme and analyzed by ICP-OES to measure the zinc contents again. Figure 2.13 shows the SDS-PAGE of His-tag cleavage of NDM-1 WT by Thrombin enzyme at different incubation time. As shown in the gel, the His-tag was completely cleaved after 3 hr incubation of Thrombin enzyme. The cleaved proteins were then incubated with the Ni-NTA agarose resin to remove the non-cleaved His-tag proteins. Finally, the samples were further purified by size-exclusion chromatography. Figure 2.14 shows the SDS-PAGE of the NDM-1 WT and mutants after the size-exclusion chromatography. As shown in the gel, the cleaved NDM-1 proteins were about 90% purity. There were still some truncated NDM-1 in the samples, which were created by over-cutting of Thrombin enzyme. It is very difficult to further purify these proteins because the size difference between the truncated proteins and full protein are too small (only 3.4 kDa in difference). Therefore, these protein samples were continued to use to measure the zinc contents.



The zinc contents of the His-tag cleaved NDM-1 samples were measured by ICP-OES. Table 2.5 shows the zinc concentration data from the ICP-OES and the protein concentration data from the Bradford assays of the His-tag cleaved NDM-1. By using the formula showed in Experimental method 2.2.2.5, the zinc content per protein molecule was calculated. As the result shown, the zinc contents of NDM-1 WT is 1.7 and the NDM-1 mutants are ranged from 1.6 to 1.8. As expected, the zinc contents were dropped below 2.0 after the His-tag was cleaved. Since the zinc content is an average value, this means the NDM-1 samples are mixed of 1 Zn and 2 Zn binding complexes. As the Zn1 site has a stronger binding affinity with zinc ion and Zn2 site is weaker<sup>87, 89-91</sup>; this result is consistent with the literatures reported. More importantly, the overall data showed that none of the mutants have a significant decrease in zinc content comparing to the WT. Therefore, the conclusion was the same as mentioned before; the mutations at position H120 did not really affect the binding of Zn1 ion in NDM-1.

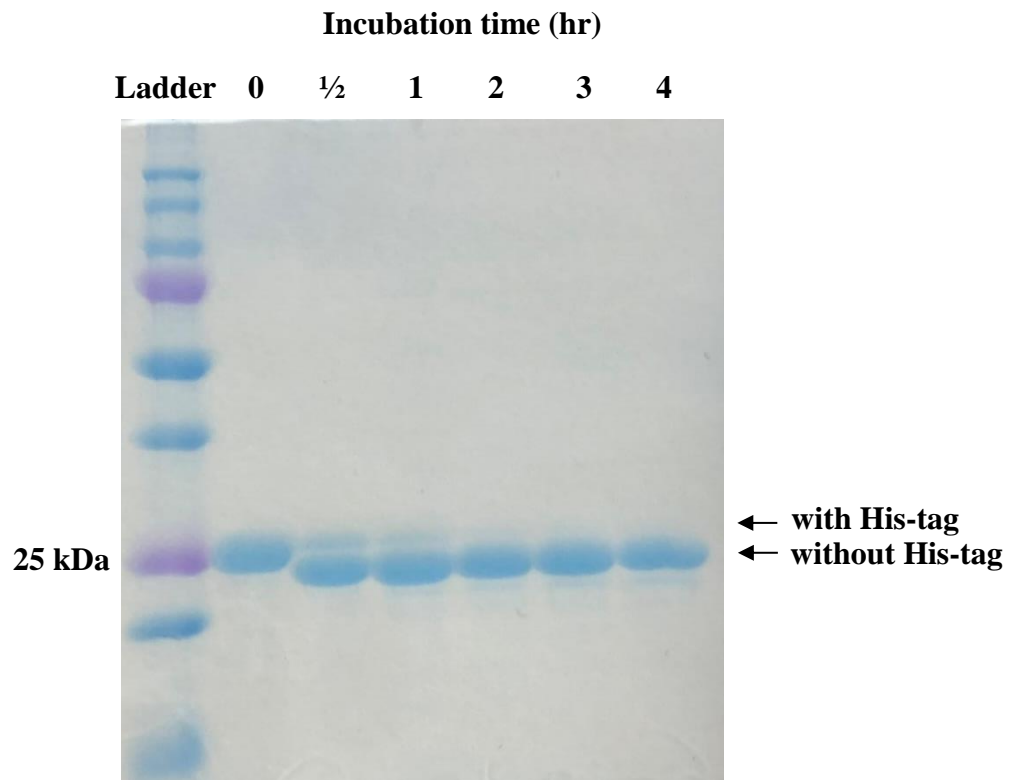


Figure 2.13 The SDS-PAGE of His-tag cleavage of NDM-1 WT by Thrombin enzyme with different incubation time. Precision Plus Protein Dual Xtra Standards Ladder (Bio-RAD) was used. The expected molecular weight (MW): His-tagged NDM-1 WT (28.39 kDa) and His-tag cleaved NDM-1 WT (24.99 kDa)

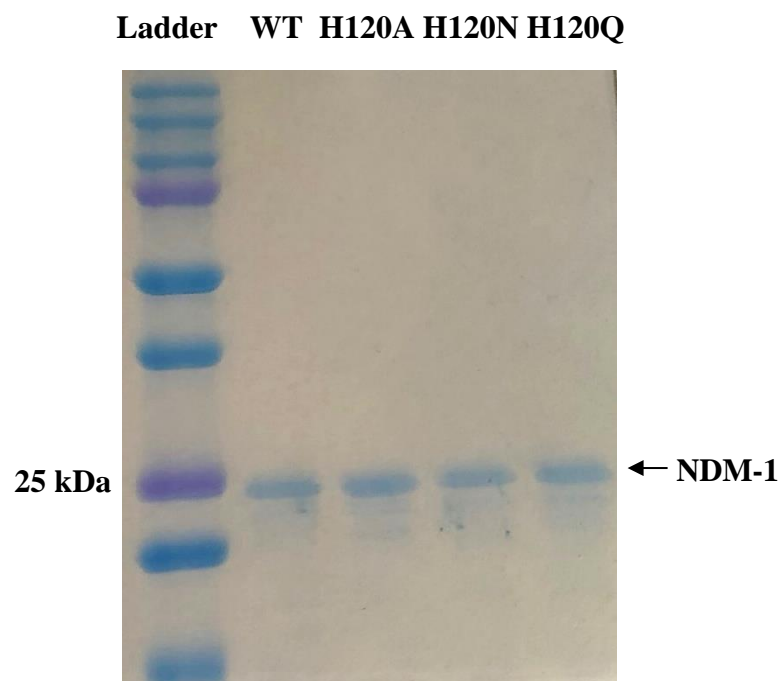


Figure 2.14 The SDS-PAGE of the NDM-1 WT and mutants after purified by the size-exclusion chromatography. Precision Plus Protein Dual Xtra Standards Ladder (Bio-RAD) was used. The expected molecular weight (MW): NDM-1 WT (24.99 kDa), H120A (24.92 kDa), H120N (24.97 kDa) and H120Q (24.98 kDa)

Table 2.5 The ICP-OES data and the calculations of zinc content of each His-tag cleaved NDM-1 samples. Each zinc concentration data was the average value of a triplicate measurement.

Proteins	Zinc Conc. (protein sample) $\mu\text{M}$	Zinc Conc. (buffer sample) $\mu\text{M}$	Protein Conc. $\mu\text{M}$	Zinc content per protein
WT	$34.3 \pm 0.6$	$30.6 \pm 0.5$	$2.2 \pm 0.1$	$1.7 \pm 0.4$
H120A	$36.6 \pm 0.3$	$30.6 \pm 0.5$	$3.4 \pm 0.2$	$1.8 \pm 0.2$
H120N	$34.8 \pm 0.5$	$30.6 \pm 0.5$	$2.6 \pm 0.1$	$1.6 \pm 0.3$
H120Q	$37.5 \pm 0.5$	$30.6 \pm 0.5$	$4.1 \pm 0.2$	$1.7 \pm 0.2$

## 2.4. Concluding Remarks

Overall, the NDM-1 WT, H120A, H120N and H120Q were expressed, purified and their zinc contents in the zinc buffer were measured. The zinc contents of NDM-1 proteins were mainly determined by ICP-OES.

At the beginning, the ICP-OES data showed that all His-tagged NDM-1 proteins (including WT and mutants) had zinc contents above 2.0, which were above the number of zinc binding sites in NDM-1. The MS analysis showed that these NDM-1 proteins samples were mixtures of 2 Zn, 3 Zn and 4 Zn binding complexes. The additional Zn were caused by the His-tag which binds this extra amount of zinc ions. As proved by our control experiment using the His-tagged BlaC TB beta-lactamase T216C enzyme, the MS analysis showed that the His-tag does bind one to two zinc ions. Therefore, in order to get an accurate zinc content measurement, it was necessary to cleave the His-tag from the NDM-1. After the His-tag cleavage by Thrombin enzyme, the zinc contents of the samples were measured again by ICP-OES. As expected the zinc content for all the samples dropped below 2.0 this time (WT = 1.7, H120A = 1.8, H120N = 1.6 and H120Q = 1.7). Overall, there were no significant decreases in the zinc contents when comparing between the WT and the mutants. This means the mutations at position H120 does not really affect the binding affinity of Zn<sup>1</sup> ion in NDM-1. This observation is unexpected and different from the

previous studies on CphA and GOB-1.<sup>93, 127</sup> It is known that H120, H122 and H189 are the three key residues of binding and holding the Zn1 ion in the NDM-1 active-site. Based on the studies from the Galleni's group<sup>127</sup> and the Bebrone's group<sup>93</sup>, it was postulated the H120 mutations will lead to the knocking out or reduction in binding affinity of Zn1 ion in NDM-1. However, the results obtained were not the same as expected. It becomes more interesting to study the exact role of the H120 residue in NDM-1.

## **Chapter 3. Beta-Lactamase Activity**

### **Assays with Different Antibiotics**

### 3.1. Introduction

Although the results from chapter 2 showed that the Zn1 ion remained in the active-site of NDM-1 after the H120 mutations, it is still interesting to test the hydrolytic activities of the mutants. As shown in Figure 3.1, the H120 residue is hidden inside the protein and isolated from the antibiotic substrate by the Zn1 ion. There should be neither direct interaction nor reaction between H120 and the antibiotic substrate. Since the Zn1 ion remained after the mutations, the activities of the NDM-1 mutants are expected to be maintained similarly to the WT.

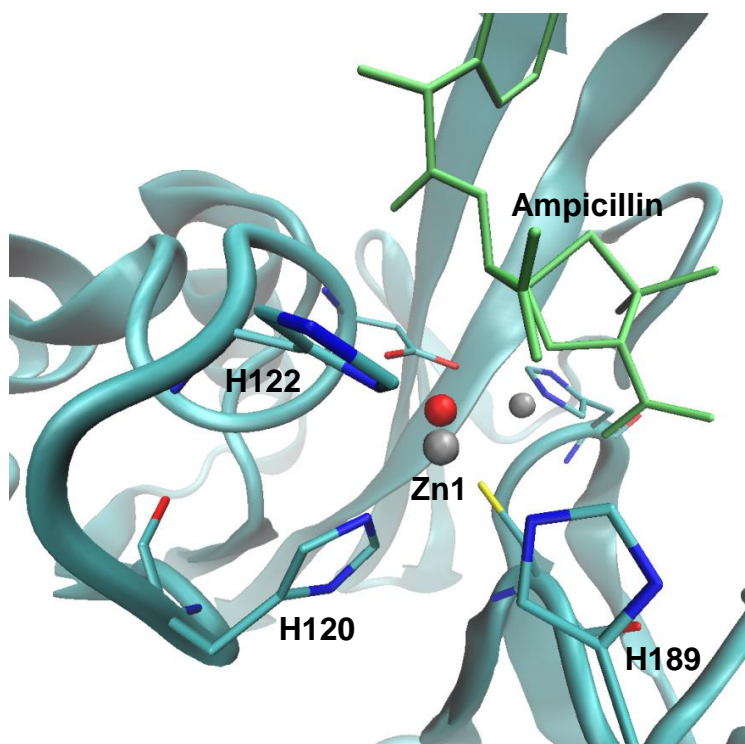


Figure 3.1 The crystal structure of NDM-1 WT binding with Ampicillin (PDB ID: 3Q6X). The H120 residue is labeled and it is isolated from the Ampicillin by the Zn1 ion. Hydroxide ion (red ball), zinc ion (grey balls), NDM-1 (cyan) and Ampicillin (green).



As NDM-1 has a broad range of target spectrum, different types of beta-lactam antibiotics will be tested for the hydrolytic activities. Two commonly known antibiotics from each type will be tested, including ampicillin and penicillin G (penicillins), cefotaxime and ceftazidime (cephalosporins), imipenem and meropenem (carbapenems). Figure 3.2 shows the scheme of the hydrolytic activity assay.<sup>134</sup> Unlike most activity assays which are measuring the amount of product formation, this hydrolytic activity assay is measuring the amount of substrate reduction during the reaction. The beta-lactam ring of each beta-lactam antibiotics absorbs UV light at a specific wavelength. When the beta-lactam ring is hydrolyzed, the product changes in its UV-Vis absorption spectrum. Therefore, by measuring the decrease in UV absorption, the initial rate of the hydrolysis reaction can be determined.

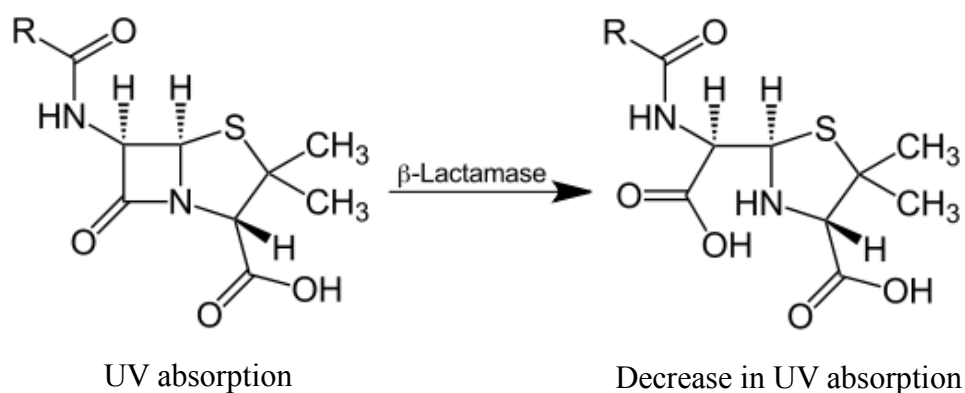


Figure 3.2 The beta-lactam ring changes in UV absorption after being hydrolyzed. The wavelength of UV absorption is different depending on the beta-lactam antibiotic.

The kinetic parameters ( $V_{\max}$ ,  $k_{\text{cat}}$  and  $K_m$ ) will be determined by the Michaelis-Menten plot (Figure 3.3a).<sup>135</sup> The initial rate of reaction ( $V$ ) will increase as the concentration of substrate increases. When the enzyme is saturated by substrates, the reaction rate will not increase anymore and this is the maximum rate of reaction ( $V_{\max}$ ) of the enzyme.

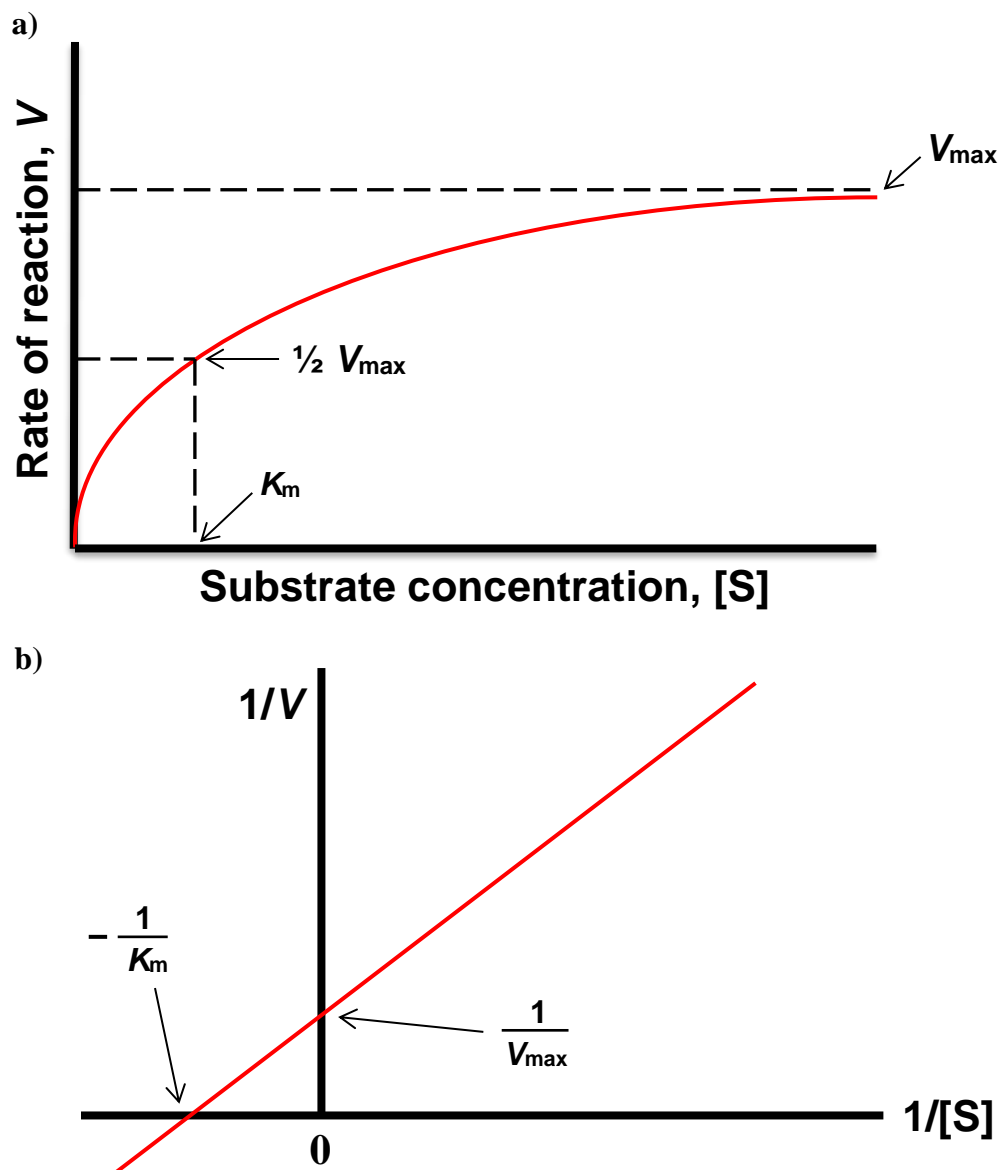


Figure 3.3 a) the Michaelis-Menten plot and b) the Lineweaver–Burk plot.

$K_m$  is the Michaelis constant of the reaction.  $K_m$  is related to the binding affinity of the enzyme to its substrate. When velocity is equal to half of the  $V_{max}$ ,  $K_m$  is equal to the substrate concentration,  $[S]$ . (Equation 3.1)<sup>135</sup>

$$\begin{aligned} \text{(Equation 3.1)} \quad V &= \frac{V_{max} [S]}{K_m + [S]} \\ \frac{V_{max}}{2} &= \frac{V_{max} [S]}{K_m + [S]} \\ V_{max} (K_m + [S]) &= 2(V_{max} [S]) \\ K_m + [S] &= 2[S] \\ K_m &= [S] \end{aligned}$$

The kinetic parameters can also be determined by the Lineweaver–Burk plots (Figure 3.3b). In comparison, the errors created by the Lineweaver–Burk plots are quite large, so the Michaelis-Menten plot is more accurate than the Lineweaver–Burk plot. In my studies, the kinetic parameters are mainly calculated by the Michaelis-Menten plots. However, since not every case can be fitted by the Michaelis-Menten plot, Lineweaver–Burk plots were also used (see Section 3.3.2).

$k_{cat}$  is a constant of the turnover number of substrate converts to product per unit time with a given concentration of enzyme,  $[E]_T$ .<sup>136</sup> As shown in Equation 3.2,  $k_{cat}$  is equal to  $V_{max}/[E]_T$ .

$$\text{(Equation 3.2)} \quad V_{max} = k_{cat} [E]_T$$

Finally, the catalytic efficiency ( $k_{\text{cat}}/K_{\text{m}}$ ) will be calculated. This value is the best value to compare the overall relative rate between the enzyme/substrate pairs.<sup>137</sup> The kinetic parameters of each NDM-1 mutants/antibiotics pairs will be measured and compared with the WT to determine the effects of the mutations.

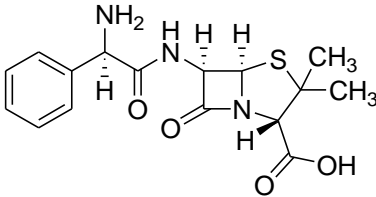
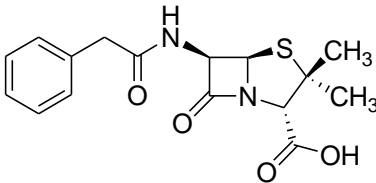
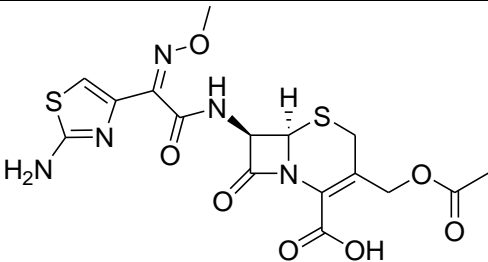
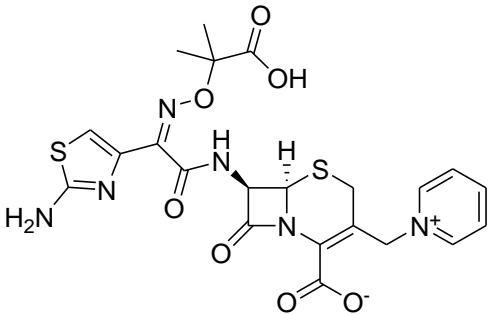
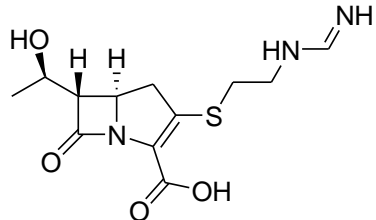
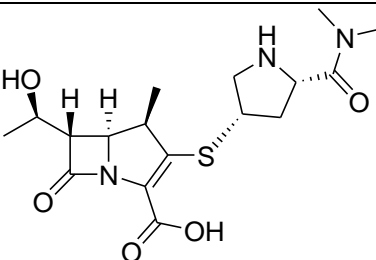
## 3.2. Experiment

### 3.2.1. Materials

#### 3.2.1.1. beta-Lactam Antibiotics

Since the classification of the beta-lactamases is highly related to their substrate specificity, the beta-lactam antibiotics from all different types will need to be tested. Table 3.1 listed the antibiotics which will be tested in the experiments and their relative extinction coefficients. Ampicillin, penicillin G, cefotaxime and ceftazidime were purchased from Sigma-Aldrich. Imipenem was purchased from TCI and the meropenem was purchased from USP.

Table 3.1 The list of testing compounds and their extinction coefficients<sup>138-139</sup>

Testing Compound		Molecular Structure	Extinction Coefficient ( $\Delta\epsilon$ , $M^{-1}cm^{-1}$ )
Penicillins	Ampicillin		$\Delta\epsilon_{235} = -900 M^{-1}cm^{-1}$
	Penicillin G		$\Delta\epsilon_{233} = -1140 M^{-1}cm^{-1}$
Cephalosporins	Cefotaxime		$\Delta\epsilon_{264} = -7250 M^{-1}cm^{-1}$
	Ceftazidime		$\Delta\epsilon_{265} = -10300 M^{-1}cm^{-1}$
Carbapenems	Imipenem		$\Delta\epsilon_{295} = -11500 M^{-1}cm^{-1}$
	Meropenem		$\Delta\epsilon_{297} = -10940 M^{-1}cm^{-1}$

### 3.2.2. Experimental Methods

#### 3.2.2.1. Optimization of Zn concentration condition for the beta-Lactamase Activity Assay

Since the zinc content of the NDM-1 enzymes is very important in our experiments, before determining the kinetic parameters, the zinc concentration to be used in the activity assays needed to be optimized in order to fully activate the NDM-1 enzymes (binding of two zinc ions in their active-site). The purified NDM-1 WT enzyme was used to measure the hydrolytic activities with ampicillin at different concentration of zinc. The activity assays were performed in 500  $\mu$ L assay buffer (15 mM sodium cacodylate, pH 6.5) with different concentration of  $\text{ZnSO}_4$  added at 25  $^{\circ}\text{C}$ . The concentrations of WT enzyme and ampicillin were fixed. A Cary 4000 UV-Vis spectrophotometer (Varian) was used to monitor the decreases in absorbance at 235 nm resulted by the hydrolysis of the beta-lactam ring of ampicillin. The absorbances were converted to concentrations by the Beer's law (Equation 3.3) and the initial rates of reaction (V) were calculated by the change in concentrations over time. The concentration of zinc required to maximize the NDM-1 activities were identified.

(Equation 3.3) 
$$A = \epsilon L c$$

Where, A = absorbance

$\epsilon$  = molar extinction coefficient ( $\text{M}^{-1}\text{cm}^{-1}$ )

L = path length (cm)

c = concentration (M)

### 3.2.2.2. beta-Lactamase Activity Assay – Kinetic Parameters

After optimized the concentration of zinc using for the activity assays, the NDM-1 WT and mutants were used to determine the kinetic parameters with different beta-lactam antibiotics. The measurements of activities were the same as method 3.2.2.1 mentioned except the zinc concentration of the assay buffer was fixed at 50  $\mu\text{M}$ . The concentrations of antibiotic substrates were increased until the rates reached the maximum rate of reaction ( $V_{\text{max}}$ ). The wavelengths of measurement for each antibiotic are shown in Table 3.1. The absorbance was converted to concentrations by the Beer's law (Equation 3.3) and the initial rate of reaction ( $V$ ) was calculated by the change in concentrations over time. Finally, the GraphPad Prism6 software was used to generate the Michaelis-Menten curves at the initial-rate conditions and the kinetic parameters ( $V_{\text{max}}$ ,  $k_{\text{cat}}$  and  $K_{\text{m}}$ ) were determined for each NDM-1/antibiotic pair. The kinetic parameters were presented as average values  $\pm$  errors based on three different sets of measurements.



### 3.3. Results and Discussions

#### 3.3.1. Optimization of Zn concentration condition for the Beta-lactamase activity assay

In order to make sure the NDM-1 enzymes have enough zinc ions binding in their active-sites to perform the activity assays, the zinc concentration condition was first tested. Figure 3.4 showed the hydrolytic activities of NDM-1 WT reacting with ampicillin under different zinc concentrations. As the results showed, any zinc concentration above 10  $\mu\text{M}$  will be enough for the NDM-1 enzyme to reach its maximum activity. For the following activity assays, zinc concentration of 50  $\mu\text{M}$  will be fixed. Since the concentration of NDM-1 mutants might not be the same in each assay, excess zinc in the buffer will be better for collecting consistent results.

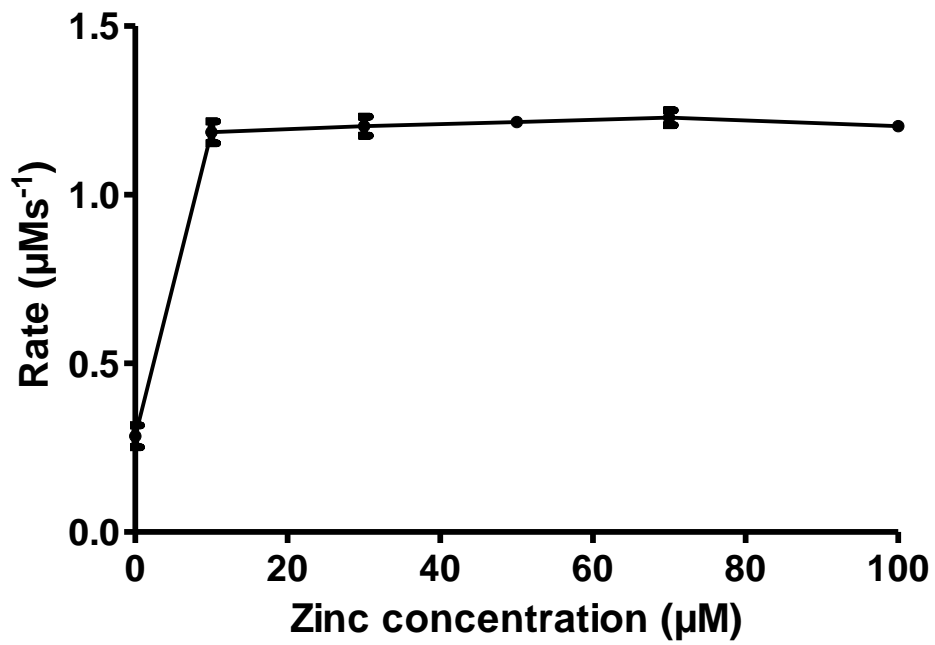


Figure 3.4 The reaction rate of NDM-1 WT (20 nM) vs. increasing concentration of zinc with fixed amount of Ampicillin (700  $\mu\text{M}$ ).

### 3.3.2. The Beta-lactamase activity assays of NDM-1 WT and mutants

Hydrolytic activities of NDM-1 WT and H120 mutants were tested with six different beta-lactam antibiotics (ampicillin, penicillin G, cefotaxime, ceftazidime, imipenem, and meropenem). Figure 3.5-3.8 shows the Michaelis-Menten curves of each NDM-1/antibiotic pair.

As shown in Figure 3.5-3.8, some of the mutants did not have very good Michaelis-Menten curves. For example, in Figure 3.6a, NDM-1 H120A vs. ampicillin, the activities of the NDM-1 H120A was too low when reacting with ampicillin, so the errors were huge. It is not possible to measure the absorbance very accurately when it is too low. Another problem of this activity assay is the way it measures the decrease of substrates over time. For example, Figure 3.6d, NDM-1 H120A vs. ceftazidime, the Michaelis-Menten curve obviously did not reach the  $V_{\max}$ , so the calculations of  $V_{\max}$  and  $K_m$  values might not be very accurate. However, it is not possible to measure higher concentration of ceftazidime either. Since the extinction coefficient is very high for the ceftazidime, the initial absorbance of ceftazidime (1 mM or above) was already over the detection range of the UV-Vis photospectrometer. The errors of measurement were huge and no accurate measurement can be done above 1 mM of ceftazidime. For this kind of mutant/antibiotic pairs, the Lineweaver-Burk plots were also generated (Figure 3.9). This included H120A vs

ceftazidime, H120A vs imipenem, H120N vs. ceftazidime, H120N vs. imipenem, H120N vs. meropenem and H120Q vs. ceftazidime (mainly when reacting with ceftazidime). In general, the kinetic parameters generated by the Lineweaver-Burk plot are less reliable than the Michaelis-Menten equation because the double reciprocal plot distorts the error structure of the data (Table 3.2). Nevertheless, when comparing the  $k_{cat}/K_m$  values, both the Lineweaver-Burk plots and Michaelis-Menten plots showed very similar  $k_{cat}/K_m$  values. It is also noted that most of the NDM-1/antibiotic pairs show very good fitting of Michaelis-Menten curves when the data reached the  $V_{max}$  value.

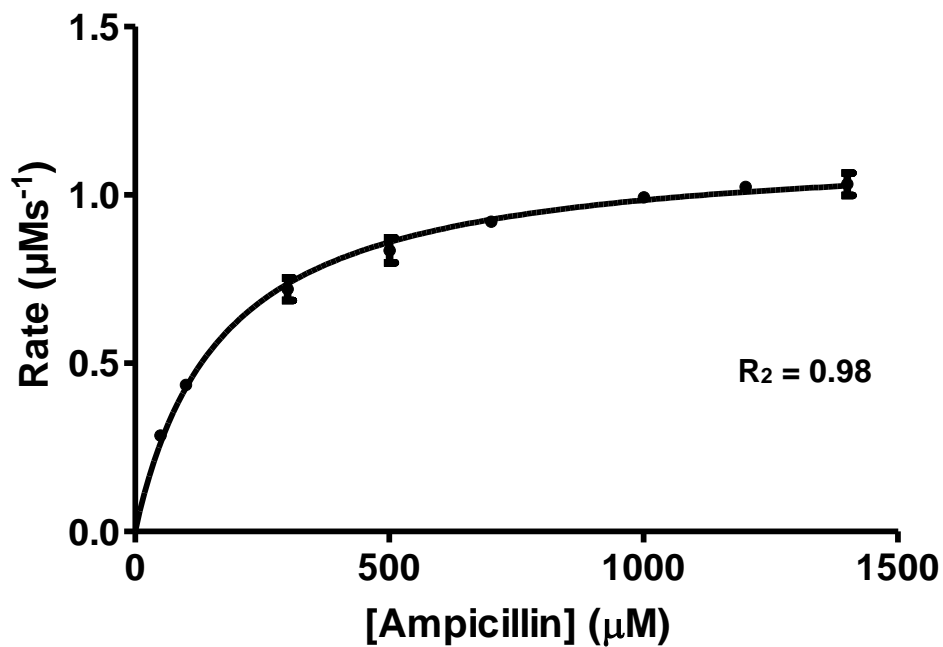
Figures 3.10-3.15 compare the activities between WT and mutants with different antibiotics. The reaction rates were normalized by the concentration of NDM-1 enzyme used in the experiment. As shown in the figures, all the mutants had a very significant reduction in reaction rate comparing to the WT NDM-1. Furthermore, Table 3.2 shows the calculated kinetic parameters for each NDM-1/antibiotic pair (all calculated by the Michaelis-Menten plots). The activities of the mutants were decreased by 6 to 810 folds comparing to the WT when hydrolyzing different antibiotic substrates. The mutants have almost lost all activities against penicillins (ampicillin and penicillin G), up to 679-810 folds of reduction. Especially for the H120N mutant, no hydrolytic activity was detected when testing with ampicillin (data not shown). On the other hand, the activities to the cephalosporins (cefotaxime and ceftazidime) were not reduced a lot comparing to the penicillins, only 19-51 folds of reduction. The decreases

in  $k_{\text{cat}}/K_m$  values are mainly due to the increases in  $K_m$  values, but the  $k_{\text{cat}}$  values are about the same as the WT. Interestingly, imipenem and meropenem are both carbapenems, but they show different activities with the mutants. For imipenem, all the mutants resulted in significant reduction in activities, up to 239 folds. However, for meropenem, there were only up to 18 folds of activity reductions. Similar to the cephalosporins, the decreases in  $k_{\text{cat}}/K_m$  values of mutants/meropenem pairs were mainly due to the increases in  $K_m$  values. These increases in  $K_m$  values suggest that the mutants bind weaker to the antibiotics. Moreover, for the H120A and H120N, the  $k_{\text{cat}}$  values are even higher than the WT when reacting with meropenem, which means these two mutants can have a higher maximum reaction rate than the WT after the mutations. Overall, the results showed that the H120 mutants had the least reductions in reaction rates when reacting with cefotaxime and meropenem.

Based on the results, the main reason of the reduction of activities is due to the increase of  $K_m$  values, which implies the weaker bindings of antibiotics. Since the Zn1 ion remains bound to the NDM-1 proteins, the reduction of hydrolytic activities must be related to the mutations at the Zn1 site. As the zinc ions are possibly involved in the binding of substrate, the H120 mutations might have changed the shape or shifted the position of the active site, so the antibiotics bind to the mutants with a weaker affinity which resulted in the increase of  $K_m$  values.

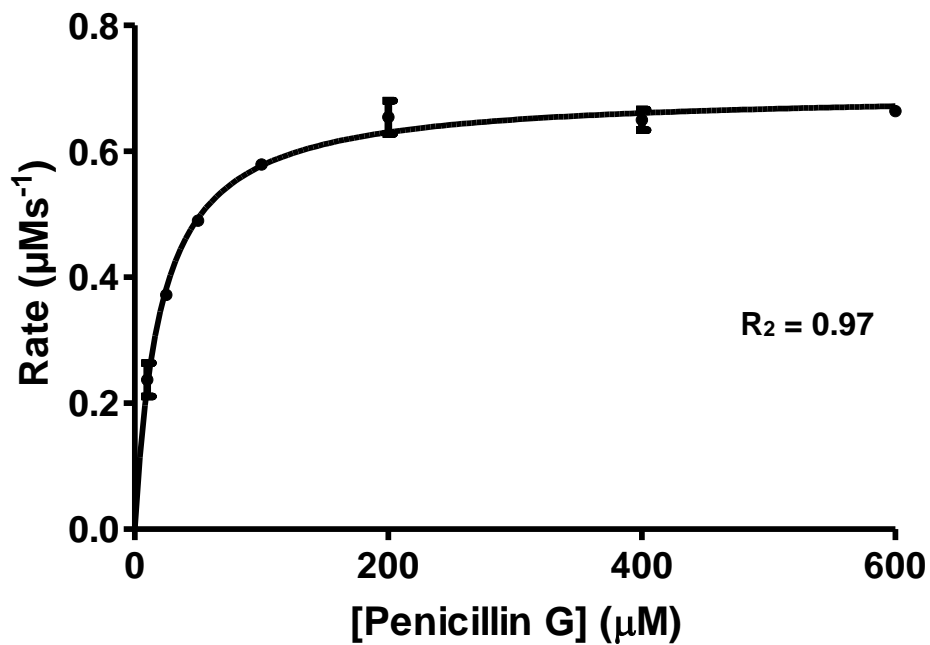
3.5a)

### WT vs Ampicillin



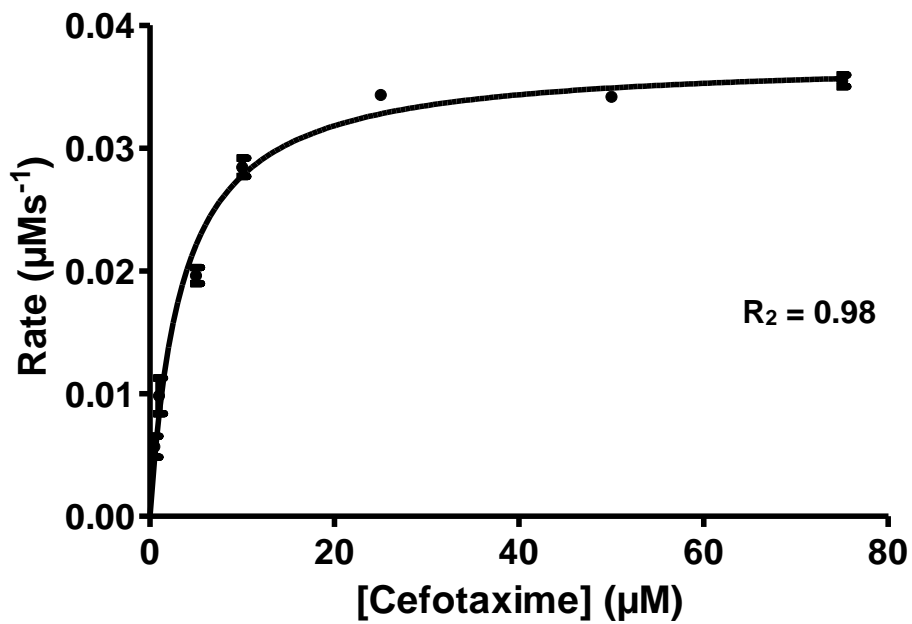
3.5b)

### WT vs Penicillin G



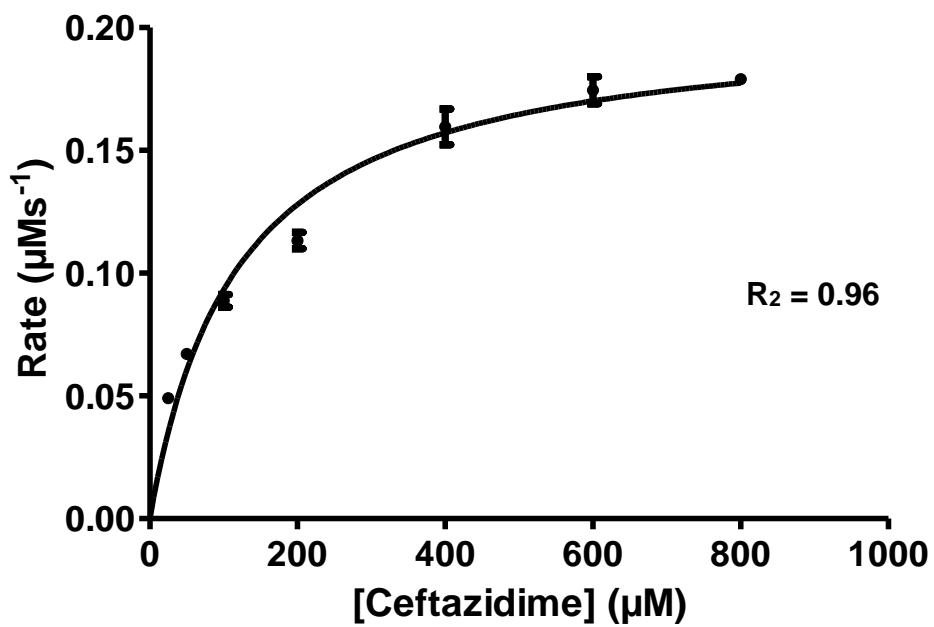
3.5c)

### WT vs Cefotaxime



3.5d)

### WT vs Ceftazidime



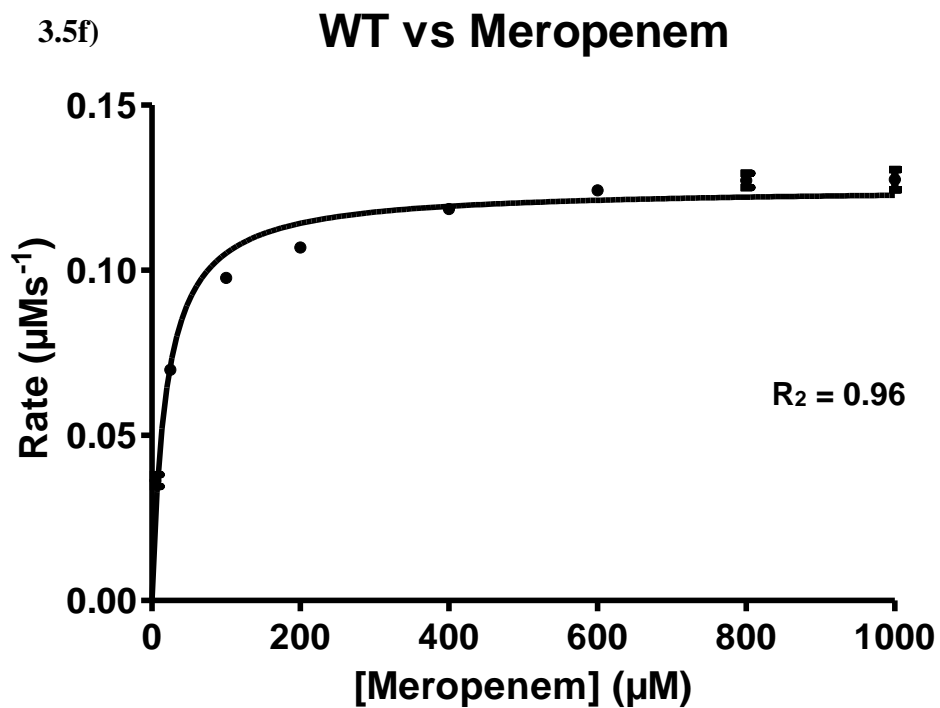
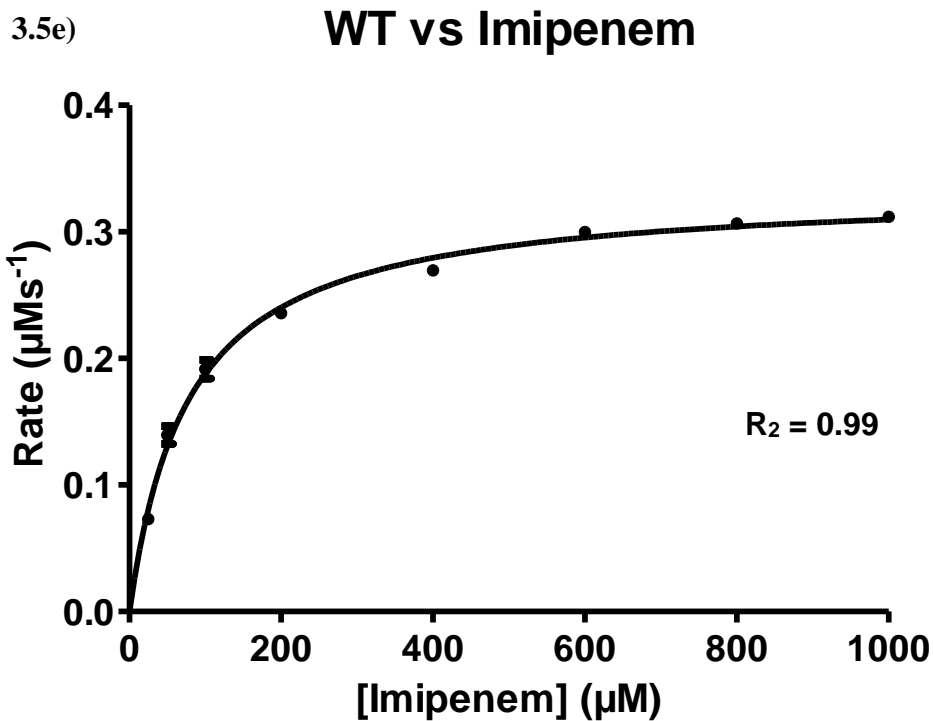
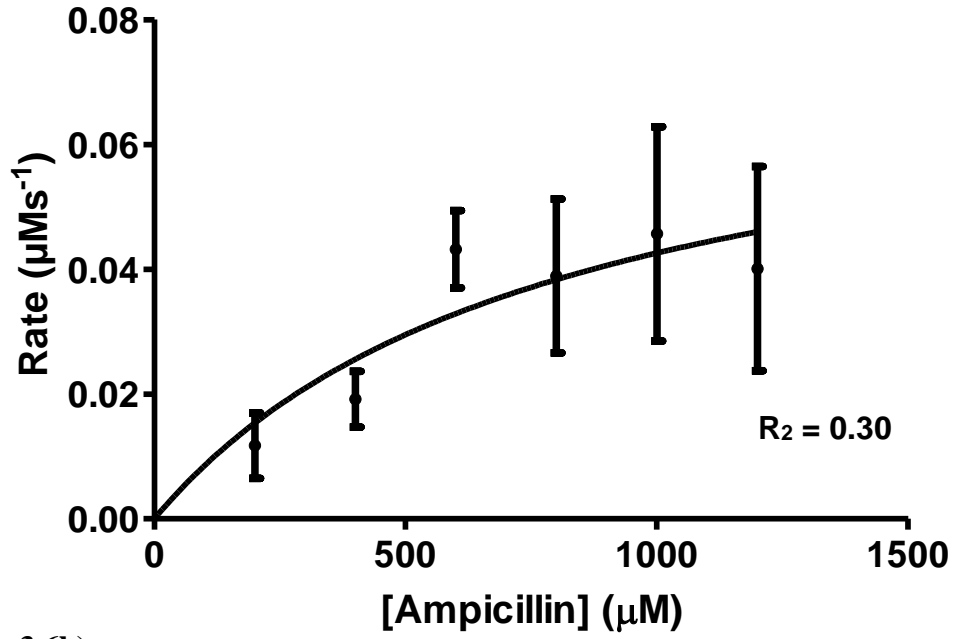


Figure 3.5 The reaction rate of NDM-1 WT vs. a) Ampicillin, b) Penicillin G, c) Cefotaxime, d) Ceftazidime, e) Imipenem, and f) Meropenem



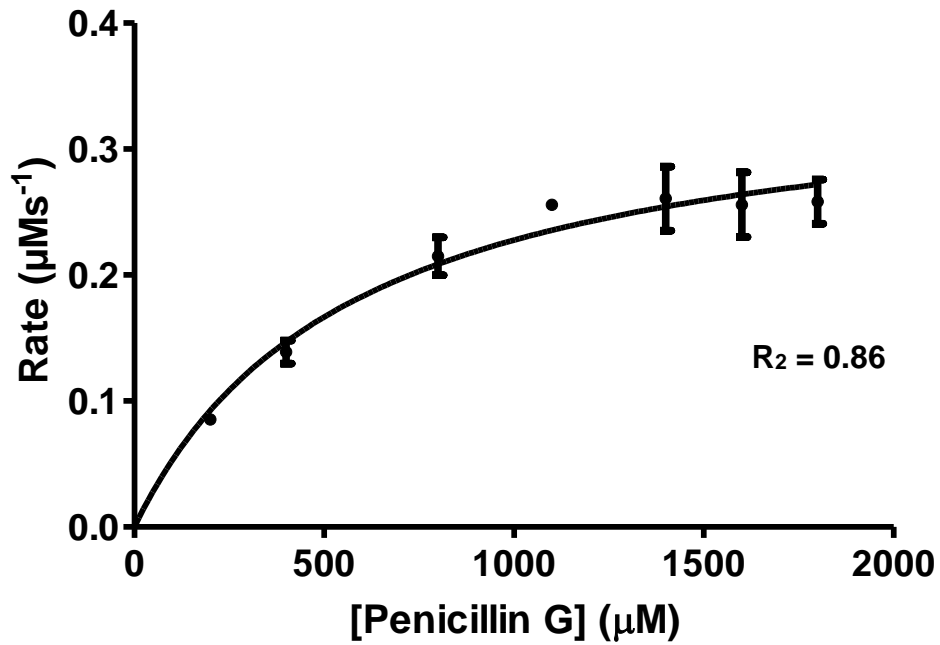
3.6a)

### H120A vs Ampicillin



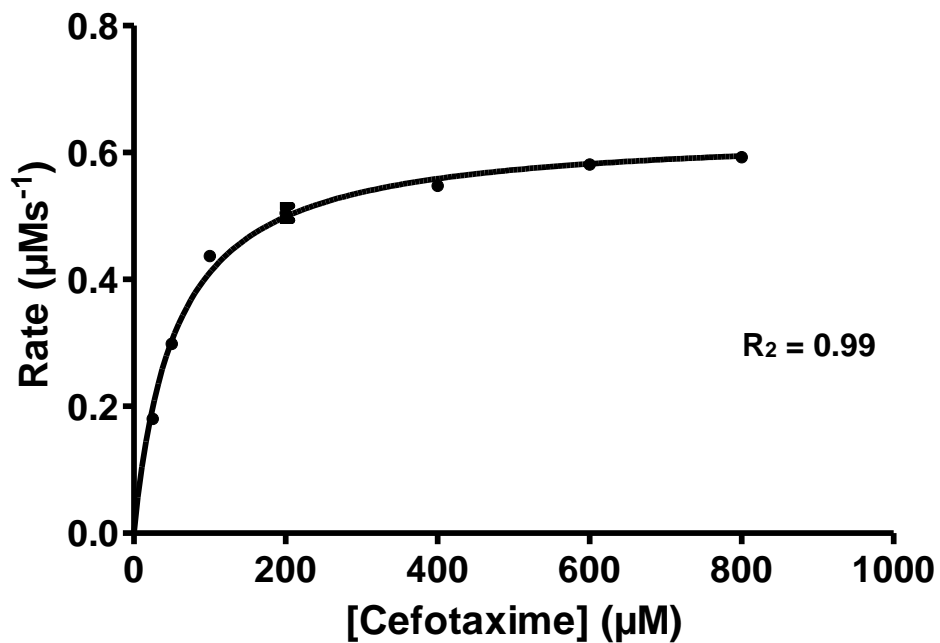
3.6b)

### H120A vs Penicillin G



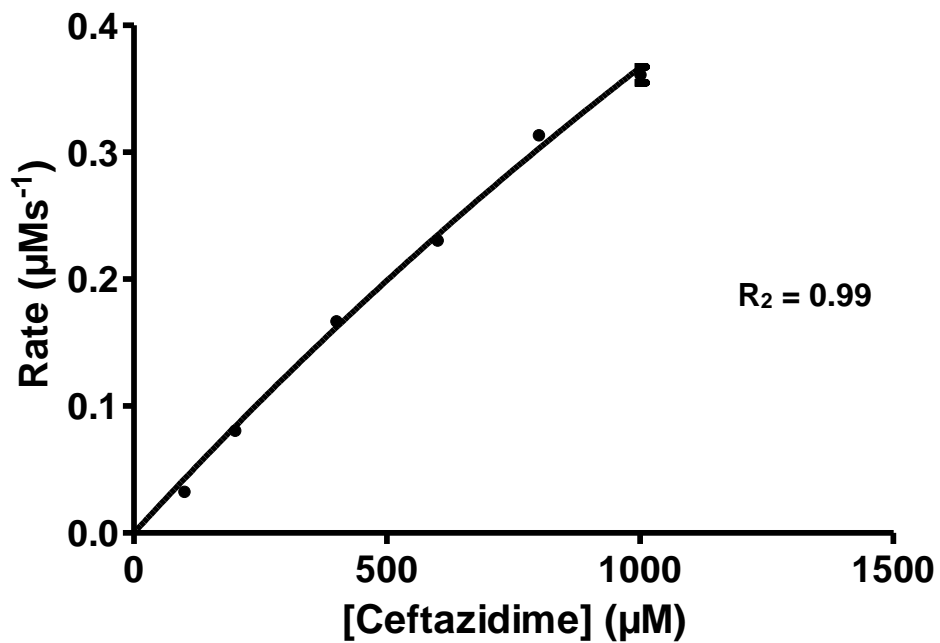
3.6c)

### H120A vs Cefotaxime



3.6d)

### H120A vs Ceftazidime



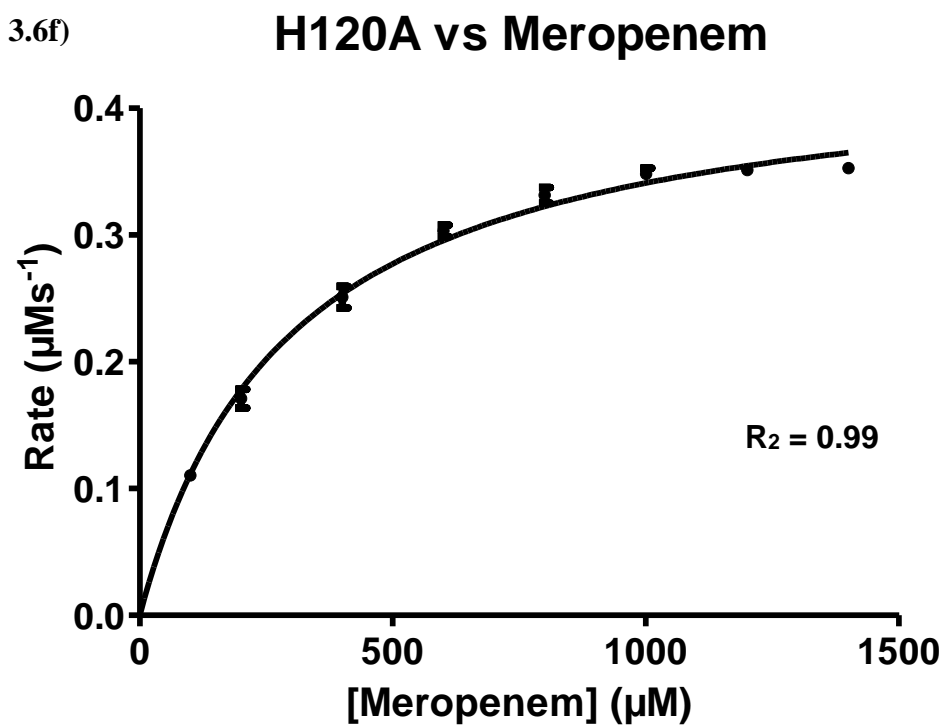
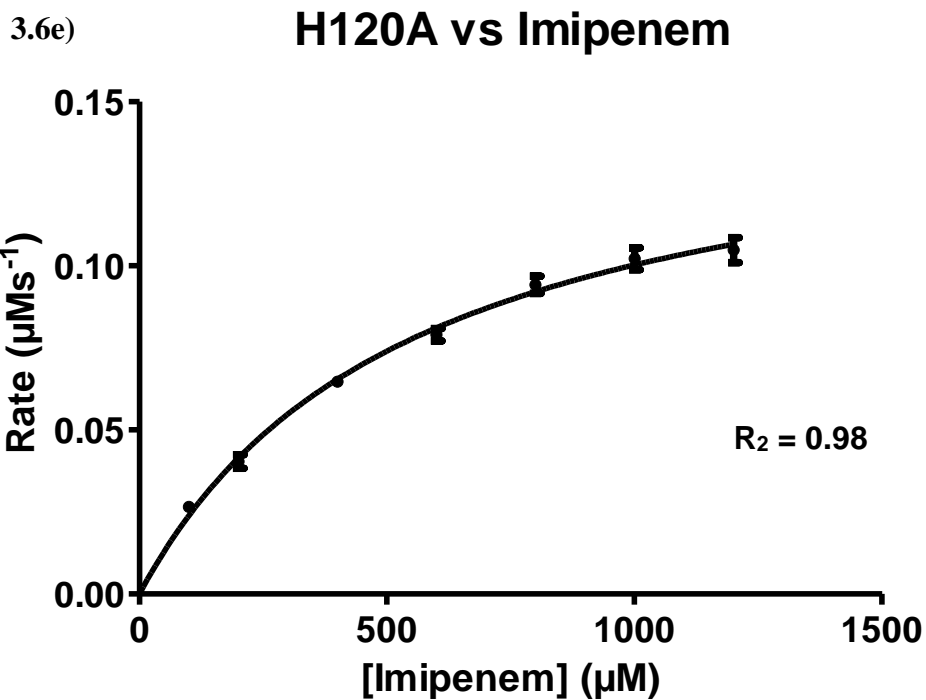
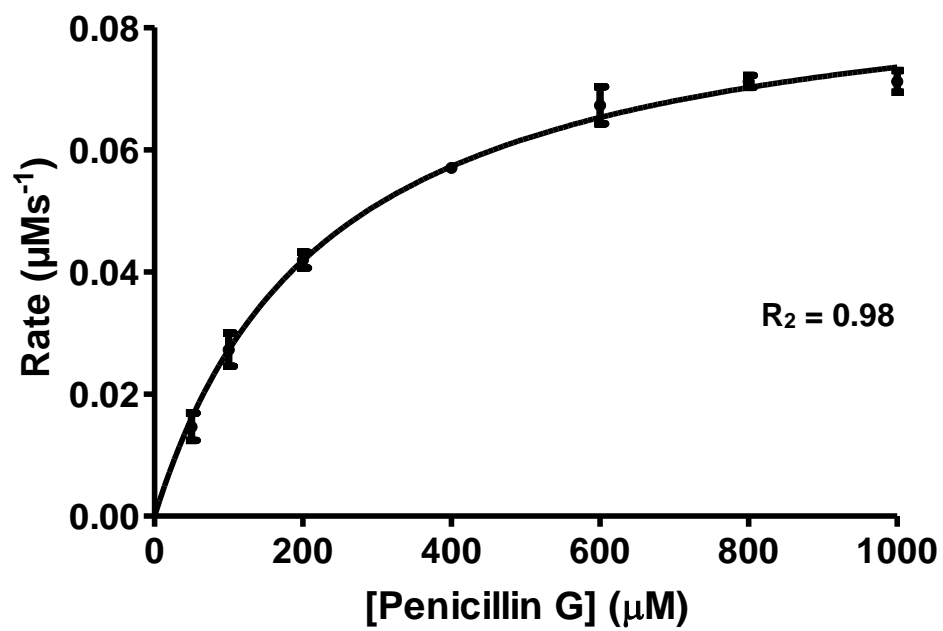


Figure 3.6 The reaction rate of NDM-1 H120A vs. a) Ampicillin, b) Penicillin G, c) Cefotaxime, d) Ceftazidime, e) Imipenem, and f) Meropenem

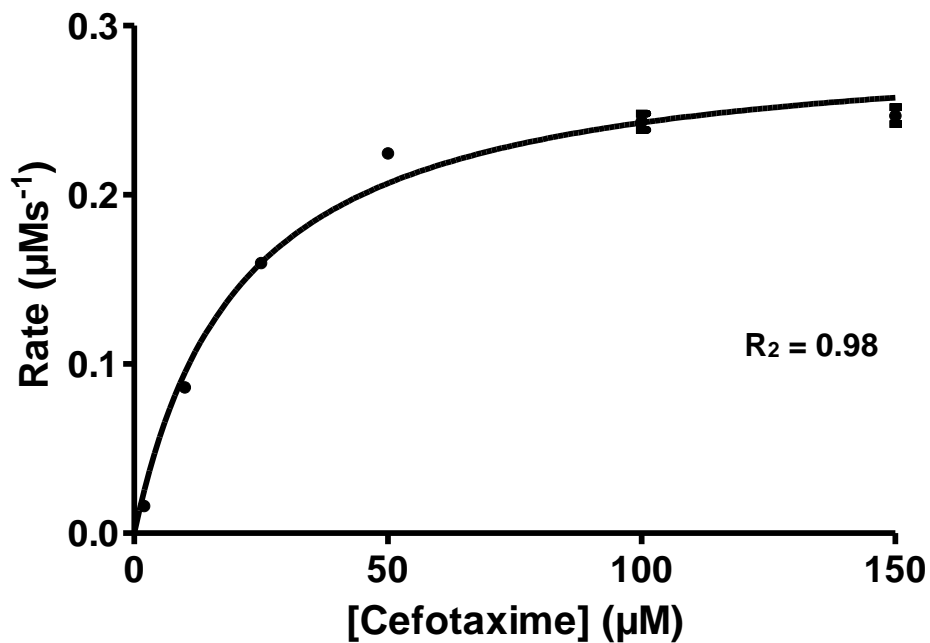
3.7a)

### H120N vs Penicillin G



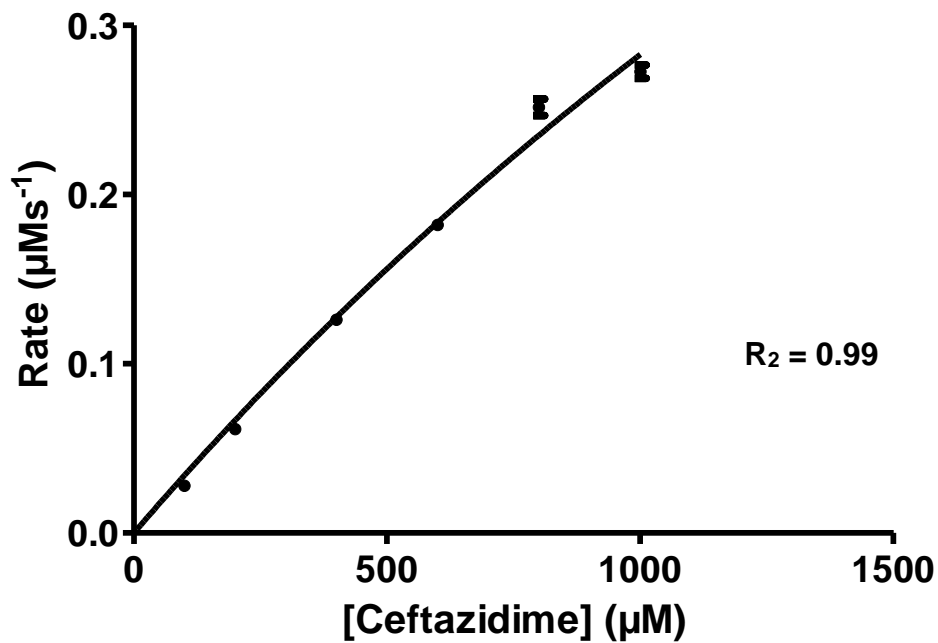
3.7b)

### H120N vs Cefotaxime



3.7c)

### H120N vs Ceftazidime



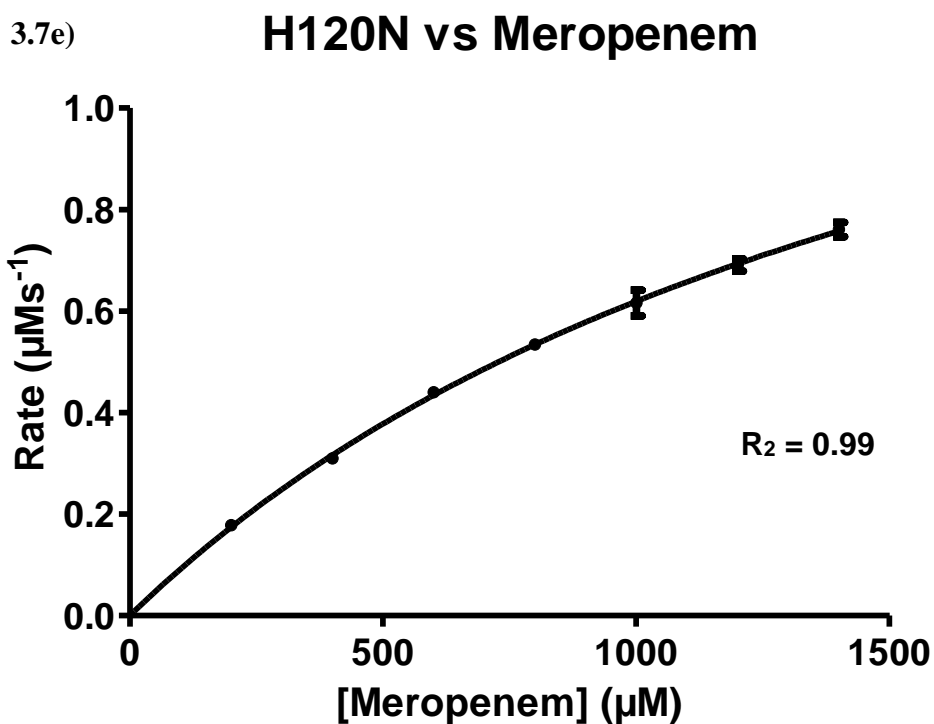
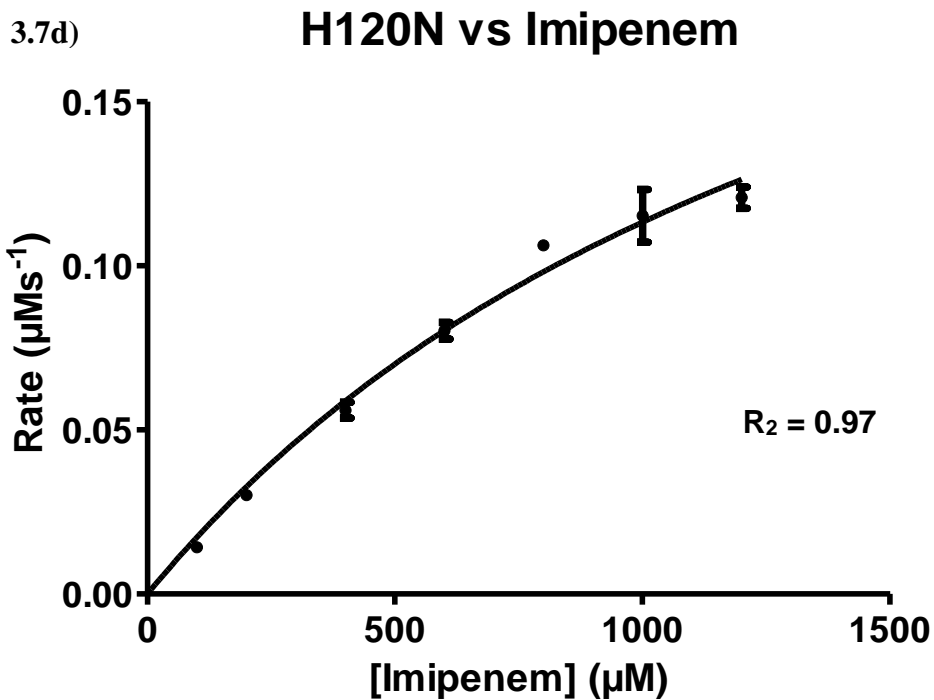
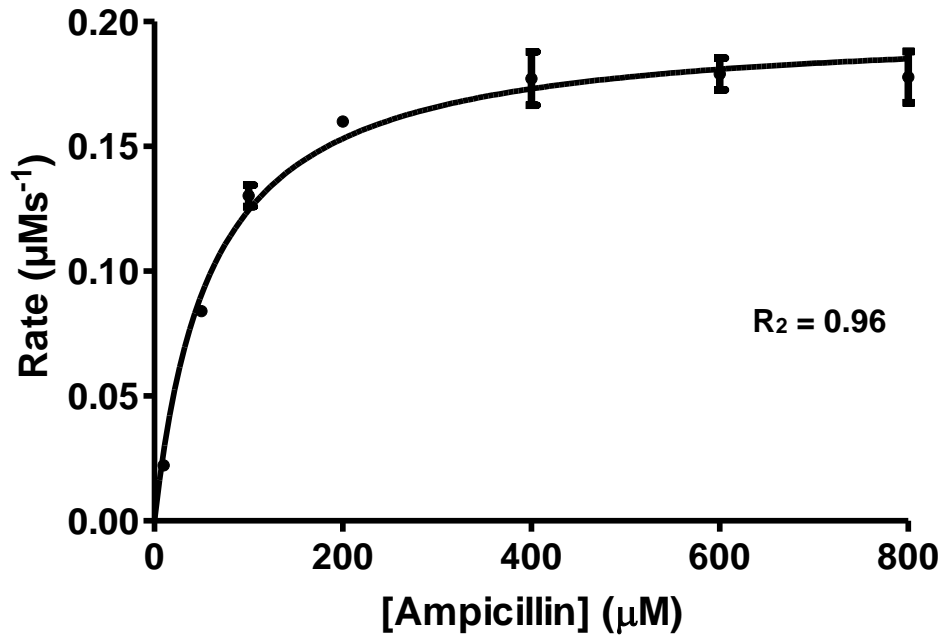


Figure 3.7 The reaction rate of NDM-1 H120N vs. a) Penicillin G, b) Cefotaxime, c) Ceftazidime, d) Imipenem, and e) Meropenem

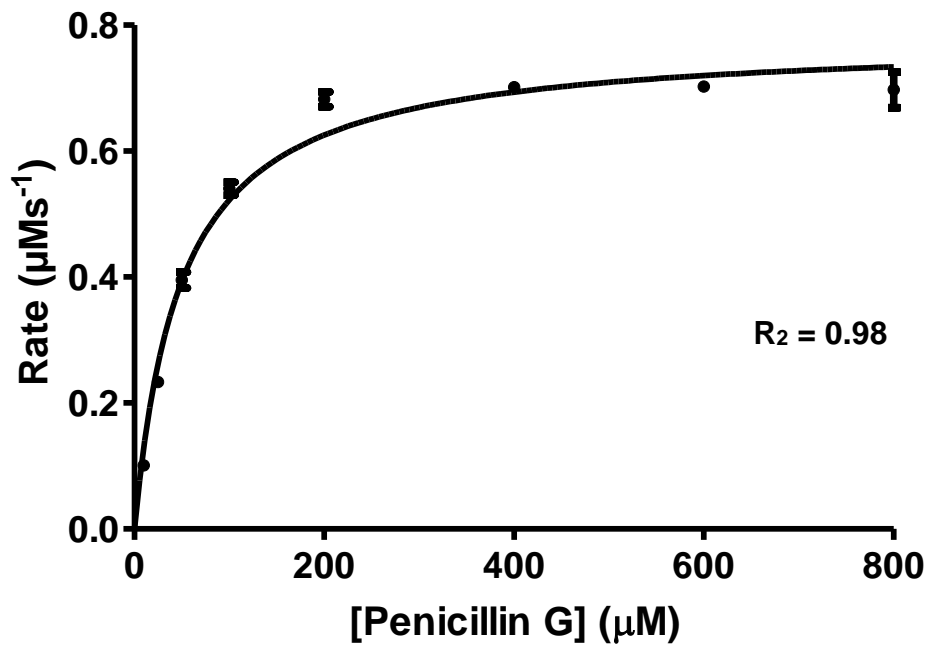
3.8a)

### H120Q vs Ampicillin



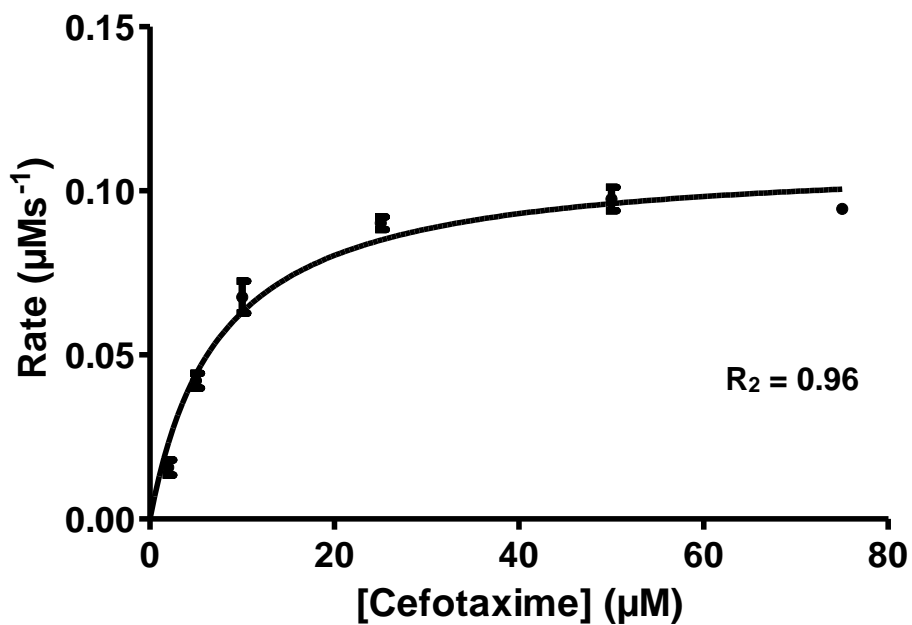
3.8b)

### H120Q vs Penicillin G



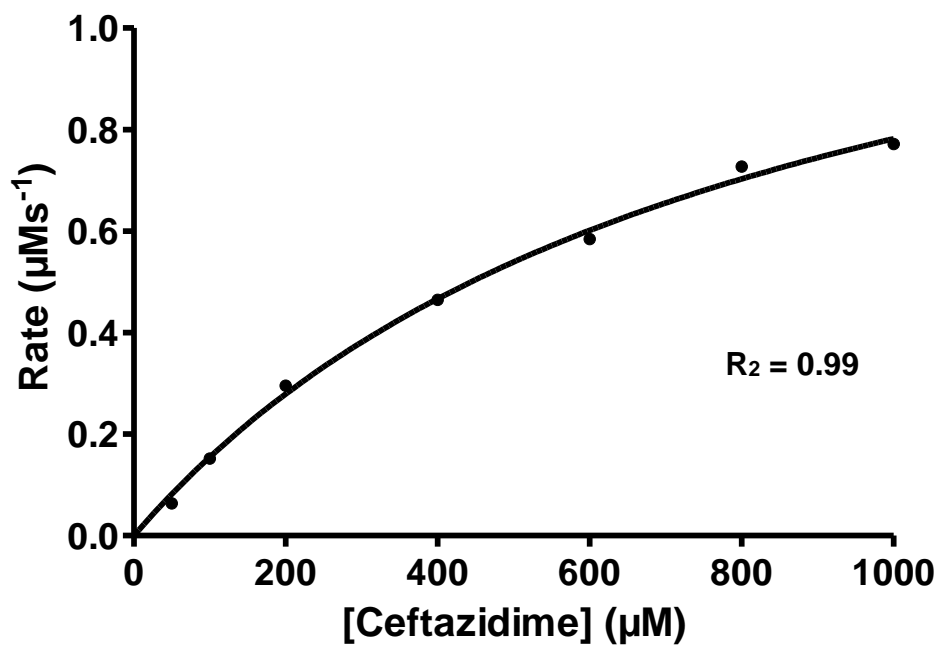
3.8c)

### H120Q vs Cefotaxime



3.8d)

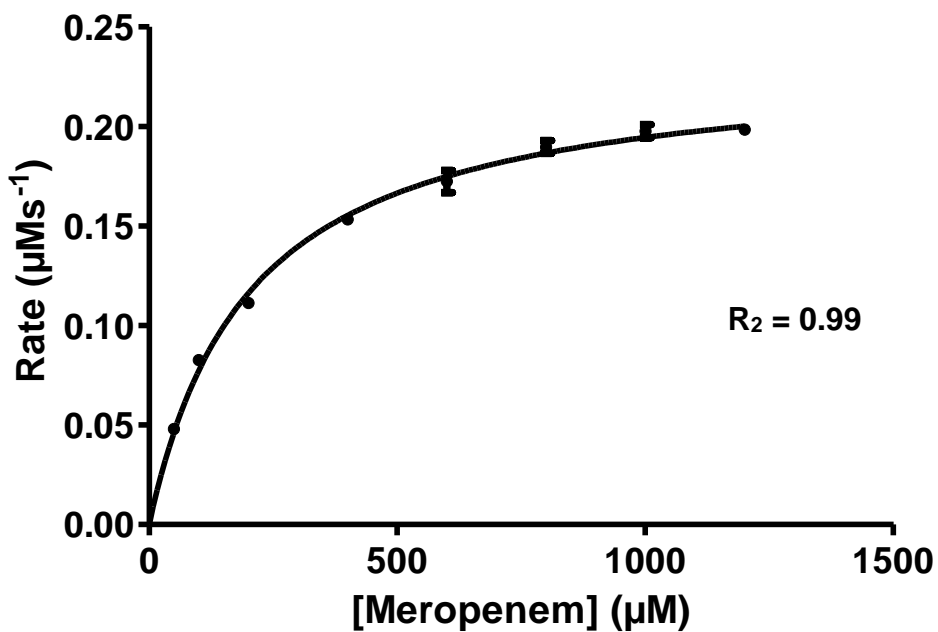
### H120Q vs Ceftazidime





3.8e)

### H120Q vs Meropenem



### H120Q vs Imipenem

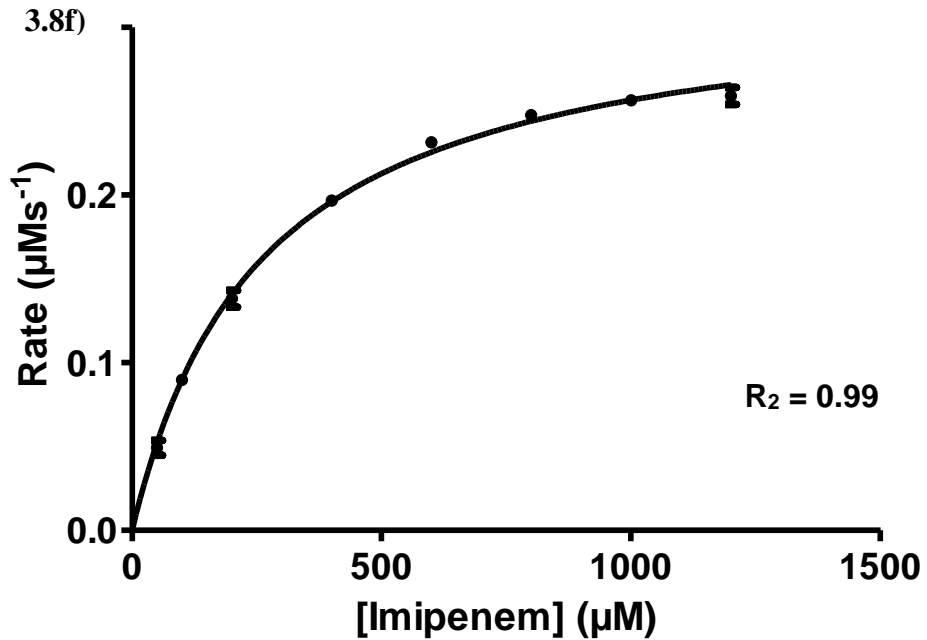
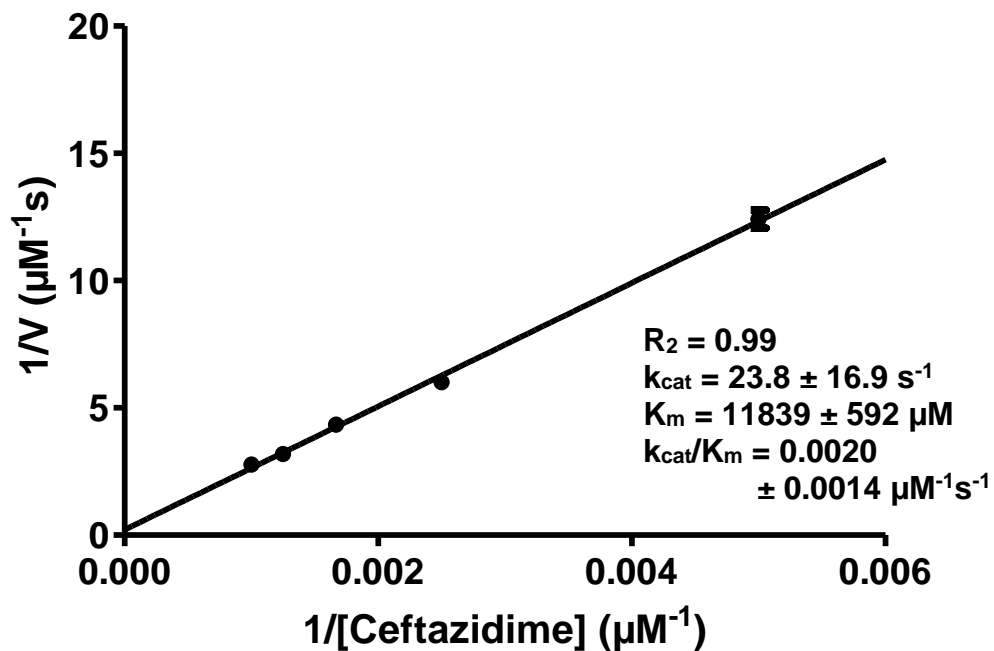


Figure 3.8 The reaction rate of NDM-1 H120Q vs. a) Ampicillin, b) Penicillin G, c) Cefotaxime, d) Ceftazidime, e) Imipenem, and f) Meropenem

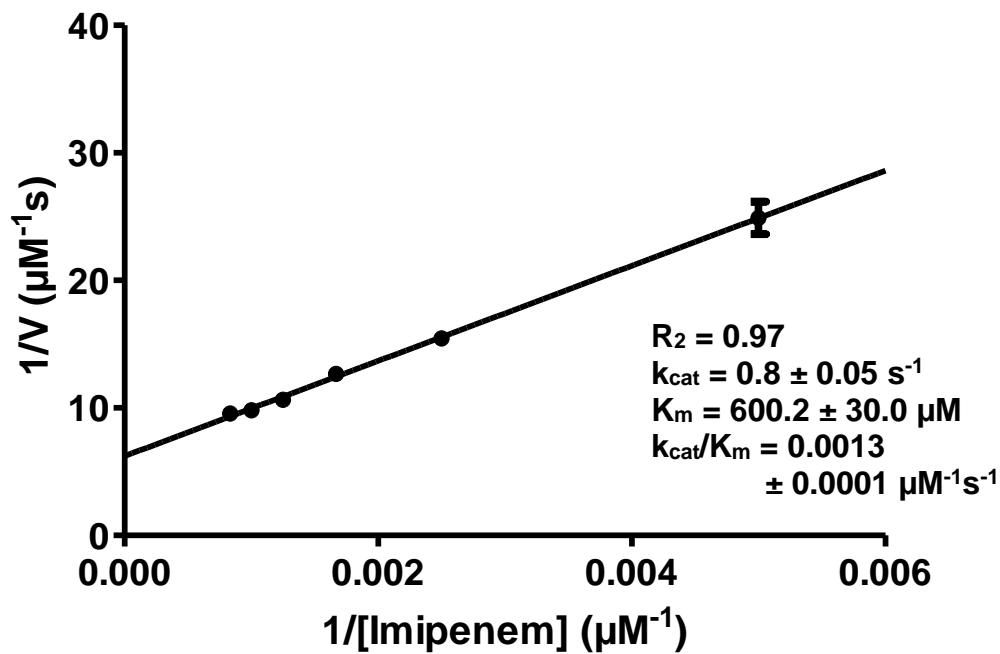
3.9a)

### H120A vs Ceftazidime



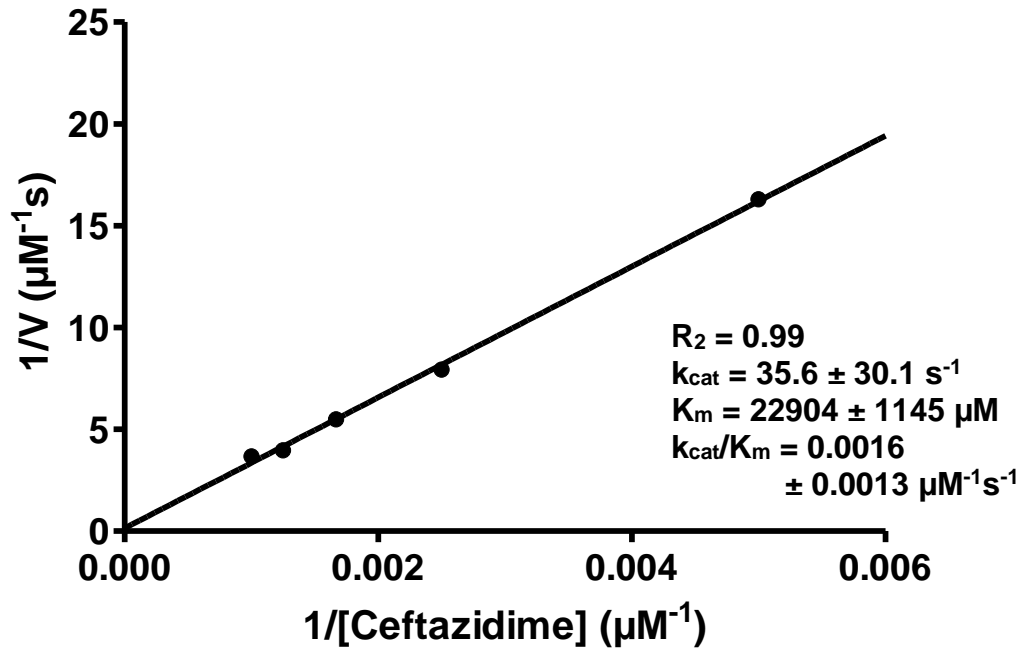
3.9b)

### H120A vs Imipenem



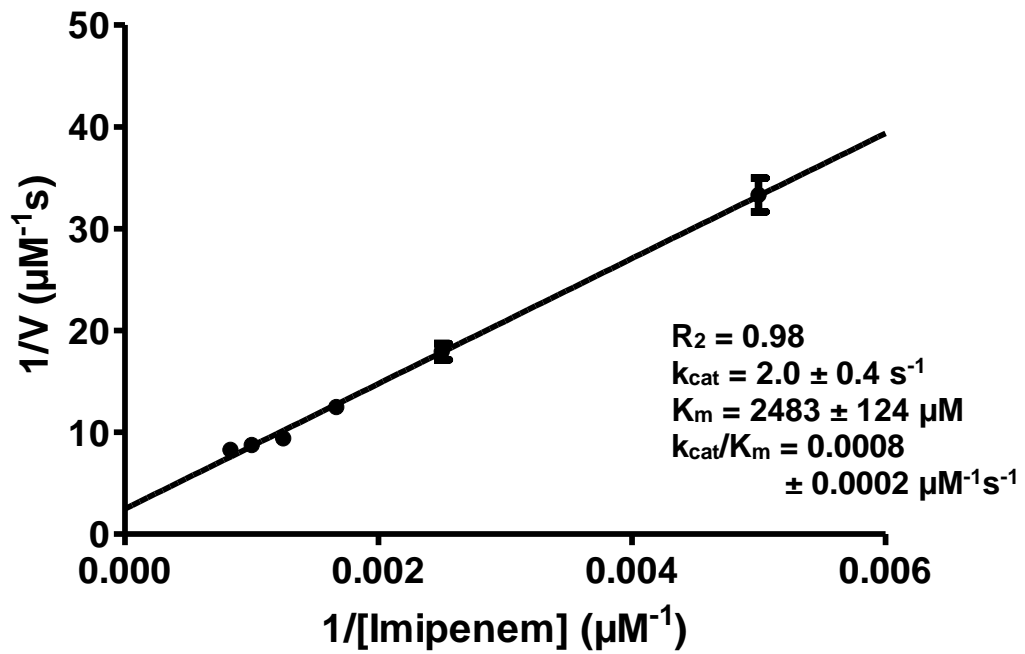
3.9c)

### H120N vs Cefprozil



3.9d)

### H120N vs Imipenem



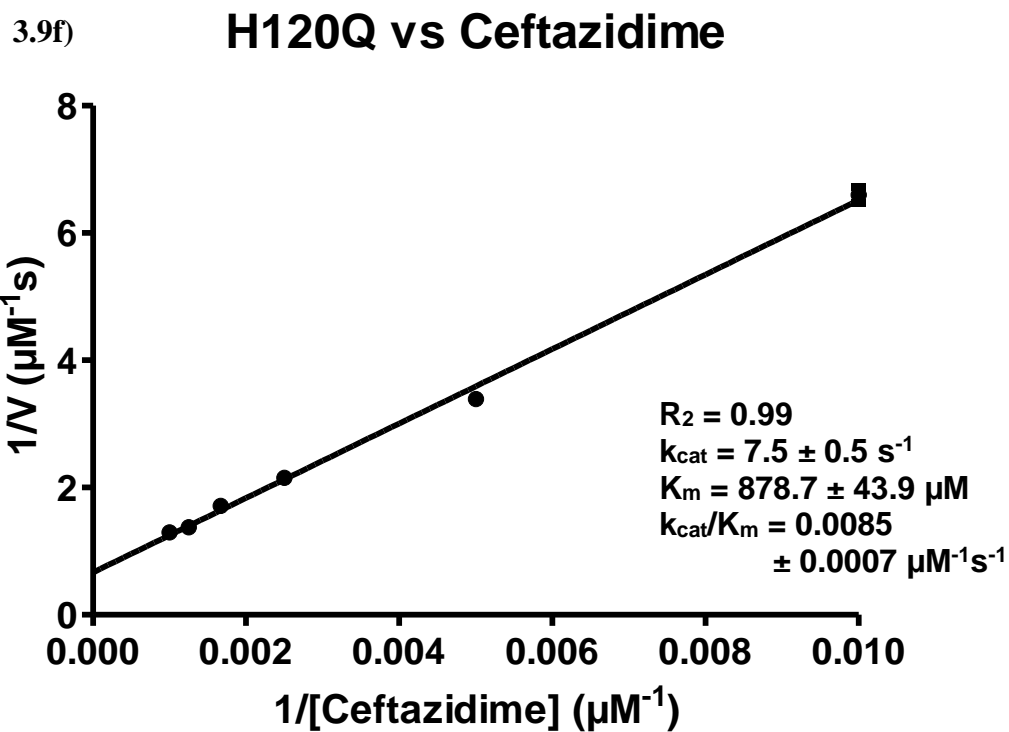
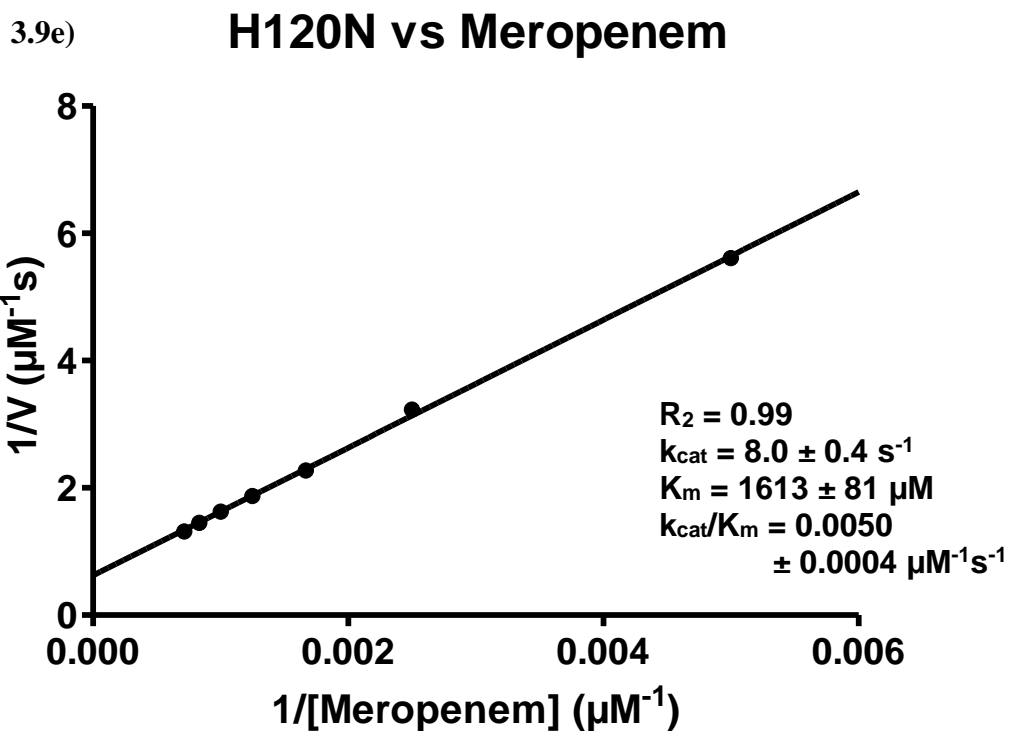


Figure 3.9 The lineweaver-burk plots of a) H120A vs Ceftazidime, b) H120A vs. Imipenem, c) H120N vs. Ceftazidime, d) H120N vs. Imipenem, e) H120N vs. Meropenem, and f) H120Q vs. Ceftazidime.

### NDM-1 mutants vs Ampicillin

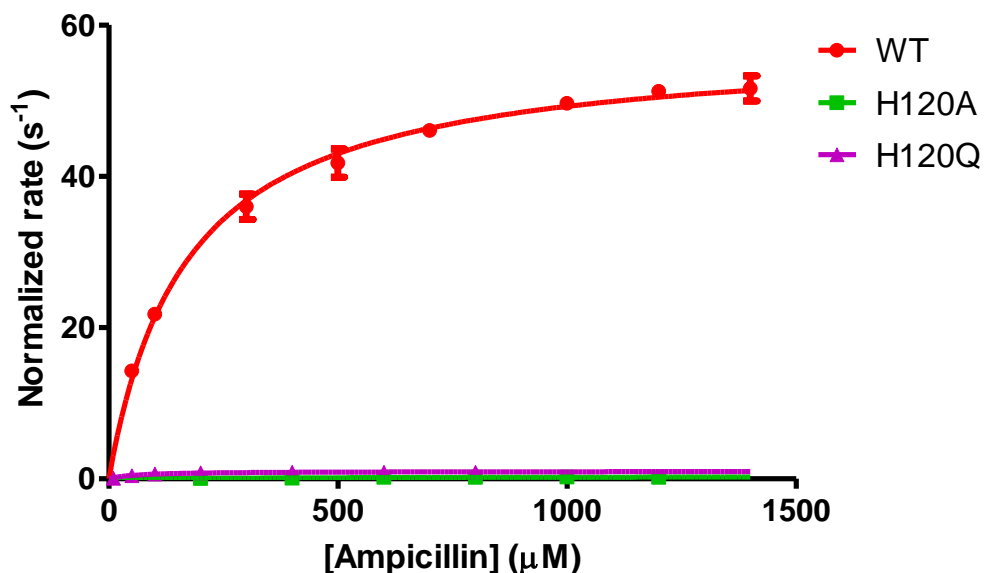


Figure 3.10 The comparison of reaction rates between all NDM-1 mutants vs. Ampicillin. The reaction rates were normalized with the enzyme concentration used in the experiment.

### NDM-1 mutants vs Penicillin G

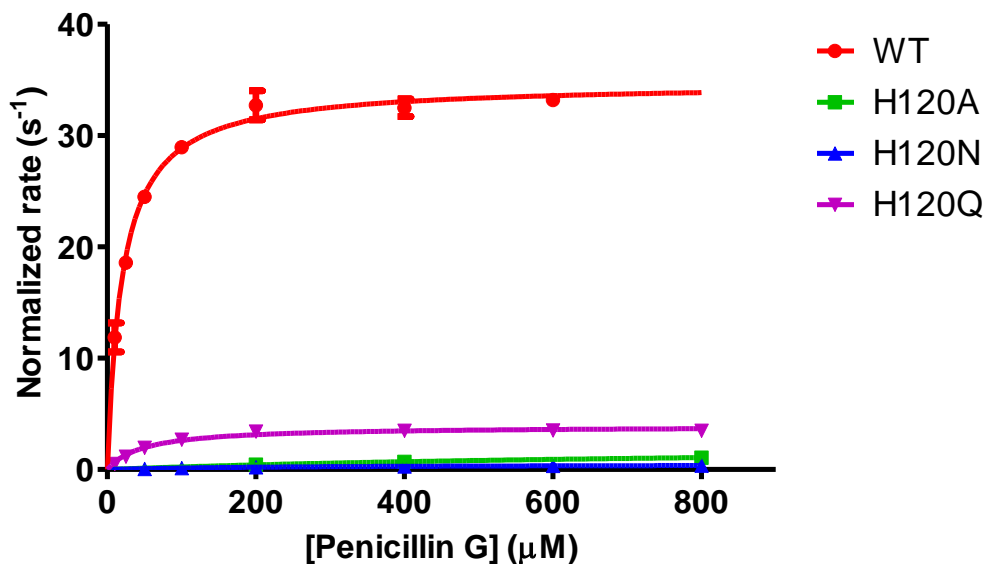


Figure 3.11 The comparison of reaction rates between all NDM-1 mutants vs. Penicillin G. The reaction rates were normalized with the enzyme concentration used in the experiment.

### NDM-1 mutants vs Cefotaxime

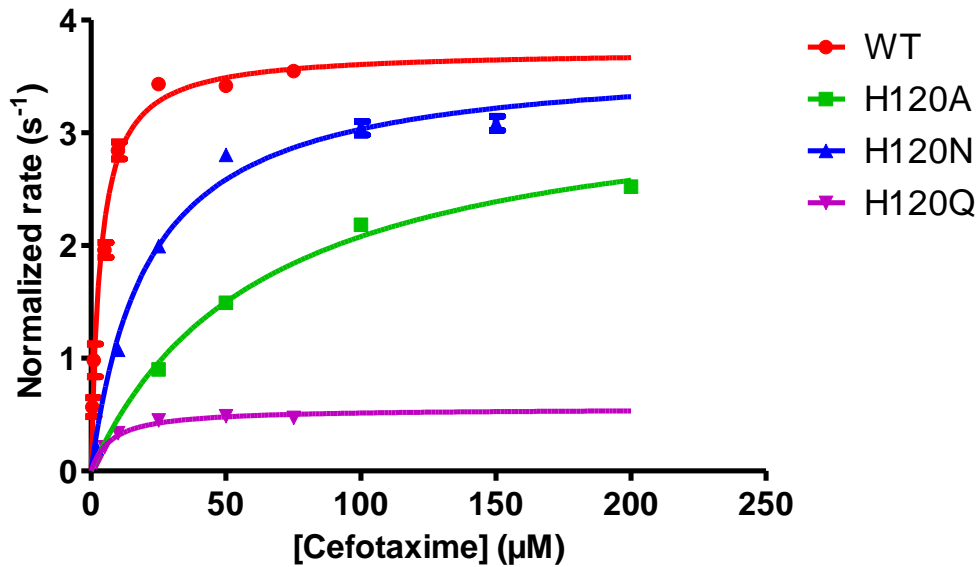


Figure 3.12 The comparison of reaction rates between all NDM-1 mutants vs. Cefotaxime. The reaction rates were normalized with the enzyme concentration used in the experiment.

### NDM-1 mutants vs Ceftazidime

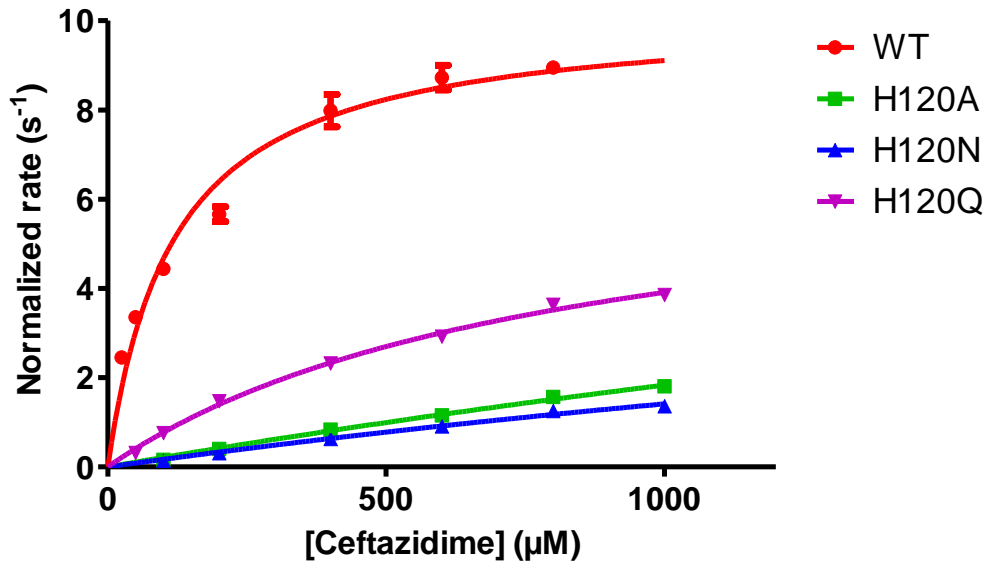


Figure 3.13 The comparison of reaction rates between all NDM-1 mutants vs. Ceftazidime. The reaction rates were normalized with the enzyme concentration used in the experiment.

### NDM-1 mutants vs Imipenem

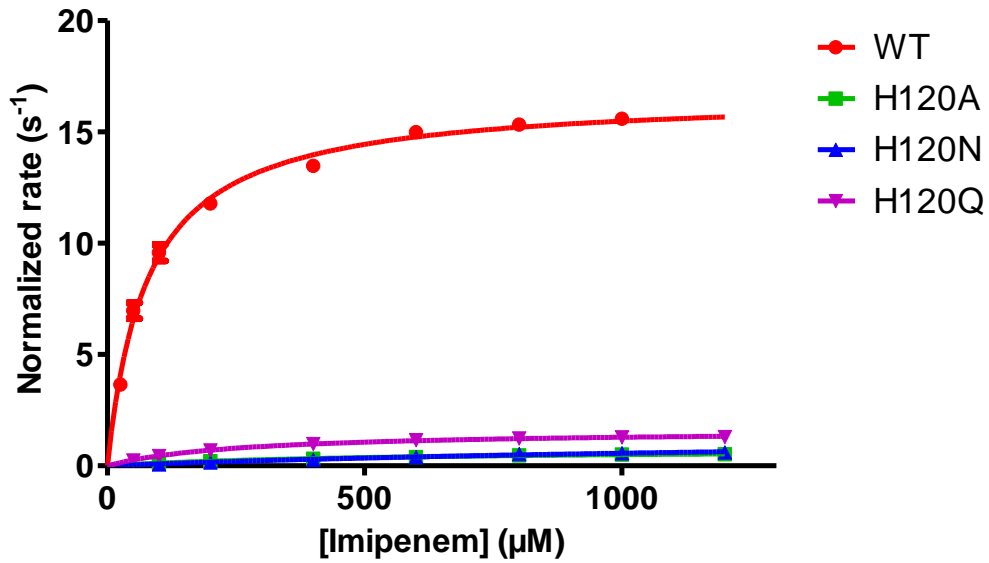


Figure 3.14 The comparison of reaction rates between all NDM-1 mutants vs. Imipenem. The reaction rates were normalized with the enzyme concentration used in the experiment.

### NDM-1 mutants vs Meropenem

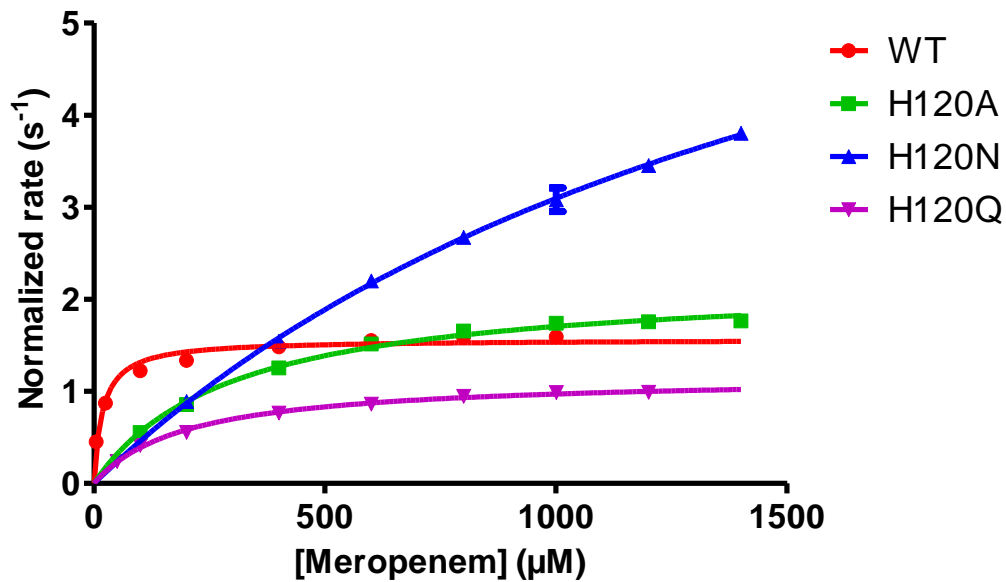


Figure 3.15 The comparison of reaction rates between all NDM-1 mutants vs. Meropenem. The reaction rates were normalized with the enzyme concentration used in the experiment.

Table 3.2 The kinetic parameters of NDM-1 mutants vs. different beta-lactam antibiotics (calculated by the Michaelis-Menten plots).

Ampicillin			
	$K_m$ ( $\mu\text{M}$ )	$k_{\text{cat}}$ ( $\text{s}^{-1}$ )	$k_{\text{cat}}/K_m$ ( $\mu\text{M}^{-1}\text{s}^{-1}$ )
WT	$169.7 \pm 11.9$	$57.6 \pm 1.0$	$0.3394 \pm 0.0245$
H120A	$798.9 \pm 1006$	$0.4 \pm 0.2$	$0.0005 \pm 0.0007$
H120N	No activity		
H120Q	$59.9 \pm 7.3$	$1.0 \pm 0.03$	$0.0167 \pm 0.0021$
Penicillin G			
	$K_m$ ( $\mu\text{M}$ )	$k_{\text{cat}}$ ( $\text{s}^{-1}$ )	$k_{\text{cat}}/K_m$ ( $\mu\text{M}^{-1}\text{s}^{-1}$ )
WT	$20.4 \pm 1.5$	$34.7 \pm 0.5$	$1.7010 \pm 0.1275$
H120A	$576.9 \pm 140$	$1.8 \pm 0.2$	$0.0031 \pm 0.0008$
H120N	$232.9 \pm 22.1$	$0.5 \pm 0.01$	$0.0021 \pm 0.0002$
H120Q	$49.0 \pm 4.2$	$3.9 \pm 0.08$	$0.0796 \pm 0.0070$
Cefotaxime			
	$K_m$ ( $\mu\text{M}$ )	$k_{\text{cat}}$ ( $\text{s}^{-1}$ )	$k_{\text{cat}}/K_m$ ( $\mu\text{M}^{-1}\text{s}^{-1}$ )
WT	$3.4 \pm 0.4$	$3.7 \pm 0.1$	$1.0882 \pm 0.1314$
H120A	$54.6 \pm 2.9$	$3.2 \pm 0.04$	$0.0586 \pm 0.0032$
H120N	$21.0 \pm 2.1$	$3.7 \pm 0.1$	$0.1762 \pm 0.0183$
H120Q	$7.5 \pm 1.0$	$0.6 \pm 0.02$	$0.0800 \pm 0.0110$
Ceftazidime			
	$K_m$ ( $\mu\text{M}$ )	$k_{\text{cat}}$ ( $\text{s}^{-1}$ )	$k_{\text{cat}}/K_m$ ( $\mu\text{M}^{-1}\text{s}^{-1}$ )
WT	$118.4 \pm 13.5$	$10.2 \pm 0.3$	$0.0861 \pm 0.0101$
H120A	$5388 \pm 1594$	$11.7 \pm 3.0$	$0.0022 \pm 0.0009$
H120N	$4300 \pm 1454$	$7.5 \pm 2.1$	$0.0017 \pm 0.0008$
H120Q	$818.3 \pm 63.3$	$7.1 \pm 0.3$	$0.0087 \pm 0.0008$
Imipenem			
	$K_m$ ( $\mu\text{M}$ )	$k_{\text{cat}}$ ( $\text{s}^{-1}$ )	$k_{\text{cat}}/K_m$ ( $\mu\text{M}^{-1}\text{s}^{-1}$ )
WT	$77.8 \pm 4.0$	$16.7 \pm 0.2$	$0.2147 \pm 0.0113$
H120A	$549.7 \pm 54.6$	$0.8 \pm 0.03$	$0.0015 \pm 0.0002$
H120N	$1608 \pm 360.6$	$1.5 \pm 0.2$	$0.0009 \pm 0.0002$
H120Q	$259.4 \pm 12.7$	$1.6 \pm 0.03$	$0.0062 \pm 0.0003$
Meropenem			
	$K_m$ ( $\mu\text{M}$ )	$k_{\text{cat}}$ ( $\text{s}^{-1}$ )	$k_{\text{cat}}/K_m$ ( $\mu\text{M}^{-1}\text{s}^{-1}$ )
WT	$18.9 \pm 2.1$	$1.6 \pm 0.02$	$0.0847 \pm 0.0095$
H120A	$297.6 \pm 18.7$	$2.2 \pm 0.04$	$0.0074 \pm 0.0005$
H120N	$1776 \pm 173.1$	$8.6 \pm 0.5$	$0.0048 \pm 0.0005$
H120Q	$200.7 \pm 11.1$	$1.2 \pm 0.02$	$0.0060 \pm 0.0003$



### 3.4. Concluding Remarks

In this chapter, hydrolytic activities of NDM-1 WT, H120A, H120N, and H120Q against six different beta-lactam antibiotics (ampicillin, penicillin G, cefotaxime, ceftazidime, imipenem, and meropenem) were measured. As shown in the results, all the NDM-1 mutants had significant decrease in activities against all types of antibiotics. Looking at the measured kinetic parameters, almost all the NDM-1 mutants had their  $K_m$  values increased significantly. However, about half of them had their  $k_{cat}$  remained the same as the NDM-1 WT. This might imply that the mutations at H120 position had weakened the binding affinity of NDM-1 to the antibiotic substrates, so that it reduced the overall activities of the enzyme. As the Zn1 ion remains bound to the NDM-1 mutants, the reduction in hydrolytic activities of the mutants must be related to factors other than the presence of  $Zn^{2+}$ . Since the residue H120 does not have any direct interaction with the antibiotic substrates, it is not known how the mutations at this position can affect the hydrolysis reaction of NDM-1. In the next chapter, Molecular Dynamics (MD) simulation will be used to find out more about this reduction in activities.

# **Chapter 4. Molecular Dynamics**

## **Simulations**

## 4.1. Introduction

Based on the results collected from the two previous chapters, the NDM-1 mutants have the Zn1 ion remained in the active-site, but the hydrolytic activities were greatly reduced. Since residue H120 cannot directly interact with the substrates, there should be some position changes to the Zn1 ion due to the mutations. In this chapter, Molecular Dynamics will be used to simulate the movement of the Zn1 ion after the mutations in order to understand what is happening in the active-site.

Molecular Dynamics (MD) is a computational simulation system using Newton's equations of motion to calculate and predict the trajectory of molecule dynamics over a period of time.<sup>140</sup> The use of MD simulations in biological molecule was started three decades ago.<sup>141-142</sup> With the improvement of computer power and development in calculation, MD simulation becomes an important technique to study the dynamics of biological molecules.<sup>143</sup> In MD simulations, the potential energy of the system is described by the interaction functions called Molecular Mechanics (MM) force field<sup>140</sup>:

$$V_{MM} = \sum_i^{N_{\text{bonds}}} V_i^{\text{bond}} + \sum_j^{N_{\text{angles}}} V_j + \sum_l^{N_{\text{torsions}}} V_l^{\text{torsion}} \\ + \sum_i^{N_{\text{MM}}} \sum_{j>i}^{N_{\text{MM}}} V_{ij}^{\text{Coul}} + \sum_i^{N_{\text{MM}}} \sum_{j>i}^{N_{\text{MM}}} V_{ij}^{\text{LJ}}$$

This equation includes the number of atoms (N) and the functions to model the bonds, angles and torsions between atoms. Other than that, the electrostatic interaction between the partial charged atoms is described by the Coulomb's law (Coul) and the Van der Waals interactions are described by the Lennard-Jones potential (LJ). However, electron movements are not described in the MM force field. Therefore, MD simulations cannot simulate any process involving electronic rearrangement, including breaking and forming of covalent bonds. This kind of electronic rearrangement process requires Quantum Mechanical (QM) description to model it.<sup>144</sup> The best way of simulation will be applying QM to every atom in the system. Unfortunately, the requirement of computational power for the QM calculations is huge, and there is no such powerful computer being able to simulate a whole protein molecule for now. Nevertheless, the QM calculations can still guide to a more accurate MM force field, which can improve the accuracy of a MD simulation.<sup>145</sup>

My goal was to simulate the movement of Zn1 ion in the active-site of NDM-1, which does not involve any kind of covalent bond formation or breaking. Theoretically, there is no need to apply QM calculations to the models. However, the zinc ions in NDM-1 have two different coordination geometries, which the Zn1 ion is in tetrahedral coordination geometry and the Zn2 ion is in trigonal bipyramidal coordination geometry (Figure 4.1).<sup>146</sup> Most of the commonly use MM force fields are not well developed for metal ions simulations, especially for this kind of different coordination geometries case.

Therefore, QM will first be used to estimate the electron density at the two zinc ions and calculate the parameters for creating a new MM force field. Then the MD simulation will be running with the new MM force field and model the two zinc ions as two special partially charged atoms.<sup>145</sup> In this way the MD simulation will be much more accurate in our studies.

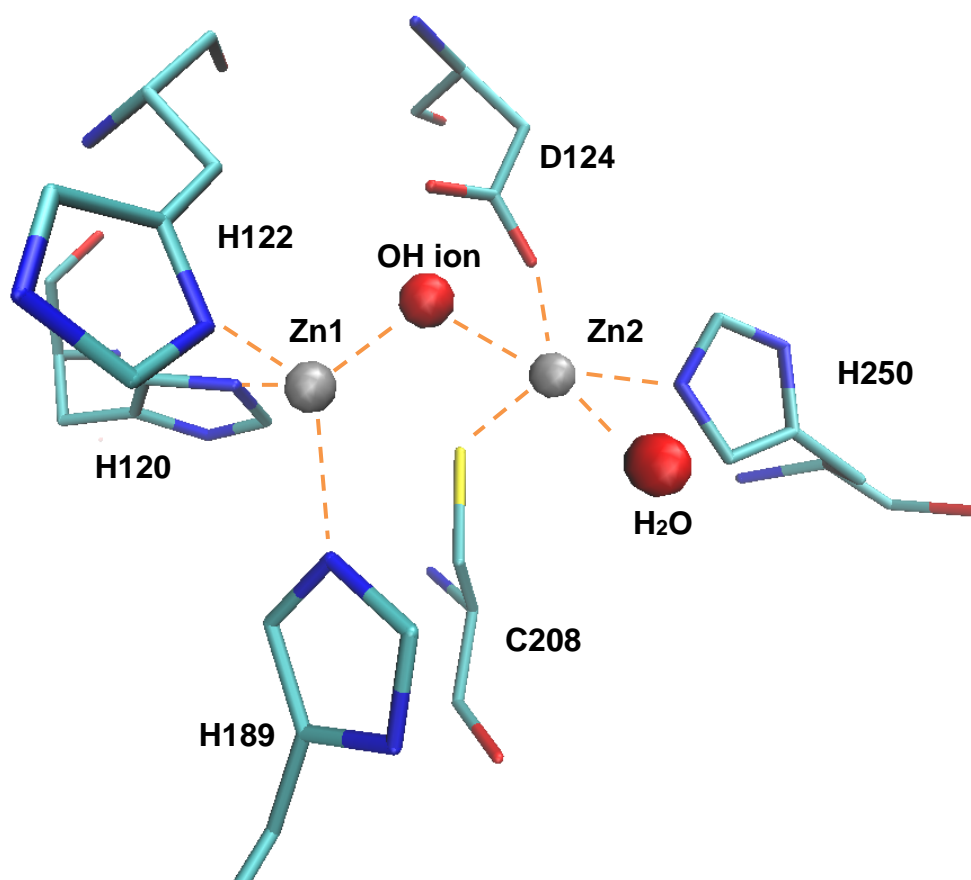


Figure 4.1 The coordination geometries of the two zinc ions of NDM-1 (PDB ID: 3SPU): tetrahedral coordination geometry for Zn1 and trigonal bipyramidal coordination geometry for Zn2.

## 4.2. Experiment

### 4.2.1. Software

Three softwares were used for simulations in this work: MCPB.py, Gaussian09 and Gromacs. MCPB.py is a python-based metal center parameter builder.<sup>147</sup> It can build a reliable force field for complexes containing metal ions. In my study, MCPB.py was used to bridge the QM calculations and MD simulation together by creating a zinc ion center force field. Gaussian09 is a software for QM calculations<sup>148-149</sup>, which was used in creating the zinc ion force field with MCPB.py. Finally, Gromacs is a software for MD simulation.<sup>150</sup> It used the zinc force field created by MCPB.py to simulate the movements of the active-site in the NDM-1 mutants.

#### 4.2.2. Experimental Methods

The overall workflow of the preparation of MM force field is shown in Figure 4.2. Firstly, the crystal structure of NDM-1 WT (PDB ID: 3SPU) was selected for simulation studies. The 3SPU structure contains 5 chains of NDM-1. Because the B chain (residues 43-268) has the most similar protein sequence to our experimental NDM-1 protein (residues 36-270), the PDB file was edited that only the B chain was used in our simulation. This PDB file was submitted to the H++ web server (<http://biophysics.cs.vt.edu/>) to add hydrogen atoms on the structure. Since the H++ will delete the zinc metal ions and water during the addition of hydrogen, the two zinc ions, bridging hydroxide ion and the coordinated water molecules were added back manually afterward. Then the MCPB.py input file and the mol2 file were created. The mol2 file is the naming file for non-standard residues, such as zinc ion and water. These two files were used to specify the zinc ions and construct the metal site for QM calculations. By using the MCPB.py program, the Gaussian and fingerprinting files were created. The fingerprinting files included the small, standard and large models, which were used for QM calculations by Gaussian09. The standard model contained the specification of residues which are bound to the zinc ions and the linkage information between them. The small model is used for calculating the force constants and the large model is used for calculating the Merz-Kollman charges at the zinc metal site. After the QM calculations of small and large models, the MCPB.py program was used to generate the final force constant parameters by the Seminario method and perform a Restrained Electrostatic

Potential (RESP) charge fit for the large model. Finally, the PDB file with the renamed metal site residues and the leap source file were generated. This leap source file is the final product of the MCPB.py program. By using this leap file, the topology and coordinate files were created and converted to Gromacs files for MD simulations.

For the mutants (H120A, H120N and H120Q), the H120 residue of the NDM-1 WT crystal structure (PDB ID: 3SPU B chain) was first mutated by using the Crystallographic Object-Oriented Toolkit (Coot) software<sup>151</sup> and the PDB files of the mutants were generated. Then these PDB files were submitted to the H++ web server and followed the method mentioned above.

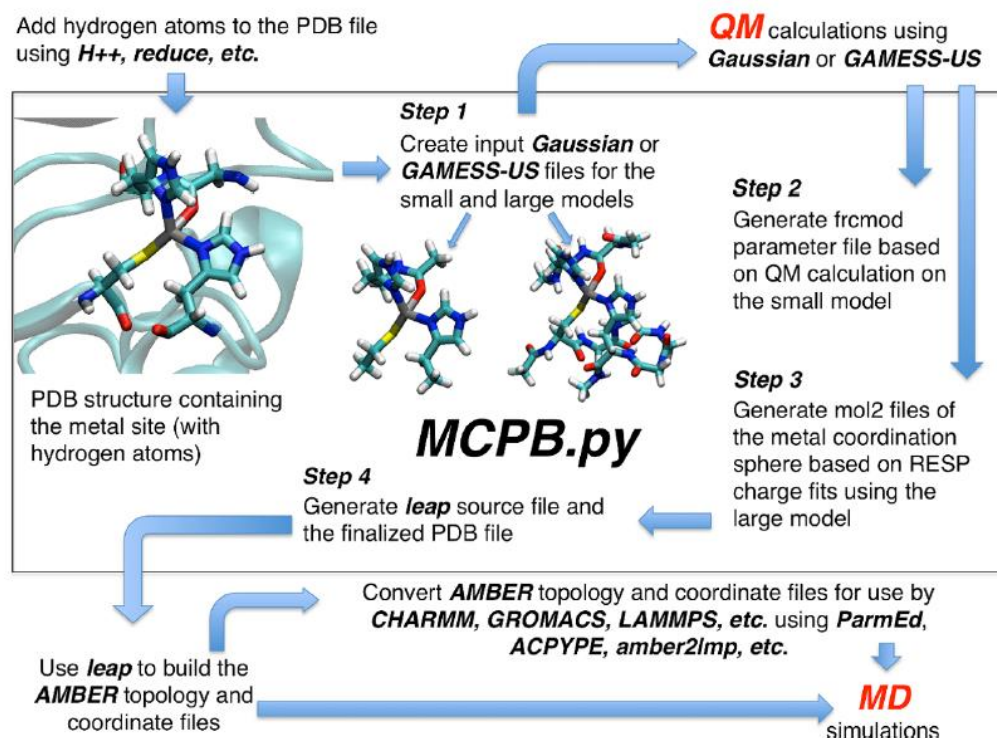


Figure 4.2 The workflow of the preparation of MM force field<sup>147</sup>



The structure for MD simulation was prepared in a cubic box containing TIP3P water<sup>152</sup> and 15 mM of NaCl (the experimental solvent concentration for activity assay was 15 mM). Before the MD simulation start, the system first went through the Energy Minimization (EM), NVT (constant Number of particles, Volume, and Temperature) and NPT (constant Number of particles, Pressure, and Temperature) equilibration by Gromacs 4.5.6. Since the system might have some steric clashes or bad geometry at the beginning, the structure was first relaxed through the EM step to make sure that the starting structure was reasonable. Then it is necessary to bring the system to an equilibrium environment before starting the simulation. However, the protein structure might collapse if the system was equilibrated without restraints at the beginning, so the equilibration was started with 1000 kJ/mol/nm restrain force on the protein. The equilibration was separated into two steps: NVT and NPT. The system was brought to 300 K reference temperature by the NVT ensemble. Then 1 bar reference pressure was applied to the system to reach the density equilibration by NPT ensemble. After these equilibrations, the restraints on the protein were slowly released from 1000 to 0.1 kJ/mol/nm. Finally, a 10 ns MD simulation was performed under no restraint condition at 300 K and 1 bar NPT ensemble. The Visual Molecular Dynamics (VMD) software<sup>153</sup> was used to visualize and analyze the results. The Root-Mean-Square Deviation (RMSD) was also calculated for each NDM-1 mutants.

### 4.3. Results and Discussions

#### 4.3.1. MD simulation of NDM-1 WT (Control)

In order to investigate the position of Zn1 ion and the changes in the active-site after the mutation, 10 ns of MD simulation was performed. NDM-1 WT was first simulated for control purpose. In Figure 4.3, the simulated NDM-1 WT Root-Mean-Square Deviation (RMSD) values comparing to the MD starting model structure were shown. Based on the RMSD plot, the RMSD values of the backbone fluctuated from 0.75 to 1.0 Å after 2.4 ns of the simulation time, and then the RMSD values stabilized at 0.9 Å for the rest of the time. This showed the overall structure is relatively stable after 2.4 ns. A snapshot of the lowest potential energy structure (Time =6.84 ns) of the NDM-1 WT active-site is shown in Figure 4.4. As shown in the figure, the nitrogen of the three histidine residues are all pointing towards the Zn1 ion and the aspartate-cysteine-histidine residues are pointing to the Zn2 ion. The bridging hydroxide ion is located between the two zinc ions and forms a hydrogen bond with D124. The distance between the hydrogen of the hydroxide ion and the oxygen of D124 was measured over the simulation time (Figure 4.5). The distance was kept at around 1.9 Å over the whole simulation, which is a stable distance of hydrogen bonding (1.5-2.5 Å is the distance for hydrogen bond)<sup>154</sup>. Overall, the NDM-1 WT simulation showed the same result as the NDM-1 WT crystal structure (PDB ID: 3SPU), which meant our simulation is consistent with the reference crystal structure.

The next step is to study our simulation model with the binding of substrate molecule. Figure 4.6-4.7 show the superimposition of the NDM-1 WT simulation structure (Time =6.84 ns) with the crystal structure of NDM-1 M67V mutant/hydrolyzed Penicillin G complex (PDB ID: 4RAM). By aligning the hydrolyzed product to the simulation structure, it is able to study the effects of the changes in the active-site due to the mutations and explain the reduction in activities. Since the starting beta-lactam antibiotic substrate has never been captured by crystal structures, only hydrolyzed products can be aligned. Also, the beta-lactam ring of all types of beta-lactam antibiotics bound in an identical way to the NDM-1 active-site, so the hydrolyzed penicillin G should be a good representative for the product molecule. Moreover, Figure 4.6 compares the overall structures between the NDM-1 WT simulation and the NDM-1 M67V mutant, in which there is no significant difference. The M67V mutation is at the L3 loop of the protein, which is far away from the active-site and has no effect on the active-site at all. Therefore, this crystal structure is good enough to study the product alignment. When looking closer at the active-site (Figure 4.7), the positions of the active-site ions and residues are very similar in both structures. The difference in position of the hydroxide ion is only 0.69 Å between the two structures. This showed the alignment with the NDM-1 M67V mutant/hydrolyzed penicillin G complex will be a fair model to study the other NDM-1 mutants' simulations.

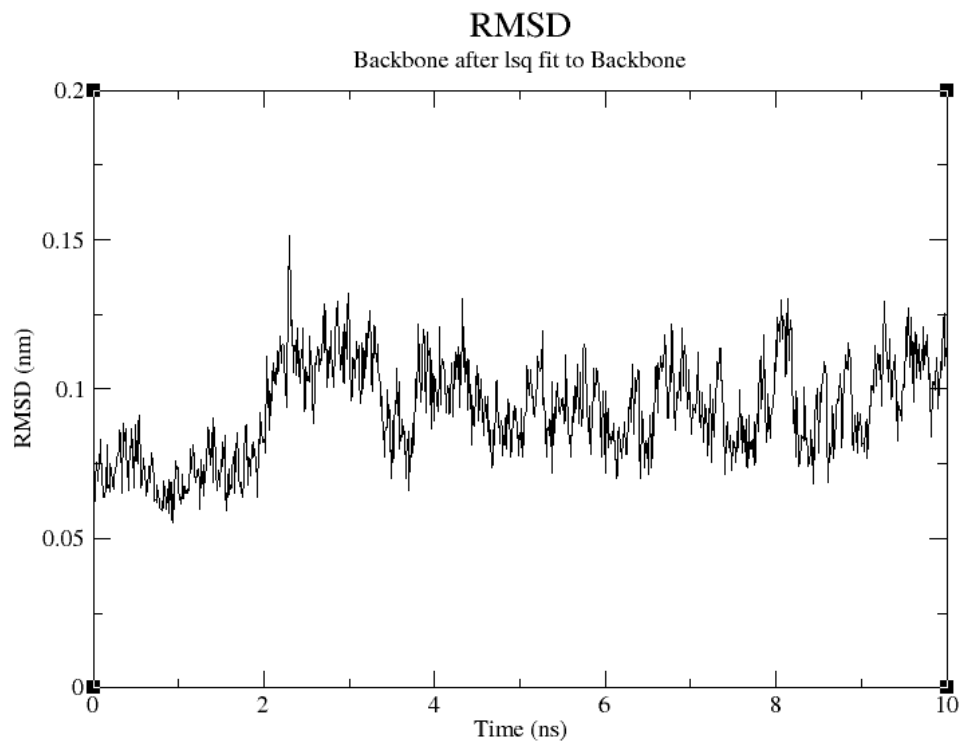


Figure 4.3 The RMSD analysis of the backbone atoms in the NDM-1 WT simulation comparing to the MD starting model structure over the simulation time.

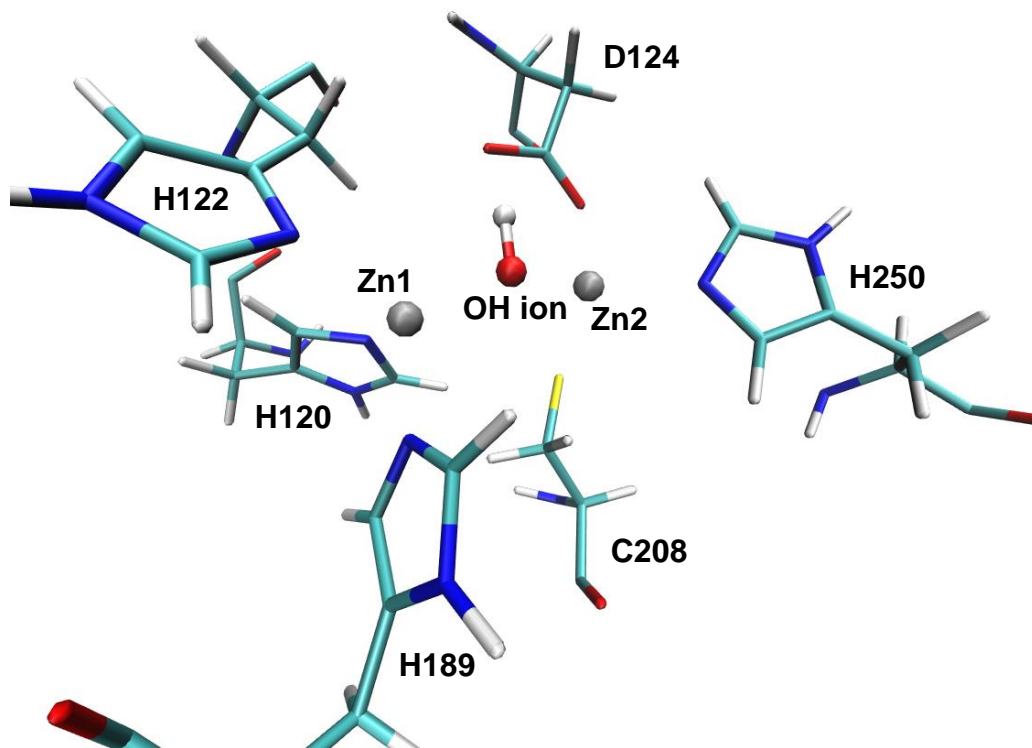


Figure 4.4 The active-site of the lowest potential energy structure of the MD simulation NDM-1 WT.

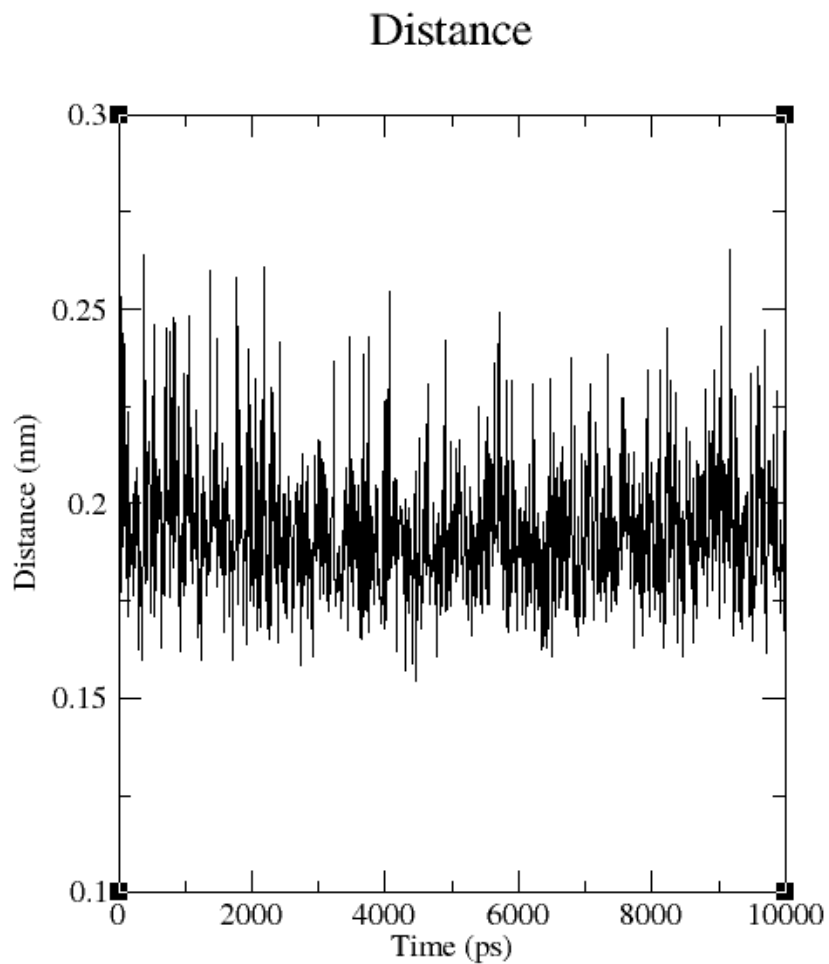


Figure 4.5 The bond distance between the hydrogen of the hydroxide ion and the oxygen of the Asp 124 residue of NDM-1 WT over the simulation time. Average distance =  $1.9 \pm 0.2 \text{ \AA}$  ( $0.1 \text{ nm} = 1 \text{ \AA}$ ).

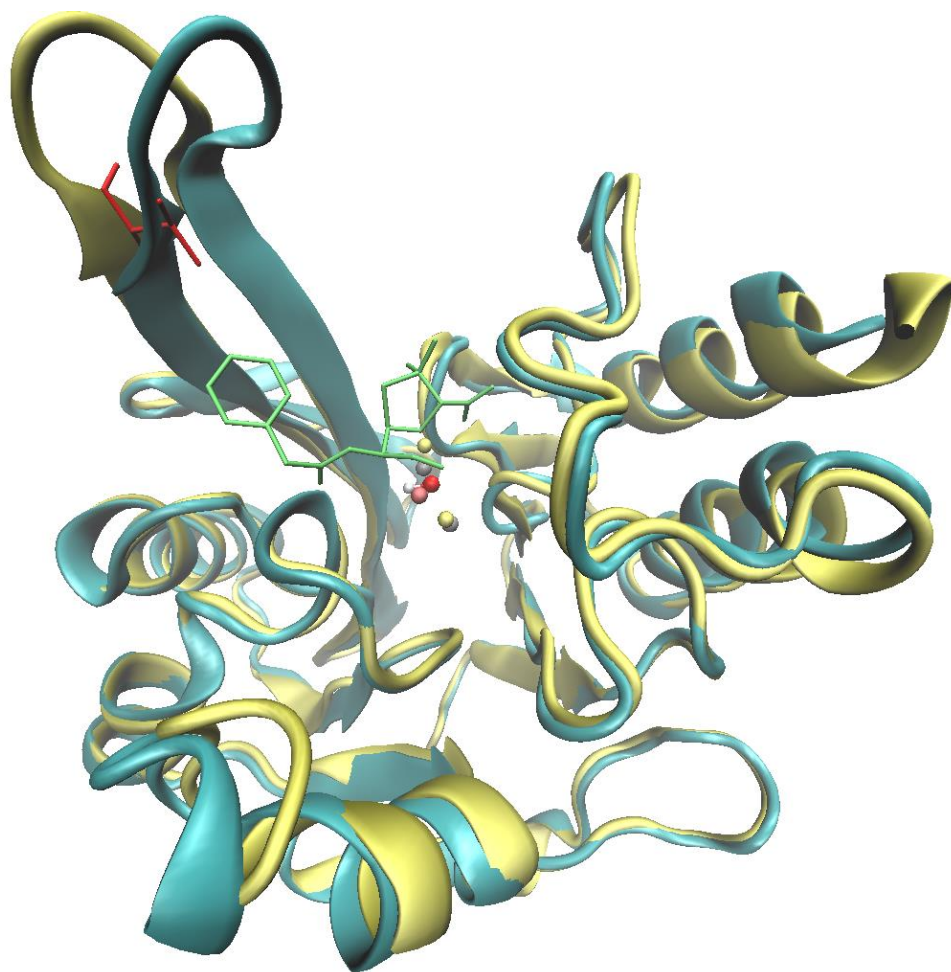


Figure 4.6 The superimposition of the lowest energy structure of the NDM-1 WT simulation with the NDM-1 M67V mutant/hydrolyzed Penicillin G complex (4RAM); WT simulation (cyan), M67V mutant (yellow), M67V mutated residue (Red), hydrolyzed Penicillin G (green), simulation zinc ion/hydroxide ion (gray/red ball) and M67V mutant's zinc ion/ hydroxide ion (yellow/pink ball).

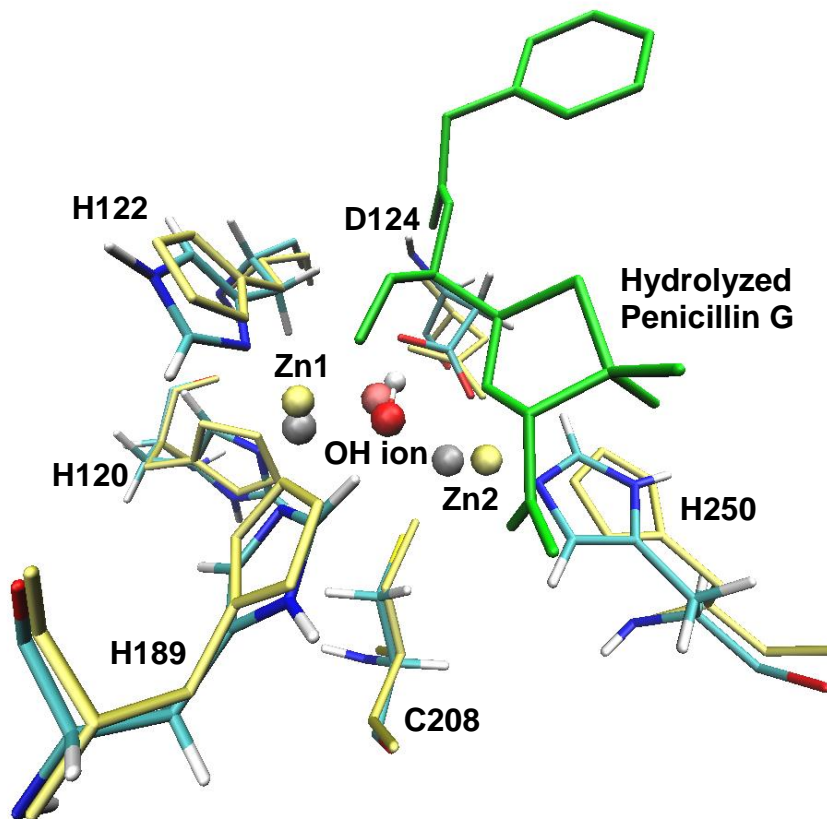


Figure 4.7 The active-site comparison between the NDM-1 WT simulation and the NDM-1 M67V mutant complexed with hydrolyzed Penicillin G (PDB ID: 4RAM); WT simulation (cyan), M67V mutant (yellow), hydrolyzed Penicillin G (green), simulation zinc ion/hydroxide ion (gray/red ball) and M67V mutant's zinc ion/ hydroxide ion (yellow/pink ball).



#### 4.3.2. MD simulation of NDM-1 H120A

Using the same method as the NDM-1 WT, a 10 ns MD simulation of NDM-1 H120A was performed. In Figure 4.8, the RMSD plot comparing to the MD starting model structure showed an average value of 0.6 Å over the whole simulation period. Although there were some small fluctuations between 5 and 8 ns, the overall RMSD values were about the same. This showed the overall structure of the protein was very stable throughout the simulation time. Figure 4.9-4.10 are snapshots of the lowest potential energy structure (Time = 3.61 ns) of the NDM-1 H120A aligning with the WT. As Figure 4.9 shows the overall protein structures are about the same between H120A and WT. However, the position of the hydroxide ion has changed significantly. Looking closer at the active-site (Figure 4.10), all active-site residues have shifted. Because of the H120A mutation, the Zn1 ion has lost a coordinating residue and moved 0.63 Å away from the WT Zn1 ion position. This correspondingly moved the hydroxide ion (1.31 Å) and Zn2 ion (0.52 Å) away from the relative WT positions. Comparing to the movements of the two zinc ions, the movement of the hydroxide ion is significant. As shown in Figure 4.11, the distance between the hydrogen of the hydroxide ion and the oxygen of the D124 residue became 4.0 Å, which means the hydrogen bond between the bridging hydroxide ion and D124 was completely broken after the mutation. This breaking of hydrogen bond has a huge impact to the hydrolytic activities of NDM-1. When aligning the crystal structure of NDM-1 M67V/hydrolyzed penicillin G to the simulation

structure (Figure 4.12), the hydroxide ions were 1.96 Å difference in position. More importantly, the hydrogen atom of the hydroxide ion was pointing towards the beta-lactam ring of the penicillin G, which is not a favorable conformation for nucleophilic attack. Therefore, the hydrolytic activities of the NDM-1 H120A were greatly reduced.

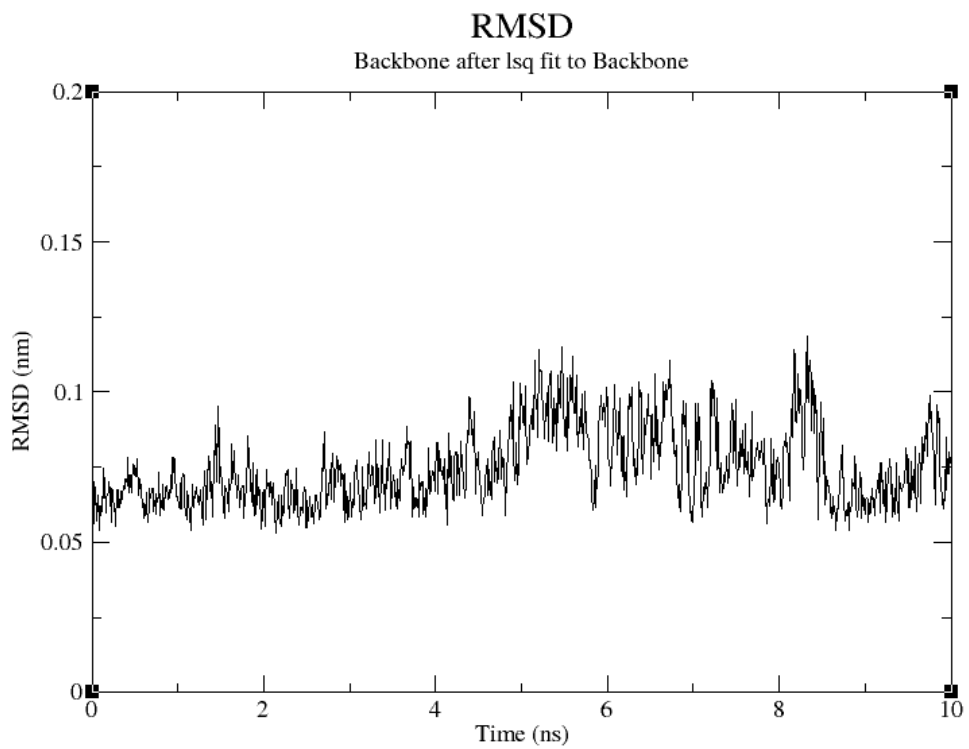


Figure 4.8 The RMSD analysis of the backbone atoms in the NDM-1 H120A simulation comparing to the MD starting model structure over the simulation time.

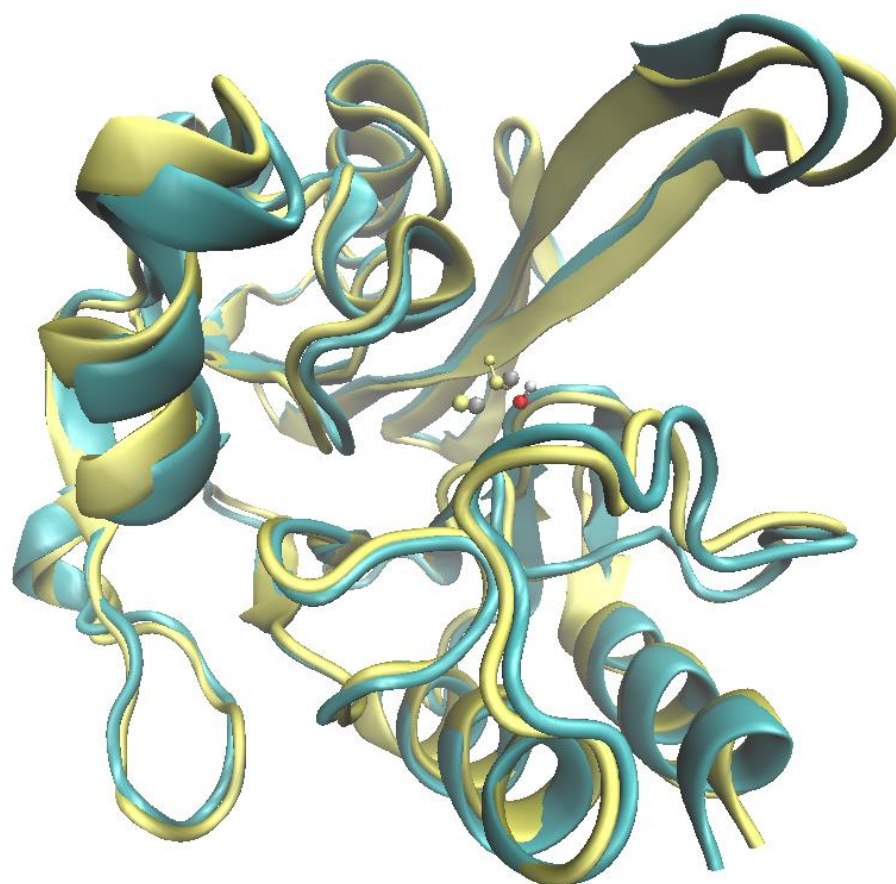


Figure 4.9 Comparison between the lowest potential energy structures of the NDM-1 WT (yellow) and H120A (cyan) simulations. WT zinc ion/hydroxide ion (yellow balls) and H120A zinc ion/hydroxide ion (gray/red ball).

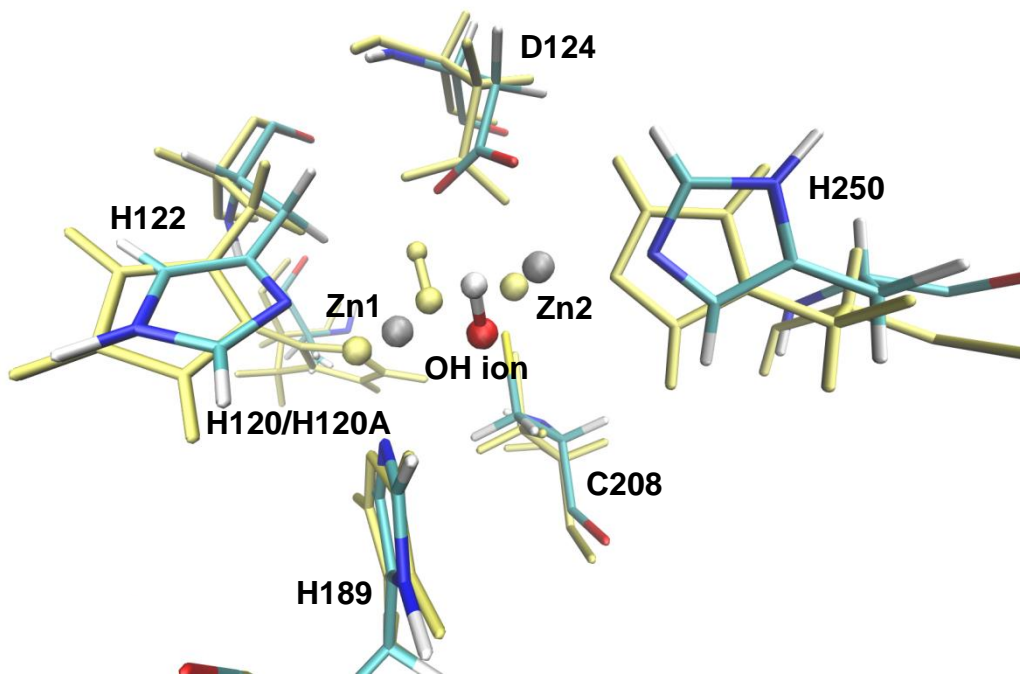


Figure 4.10 Comparison between the active-sites of the lowest potential energy structures of NDM-1 WT (yellow) and H120A (cyan) simulations. WT zinc ion/ hydroxide ion (yellow balls) and H120A zinc ion/hydroxide ion (gray/red ball).

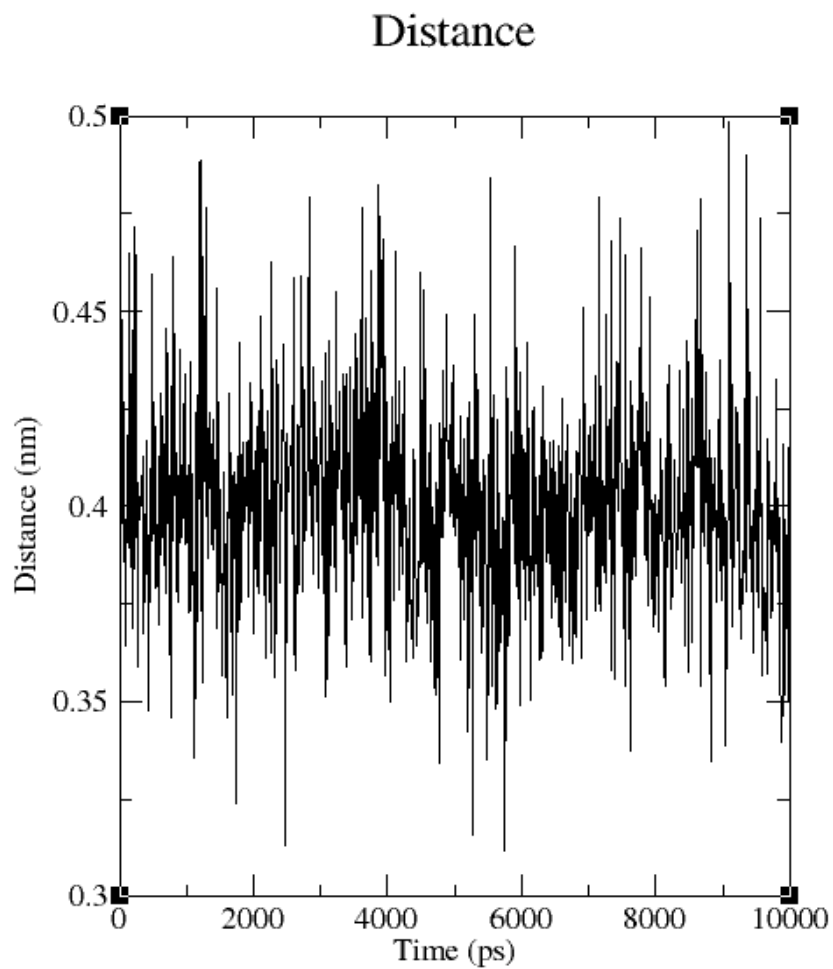


Figure 4.11 The bond distance between the hydrogen of the hydroxide ion and the oxygen of the Asp 124 residue of NDM-1 H120A over the simulation time. Average distance =  $4.0 \pm 0.3 \text{ \AA}$  ( $0.1 \text{ nm} = 1 \text{ \AA}$ ).

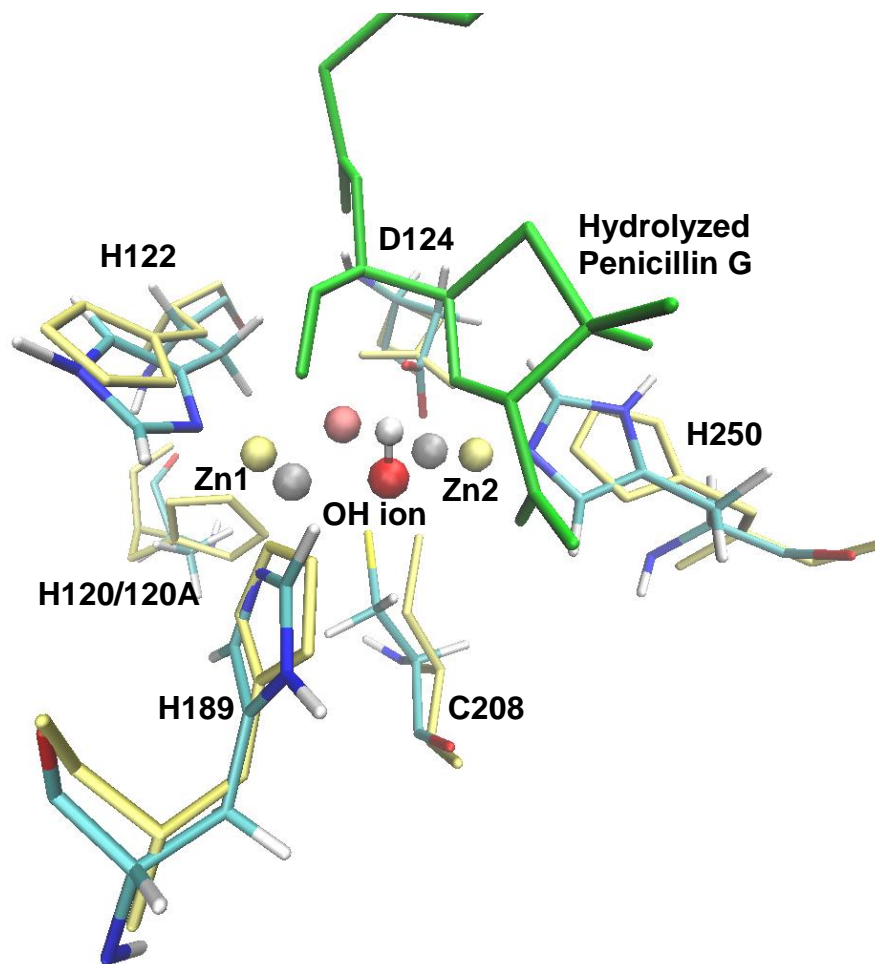


Figure 4.12 The active-site comparison between the NDM-1 H120A simulation and the NDM-1 M67V mutant complexed with hydrolyzed Penicillin G (PDB ID: 4RAM); H120A simulation (cyan), M67V mutant (yellow), hydrolyzed Penicillin G (green), simulation zinc ion/hydroxide ion (gray/red ball) and M67V mutant's zinc ion/ hydroxide ion (yellow/pink ball).

#### 4.3.3. MD simulation of NDM-1 H120N

Following the NDM-1 H120A, 10 ns MD simulation of NDM-1 H120N was performed. Figure 4.13 showed a RMSD plot of NDM-1 H120N backbone atoms comparing to the MD starting model structure over the simulation time. An average RMSD value of 0.7 Å was found throughout the whole simulation time, which means the overall structure of NDM-1 H120N simulation was very stable. However, there were significant changes in the active-site during this simulation. Two snapshots during the H120N simulation were taken: Time = 4.90 ns (bonding) and Time = 8.26 ns (non-bonding). Bonding here means there is a hydrogen bond between the hydroxide ion and D124 and non-bonding means the hydrogen bond is broken between the hydroxide ion and D124. Figure 4.14 showed the comparison of the overall structures of these two forms with the NDM-1 WT. As shown in the figures, both the bonding and non-bonding forms have no significant difference in overall structures when comparing to the WT or between the two forms. The critical differences between the two forms were in the active-site. Figure 4.15 showed the comparisons between the active-sites of NDM-1 WT and H120N with both forms. In the bonding form, there were no big differences in positions of the ions between H120N and WT (Zn1 = 0.79 Å, OH = 0.23 Å and Zn2 = 0.34 Å). However, in the non-bonding form, the position difference of the hydroxide ions between H120N and WT was very big (Zn1 = 0.64 Å, OH = 1.23 Å and Zn2 = 0.15 Å). When transforming from the bonding to non-bonding form, the



hydroxide ion moved about 1.0 Å where the other two zinc ions did not really move at all. Figure 4.16 showed the bond distance between the hydrogen atom of the hydroxide ion and the oxygen atom of D124 over the simulation time. As shown in the plot, the distances fluctuated between 2.3 Å and 4.4 Å forward and backward (1.5-2.5 Å is the ideal distance for hydrogen bond)<sup>154</sup>, which meant the hydrogen bond was constantly forming and breaking. Also, NDM-1 H120N was in the non-bonding form for most of the time, 79.5% of the simulation time. When aligning with the crystal structure of NDM-1 M67V/hydrolyzed penicillin G to H120N (Figure 4.17), the difference in hydroxide ion position between the structures were 0.62 Å (bonding) and 1.92 Å (non-bonding), which was a significant change. It is noticed that the active-site of the bonding form was very similar to the WT and the non-bonding form was very similar to the H120A mutant. Therefore, for the same reason as the H120A, the hydrogen atom of the hydroxide ion in the non-bonding form was pointing towards the beta-lactam ring of the penicillin G, so it does not favor the nucleophilic attack. Since H120N is staying in the non-bonding form for most of the time, this greatly reduces the hydrolytic activities of this NDM-1 mutant.

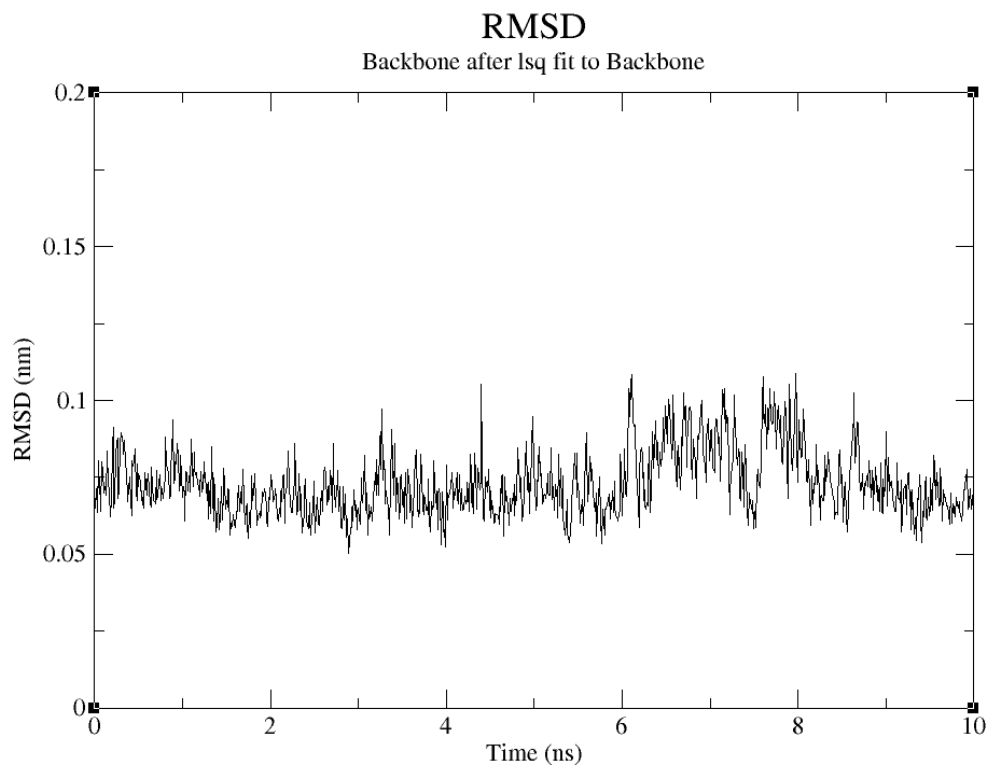
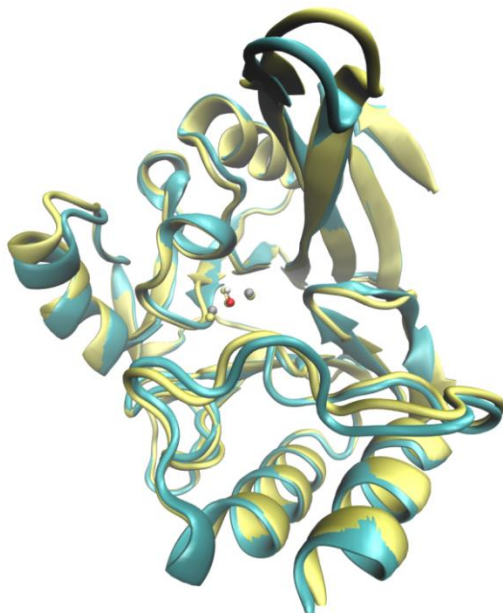


Figure 4.13 The RMSD analysis of the backbone atoms in the NDM-1 H120N simulation comparing to the MD starting model structure over the simulation time.

a)



b)

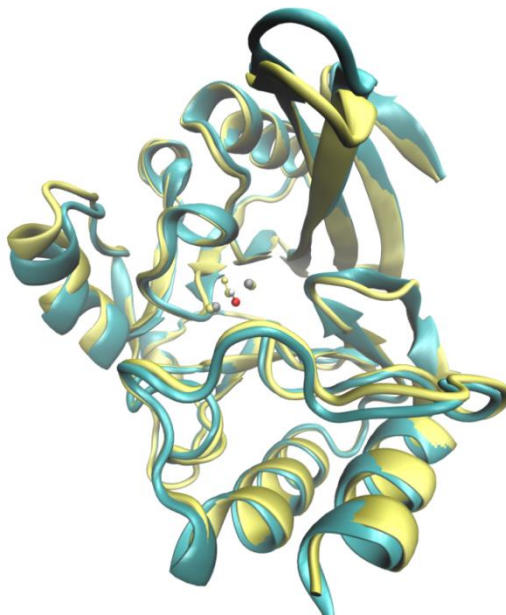


Figure 4.14 Comparison between the protein structures of the NDM-1 WT (yellow) and H120N (cyan) simulations. a) Time = 4.90 ns, b) Time = 8.26 ns. WT zinc ion/ hydroxide ion (yellow balls) and H120A zinc ion/hydroxide ion (gray/red ball).

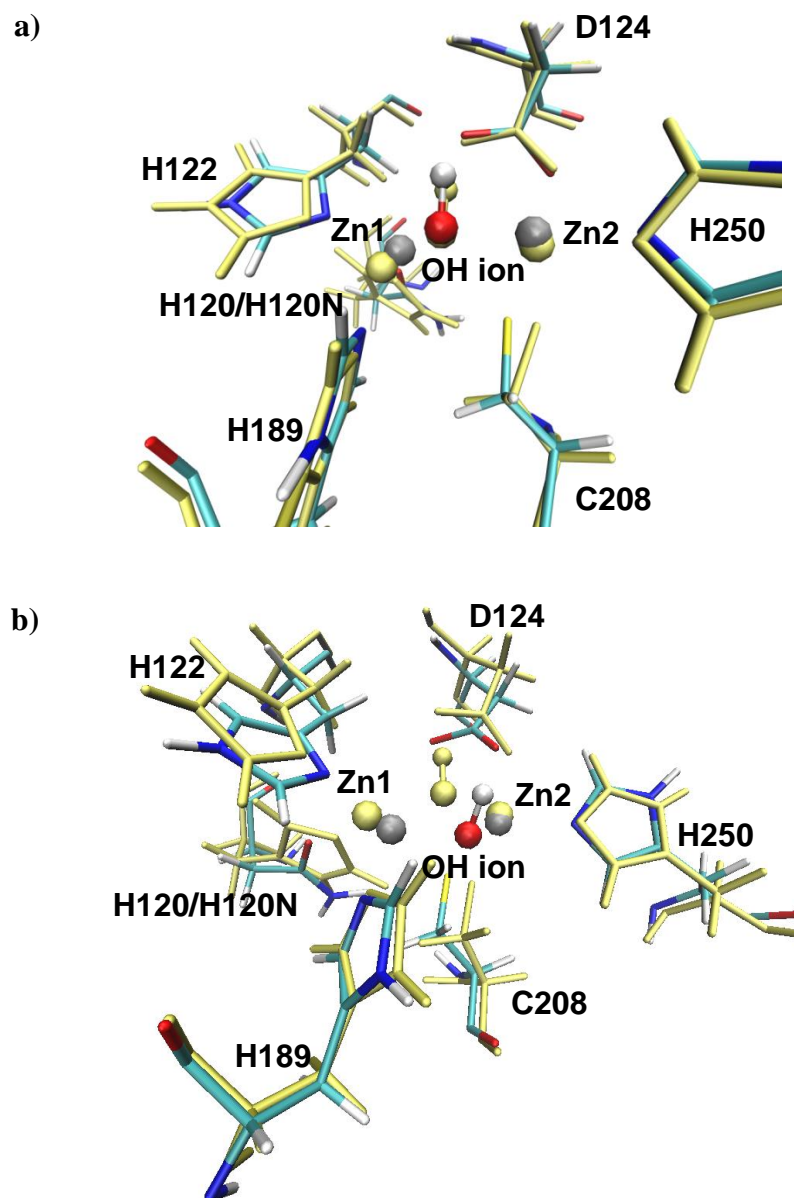


Figure 4.15 Comparison between the active-sites of NDM-1 WT (yellow) and H120N (cyan) simulations. a) Time = 4.90 ns, b) Time = 8.26 ns. WT zinc ion/ hydroxide ion (yellow balls) and H120N zinc ion/hydroxide ion (gray/red ball). The distances between the WT hydroxide ion and the H120N hydroxide ion were 0.23 Å at Time = 4.90 ns and 1.23 Å at Time = 8.26 ns. The hydroxide ion moved 1.0 Å when the hydrogen bond between D124 broke.

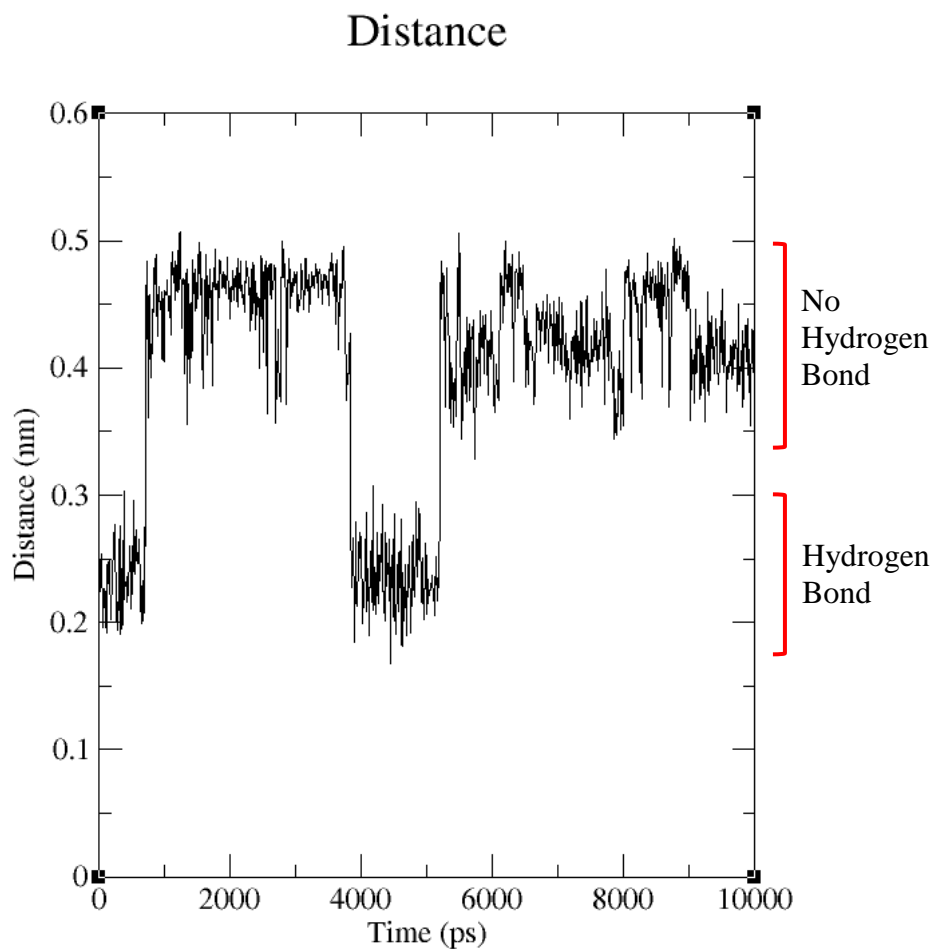


Figure 4.16 The bond distance between the hydrogen of the hydroxide ion and the oxygen of the Asp 124 residue of NDM-1 H120N over the simulation time. 20.5 % of the simulation time is in bonding form and 79.5 % is in non-bonding form. Average distance when bonding =  $2.3 \pm 0.3 \text{ \AA}$  and non-bonding =  $4.4 \pm 0.4 \text{ \AA}$  ( $0.1 \text{ nm} = 1 \text{ \AA}$ ).

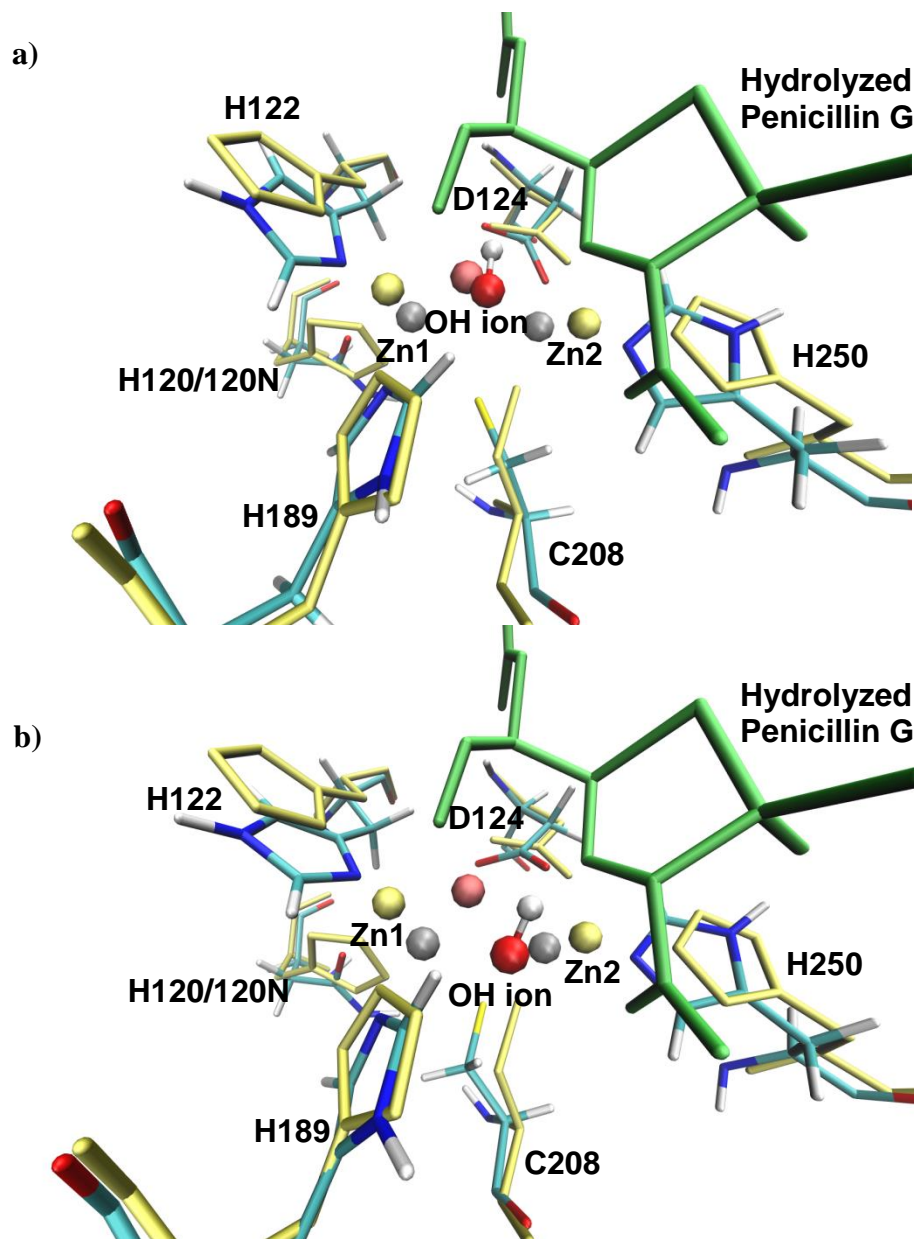


Figure 4.17 The active-sites comparison between the NDM-1 H120N simulation and the NDM-1 M67V mutant complexed with hydrolyzed Penicillin G (PDB ID: 4RAM). a) Time = 4.90 ns, b) Time = 8.26 ns; H120N simulation (cyan), M67V mutant (yellow), hydrolyzed Penicillin G (green), simulation zinc ion/hydroxide ion (gray/red ball) and M67V mutant's zinc ion/hydroxide ion (yellow/pink ball).

#### 4.3.4. MD simulation of NDM-1 H120Q

Finally, a 10 ns MD simulation of NDM-1 H120Q was performed. Figure 4.18 shows the RMSD plot of the backbone atoms of H120Q simulation comparing to the MD starting model structure over the simulation time. The RMSD values fluctuated at 1 ns and changed from 0.75 Å to 0.95 Å and stayed at 0.95 Å for the rest of the simulation. Therefore, the overall structure of the protein was very stable throughout most of the simulation period. Figure 4.19-4.20 are the snapshots of the lowest potential energy structure (Time = 6.92 ns) of the H120Q simulation comparing to the WT. Same as the other mutants, H120Q also had no significant change to its overall structure comparing to the WT (Figure 4.19). However, the active-site was very different from the other mutants. As shown in Figure 4.20, unlike the other mutants that the ions are moving outward from the active-site, all components of the whole active-site of H120Q (including the zinc ions, hydroxide ion and the coordinating residues) are shifted towards the Zn1 site direction. The Zn1, OH and Zn2 ions are shifted by 0.67 Å, 0.98 Å and 1.31 Å, respectively as compared to the WT. The coordinating residues to the two zinc ions were also greatly shifted. The movement of Zn2 ion was significant as compared to the other two ions. Interestingly, the hydrogen bond between the hydroxide ion and D124 was kept throughout the whole simulation. Shown in Figure 4.21, the distances between the hydrogen atom of the hydroxide ion and the oxygen atom of D124 were kept at 1.8 Å, which was a very strong hydrogen bond distance. And there was

no breakage of this hydrogen bond like in other mutants. When aligning the crystal structure of NDM-1 M67V/hydrolyzed penicillin G to the H120Q simulation structure (Figure 4.22), the hydroxide ions only had 0.52 Å difference in position, which was considered to be about the same position. On the other hand, the Zn<sup>2+</sup> ions had 2.13 Å difference in position. This movement of the Zn<sup>2+</sup> ion had a huge impact to the hydrolytic activities. Since the Zn<sup>2+</sup> ion is involved in substrate interaction and stabilizes the negatively charged intermediate (by interacting with the C3 carboxylate group and negatively charged N4 of the penicillins ring)<sup>126</sup>, the movement of the Zn<sup>2+</sup> ion is not favorable for these interactions, so the hydrolytic activities of the H120Q mutant were reduced.



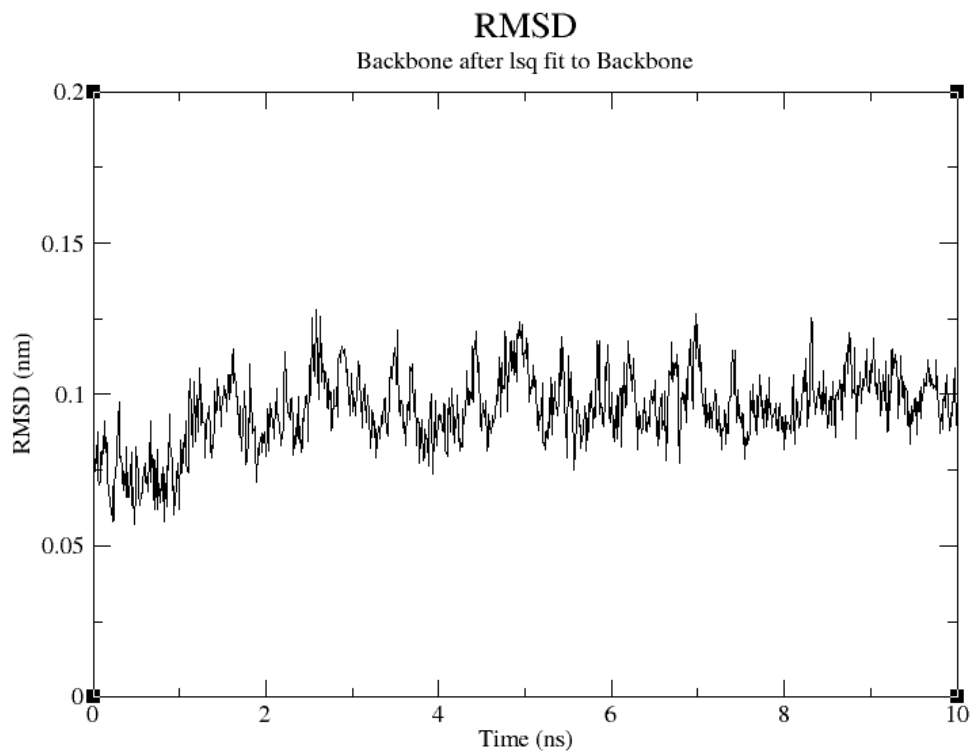


Figure 4.18 The RMSD analysis of the backbone atoms in the NDM-1 H120Q simulation comparing to the MD starting model structure over the simulation time.

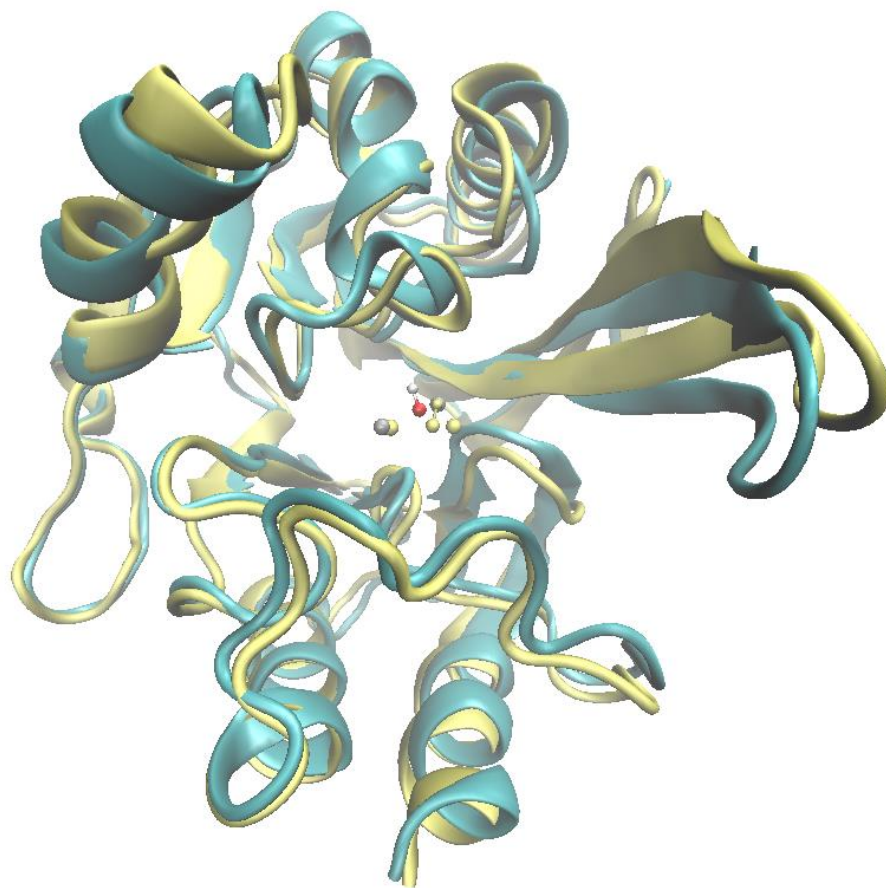


Figure 4.19 Comparison between the lowest potential energy structures of the NDM-1 WT (yellow) and H120Q (cyan) simulations. WT zinc ion/hydroxide ion (yellow balls) and H120Q zinc ion/hydroxide ion (gray/red ball).

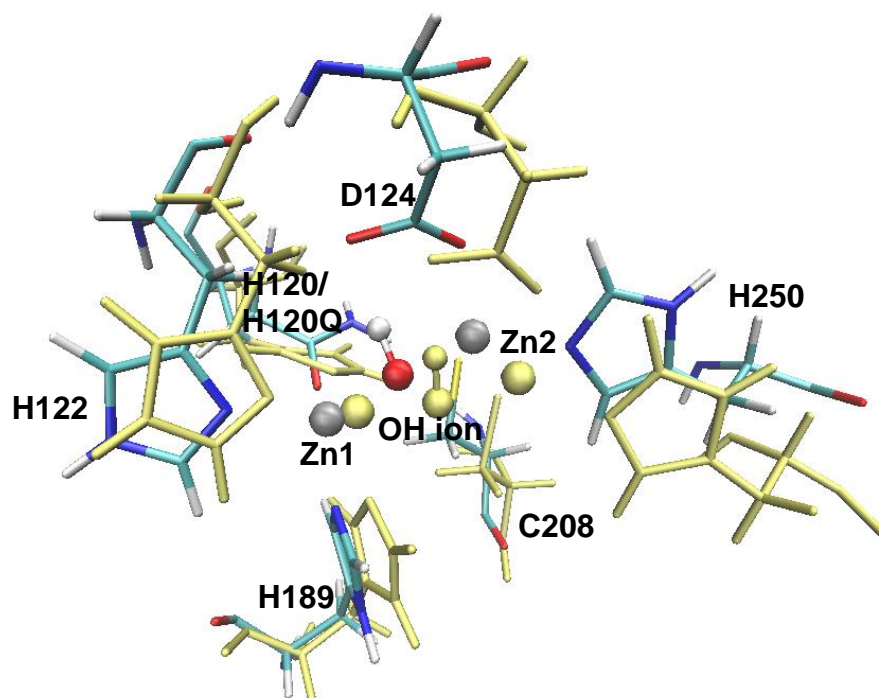


Figure 4.20 Comparison between the active-sites of the lowest potential energy structures of NDM-1 WT (yellow) and H120Q (cyan) simulations. WT zinc ion/ hydroxide ion (yellow balls) and H120A zinc ion/hydroxide ion (gray/red ball). The Zn1, OH and Zn2 ions were shifted sideward to the Zn1 site direction. All coordinating residues were greatly shifted together with the zinc ions. However, the hydrogen bond between the hydroxide ion and the D124 residue was maintained.

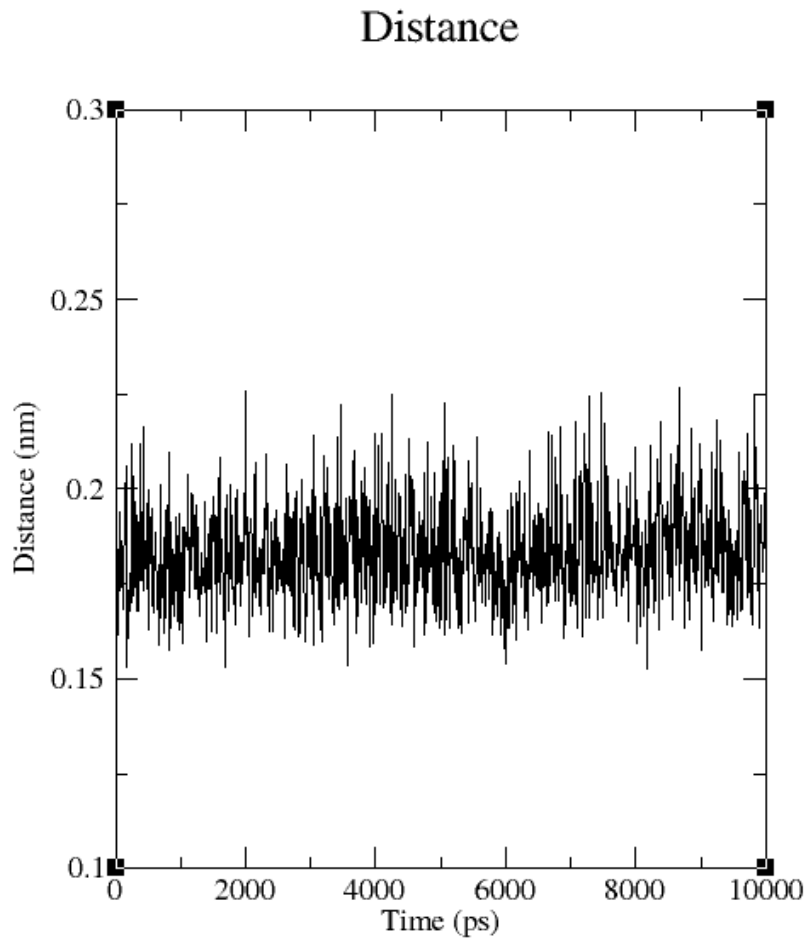


Figure 4.21 The bond distance between the hydrogen of the hydroxide ion and the oxygen of the Asp 124 residue of NDM-1 H120Q over the simulation time. Average distance =  $1.8 \pm 0.1 \text{ \AA}$  ( $0.1 \text{ nm} = 1 \text{ \AA}$ ).

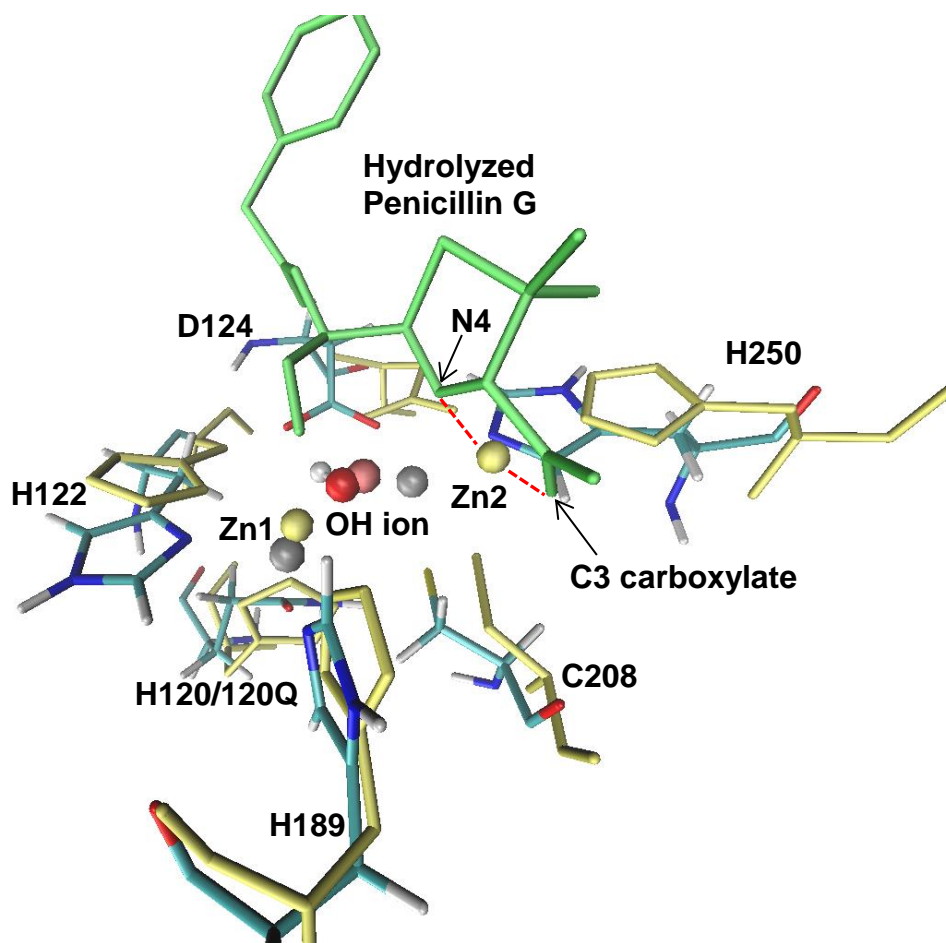


Figure 4.22 The active-site comparison between the NDM-1 H120Q simulation and the NDM-1 M67V mutant complexed with hydrolyzed Penicillin G (PDB ID: 4RAM); H120Q simulation (cyan), M67V mutant (yellow), hydrolyzed Penicillin G (green), simulation zinc ion/hydroxide ion (gray/red ball) and M67V mutant's zinc ion/ hydroxide ion (yellow/pink ball). The Zn2 ion stabilizes the negatively charged intermediate by interacting with the C3 carboxylate group and negatively charged N4 of the penicillins ring<sup>126</sup>, however, the movement of the Zn2 ion in the H120Q mutant was not favorable for these interactions.

#### 4.4. Concluding Remarks

In this chapter, MD simulations of NDM-1 WT, H120A, H120N and H120Q were successfully performed. The changes in the active-site due to the mutations were identified and the reasons of the reduction in hydrolytic activities were discussed.

In the H120A and H120N mutations, very similar changes in their active-site were observed. The Zn1 ion was moved outward from the active-site due to the residue 120 mutations, which led to the bridging hydroxide ion and Zn2 ion to move out too. Because the hydroxide ion moves away from the active-site, the hydrogen bond between the hydroxide ion and D124 is broken. This hydrogen bond is very important to the NDM-1 hydrolytic activities, as the hydrogen bond is used to orient the hydroxide ion to the correct position and angle to perform the nucleophilic attack and protonation.<sup>126</sup> When aligning the hydrolyzed penicillin G on to the hydrogen bond broken conformations of these two mutants, the hydrogen atom of the hydroxide ion was pointing toward the beta-lactam ring of the penicillin G, which was a very unfavorable conformation for nucleophilic attack. Therefore, the H120A and H120N mutants had their hydrolytic activities greatly reduced comparing to the WT. The only difference between H120A and H120N was that the H120A mutant had its hydrogen bond completely broken but H120N was continuously

forming and breaking the hydrogen bond, so the reduction of hydrolytic activities in H120N is smaller than H120A.

Unlike the H120A and H120N mutants, the H120Q mutant had a totally different result. In H120Q, the Zn1 ion moved towards the Zn1 site direction after the mutation and this pulled the whole active-site towards the Zn1 site direction (including the hydroxide ion, Zn2 ion and all the ions coordinating residues). Interestingly, the hydrogen bond between the hydroxide ion and D124 did not break like in the other two mutants. More importantly, the biggest change was the movement of the Zn2 ion, which shifted up by 2.13 Å. When aligning the hydrolyzed penicillin G to this H120Q conformation, the Zn2 ion is located very far away from the C3 carboxylate group and N4 of the penicillin G and this position is not favorable for stabilizing the negatively charged intermediate.

Referring back to the results from Chapter 3, the reduction of reaction rates of all the mutants are mainly due to the increase in  $K_m$  values, which implies that the mutants might have weaker binding affinities to the antibiotics. Based on our simulation results, the movements of the two zinc ions also moved the coordinating residues of the active site together, which did affect the positions of the active site. For example, in Figure 4.22, the active site of H120Q mutant was completely shifted in position. Since the zinc ions might affect the binding

of the substrates, the movement of the active site can have significant impact on the binding affinity to the antibiotics which results in the increase of  $K_m$  values.



## **Chapter 5. Conclusions**

In this project, site-direct mutagenesis studies were performed to understand the role of Zn1 ion in the enzyme NDM-1. Residue H120 of the Zn1 site was selected for mutations to alanine (A), asparagine (N) and glutamine (Q) in order to knock out the binding of the Zn1 ion. Based on the zinc content measurements, all three mutants had the Zn1 ion remained in their Zn1 site and the knockout of Zn1 ion has failed. Hydrolytic activities of the three mutants were tested against six different types of beta-lactam antibiotics: ampicillin and penicillin G (Penicillins), cefotaxime and ceftazidime (Cephalosporins), imipenem and meropenem (Carbapenems). The results showed that all three NDM-1 mutants have significant reduction in activities as compared to the WT (6-810 folds of reductions). Some of the reductions in activities were caused by the increase in  $K_m$  values, which might be due to the weaker binding affinities of antibiotics. Nevertheless, the reductions of activities were very obvious to all types of antibiotics.

The H120 residue is located deeply inside the active-site pocket of NDM-1 and should not have any direct interaction with antibiotics substrates. Therefore, the reduction in hydrolytic activities must be caused by the mutations on the Zn1 site. It is possible that the mutations at the H120 position changed the electronic environment of the active site. For example, the glutamine of H120Q is a weaker electron donor comparing to the histidine of the WT, which will result in a stronger Lewis acid Zn1 ion. This stronger Lewis acid Zn1 ion might have a stronger interaction to the carboxylic group of the opened beta-lactam ring

(Figure 1.11, step 4), so it is more difficult to release the product molecule and eventually reduced the overall hydrolytic activities.<sup>97-104</sup> Nevertheless, MD simulations showed that the Zn1 ion moved away from its original location after the mutations and consequently affected the positions of the bridging hydroxide ion and Zn2 ion. Interestingly, the movement of the Zn1 ion itself was relatively small, but the related movements of the bridging hydroxide ion and Zn2 ion were quite significant. The importance of the Zn2 ion and the Zn2 site residues have already been reported previously.<sup>126</sup> The position of the Zn2 ion must be very precise in order to stabilize the intermediate and the hydrogen bond between the bridging hydroxide ion and D124 of the Zn2 site is required to orient the hydroxide ion to perform the nucleophilic attack and protonation.<sup>126</sup> Therefore, the related movements of the bridging hydroxide ion and Zn2 ion resulted in a huge impact to the hydrolytic activities of NDM-1.

Overall, my studies suggested a new role of the Zn1 ion played in the NDM-1. The exact location of the Zn1 ion is critical for hydrolytic activities. The relative location of the Zn1 ion is important for the formation of the Zn1-OH-Zn2 bridge and it has a position control function to the hydroxide ion and the Zn2 ion. A specific location of the Zn1 ion is required to hold the hydroxide ion and the Zn2 ion at the correct position to perform the nucleophilic attack for the hydrolysis reaction and to stabilize the negatively charged intermediate.

Since the two zinc ions are very important for the functions of the NDM-1, targeting the zinc ions might be a good strategy for developing new inhibitors. For example, the Ebselen reported by the Chen's group can knock out the binding of the Zn<sup>2+</sup> ion and resulted in very good inhibition effects to the NDM-1.<sup>122</sup> In another very recent publication, the bismuth drugs reported by the Sun's group can even displace both zinc ions in the active site of NDM-1.<sup>155</sup> The bismuth drugs are highly potential drugs for treating NDM-1. This kind of inhibitors targeting the binding of zinc ions possibly are the potential inhibitors for treating NDM-1 or even for the whole Class B beta-lactamases.

# References

1. Russell, A. D., *Types of antibiotics and synthetic antimicrobial agents*. In: Denyer S. P., Hodges N. A. & German S. P. (eds.) *Hugo and Russell's pharmaceutical microbiology. 7th Ed. Blackwell Science, UK. 2004*; p 152-186.
2. Schlegel, H. G., *General microbiology. 7th Ed. Cambridge University Press, Cambridge. 2003*.
3. Walsh, C., *Antibiotics: actions, origins, resistance. 1st Ed. ASM Press, Washington, DC. 2003*.
4. van Hoek, A. H. A. M.; Mevius, D.; Guerra, B.; Mullany, P.; Roberts, A. P.; Aarts, H. J. M., Acquired Antibiotic Resistance Genes: An Overview. *Frontiers in Microbiology* **2011**, 2, 203.
5. Frank, U.; Tacconelli, E., The Daschner Guide to In-Hospital Antibiotic Therapy. European standards. **2012**.
6. Adzitey, F., Antibiotic classes and antibiotic susceptibility of bacterial isolates from selected poultry; a mini review. *World Vet. J.* **2015**, 5 (3), 36-41.
7. Calderon, C. B.; Sabundayo, B. P., *Antimicrobial classifications: Drugs for bugs*. In: Schwalbe R, Steele-Moore L & Goodwin AC (eds). *Antimicrobial susceptibility testing protocols. CRC Press, Taylor and Frances group. ISBN 978-0-8247-4100-6. 2007*.
8. Tidwell, T. T., Hugo (Ugo) Schiff, Schiff bases, and a century of beta-lactam synthesis. *Angew Chem Int Ed Engl* **2008**, 47 (6), 1016-20.

9. Heesemann, J., Mechanisms of resistance to beta-lactam antibiotics. *Infection* **1993**, *21* (1), S4-9.
10. McGeer, A.; Fleming, C. A.; Gree, K.; Low, D. E., Antimicrobial resistance in Ontario: Are we making progress? *Laboratory Proficiency Testing Program Newsletter* **2001**, *293*, 1-2.
11. Holten, K. B.; Onusko, E. M., Appropriate prescribing of oral beta-lactam antibiotics. *Am Fam Physician* **2000**, *62* (3), 611-20.
12. Zahner, H.; Maas, W., *Biology of Antibiotics*. Springer-Verlag, New York. 1972.
13. Boundless Antibiotic Classifications. Boundless microbiology. <https://www.boundless.com/microbiology/textbooks/boundless-microbiology-textbook/antimicrobial-drugs-13/overview-of-antimicrobial-therapy-153/antibiotic-classifications-775-4905/>. (accessed May 21, 2018).
14. Talaro, K. P.; Chess, B., *Foundations in microbiology*. 8th Ed. McGraw Hill, New York. 2008.
15. Poirel, L.; Brinas, L.; Verlinde, A.; Ide, L.; Nordmann, P., BEL-1, a novel clavulanic acid-inhibited extended-spectrum beta-lactamase, and the class 1 integron In120 in *Pseudomonas aeruginosa*. *Antimicrob Agents Chemother* **2005**, *49* (9), 3743-8.

16. Pegler, S.; Healy, B., In patients allergic to penicillin, consider second and third generation cephalosporins for life threatening infections. *BMJ* **2007**, 335 (7627), 991.
17. Abraham, E. P., Cephalosporins 1945-1986. *Drugs* **1987**, 34 Suppl 2, 1-14.
18. Bonner, D. P.; Sykes, R. B., Structure activity relationships among the monobactams. *J Antimicrob Chemother* **1984**, 14 (4), 313-27.
19. Sykes, R. B.; Bonner, D. P., Discovery and development of the monobactams. *Clin. Infect. Dis.* **1985**, 7 (4), S579-S593.
20. Sykes, R. B.; Cimarusti, C. M.; Bonner, D. P.; Bush, K.; Floyd, D. M.; Georgopapadakou, N. H.; Koster, W. M.; Liu, W. C.; Parker, W. L.; Principe, P. A.; Rathnum, M. L.; Slusarchyk, W. A.; Trejo, W. H.; Wells, J. S., Monocyclic beta-lactam antibiotics produced by bacteria. *Nature* **1981**, 291 (5815), 489-91.
21. Papp-Wallace, K. M.; Endimiani, A.; Taracila, M. A.; Bonomo, R. A., Carbapenems: past, present, and future. *Antimicrob Agents Chemother* **2011**, 55 (11), 4943-60.
22. Kropp, H.; Kahan, J. S.; Kahan, F. M.; Sandolf, J.; Darland, G.; Birnbaum, J., Abstract on 16th Interscientific conference on antimicrobial agents and chemotherapy. *Am. Soc. Microbiol.* **1976**, Abstract 228.



23. Cassidy, P. J.; Albers-Schonberg, G.; Goegelman, R. T.; Miller, T.; Arison, B.; Stapley, E. O.; Birnbaum, J., Epithienamycins. II. Isolation and structure assignment. *J Antibiot (Tokyo)* **1981**, *34* (6), 637-48.
24. Kobayashi, F.; Saino, Y.; Koshi, T.; Hattori, Y.; Nakayama, M.; Iwasaki, A.; Mori, T.; Mitsuhashi, S., Antimicrobial and beta-lactamase inhibitory activities of carpetimycins A and B, new carbapenem antibiotics. *Antimicrob Agents Chemother* **1982**, *21* (4), 536-44.
25. Torres, J. A.; Villegas, M. V.; Quinn, J. P., Current concepts in antibiotic-resistant gram-negative bacteria. *Expert Rev Anti Infect Ther* **2007**, *5* (5), 833-43.
26. Brink, A. J.; Feldman, C.; Grolman, D. C.; Muckart, D.; Pretorius, J.; Richards, G. A.; Senekal, M.; Sieling, W., Appropriate use of the carbapenems. *S Afr Med J* **2004**, *94* (10 Pt 2), 857-61.
27. Livermore, D. M.; Warner, M.; Mushtaq, S.; Doumith, M.; Zhang, J.; Woodford, N., What remains against carbapenem-resistant Enterobacteriaceae? Evaluation of chloramphenicol, ciprofloxacin, colistin, fosfomycin, minocycline, nitrofurantoin, temocillin and tigecycline. *Int J Antimicrob Agents* **2011**, *37* (5), 415-9.
28. Patel, G.; Bonomo, R. A., Status report on carbapenemases: challenges and prospects. *Expert Rev Anti Infect Ther* **2011**, *9* (5), 555-70.

29. Goossens, H.; Ferech, M.; Vander Stichele, R.; Elseviers, M., Outpatient antibiotic use in Europe and association with resistance: a cross-national database study. *The Lancet* **2005**, *365* (9459), 579-587.
30. Levy, S., From tragedy the antibiotic age is born . The Antibiotic Paradox. Springer. **1992**, 1-12.
31. Laxminarayan, R.; Brown, G. M., Economics of antibiotic resistance: A theory of optimal use. *J Environ Econ Manage* **2001**, *40*, 183-206.
32. Levy, S. B., Antibiotic Resistance: An Ecological Imbalance, in Ciba Foundation Symposium 207 - Antibiotic Resistance: Origins, Evolution, Selection and Spread. Chadwick DJ, Goode J. John Wiley & Sons, Ltd. (ed): Chichester, UK, 2007. **2007**, *1*, 1-14.
33. McEwen, S. A.; Fedorka-Cray, P. J., Antimicrobial Use and Resistance in Animals. *Clinical Infectious Diseases* **2002**, *34* (Supplement\_3), S93-S106.
34. Witte, W., Medical consequences of antibiotic use in agriculture. *Science* **1998**, *279* (5353), 996-7.
35. Levy, S. B.; Marshall, B., Antibacterial resistance worldwide: causes, challenges and responses. *Nat Med* **2004**, *10*, 122-129.
36. Overview of Bacteria.  
<http://www.merckmanuals.com/home/infections/bacterial-infections/overview-of-bacteria> (accessed May 21, 2018).

37. Davies, J.; Davies, D., Origins and evolution of antibiotic resistance. *Microbiol Mol Biol Rev* **2010**, *74* (3), 417-33.
38. Worthington, R. J.; Melander, C., Overcoming Resistance to  $\beta$ -Lactam Antibiotics. *The Journal of Organic Chemistry* **2013**, *78* (9), 4207-4213.
39. Chopra, I.; Roberts, M., Tetracycline antibiotics: mode of action, applications, molecular biology, and epidemiology of bacterial resistance. *Microbiol Mol Biol Rev* **2001**, *65* (2), 232-60 ; second page, table of contents.
40. Avorn, J.; Barrett, J. F.; Davey, P. G.; McEwen, S. A.; F, F. T., Antibiotic resistance: Synthesis of recommendations by expert policy. **2001**.
41. Padhi, S., New Delhi metallo-beta-lactamase: a weapon for the newly emerging drug-resistant bacteria. *Indian J Med Sci* **2011**, *65* (8), 317-20.
42. Khan, A. U.; Maryam, L.; Zarrilli, R., Structure, Genetics and Worldwide Spread of New Delhi Metallo- $\beta$ -lactamase (NDM): a threat to public health. *BMC Microbiology* **2017**, *17* (1), 101.
43. Yong, D.; Toleman, M. A.; Giske, C. G.; Cho, H. S.; Sundman, K.; Lee, K.; Walsh, T. R., Characterization of a new metallo-beta-lactamase gene, bla(NDM-1), and a novel erythromycin esterase gene carried on a unique genetic structure in *Klebsiella pneumoniae* sequence type 14 from India. *Antimicrob Agents Chemother* **2009**, *53* (12), 5046-54.

44. Kaase, M.; Nordmann, P.; Wichelhaus, T. A.; Gatermann, S. G.; Bonnin, R. A.; Poirel, L., NDM-2 carbapenemase in *Acinetobacter baumannii* from Egypt. *J Antimicrob Chemother* **2011**, *66* (6), 1260-2.
45. Khan, A. U.; Nordmann, P., Spread of carbapenemase NDM-1 producers: the situation in India and what may be proposed. *Scand J Infect Dis* **2012**, *44* (7), 531-5.
46. Williamson, D. A.; Sidjabat, H. E.; Freeman, J. T.; Roberts, S. A.; Silvey, A.; Woodhouse, R.; Mowat, E.; Dyet, K.; Paterson, D. L.; Blackmore, T.; Burns, A.; Heffernan, H., Identification and molecular characterisation of New Delhi metallo-beta-lactamase-1 (NDM-1)- and NDM-6-producing Enterobacteriaceae from New Zealand hospitals. *Int J Antimicrob Agents* **2012**, *39* (6), 529-33.
47. Khan, A. U.; Parvez, S., Detection of bla(NDM-4) in *Escherichia coli* from hospital sewage. *J Med Microbiol* **2014**, *63* (Pt 10), 1404-6.
48. Bush, K., Bench-to-bedside review: The role of  $\beta$ -lactamases in antibiotic-resistant Gram-negative infections. *Critical Care* **2010**, *14* (3), 224-224.
49. Bush, K.; Jacoby, G. A., Updated functional classification of beta-lactamases. *Antimicrob Agents Chemother* **2010**, *54* (3), 969-76.

50. Bush, K.; Jacoby, G. A.; Medeiros, A. A., A functional classification scheme for beta-lactamases and its correlation with molecular structure. *Antimicrob Agents Chemother* **1995**, *39* (6), 1211-33.
51. Hall, B. G.; Barlow, M., Revised Ambler classification of {beta}-lactamases. *J Antimicrob Chemother* **2005**, *55* (6), 1050-1.
52. Ambler, R. P., The structure of beta-lactamases. *Philos Trans R Soc Lond B Biol Sci* **1980**, *289* (1036), 321-31.
53. Meini, M. R.; Llarrull, L. I.; Vila, A. J., Overcoming differences: The catalytic mechanism of metallo-beta-lactamases. *FEBS Lett* **2015**, *589* (22), 3419-32.
54. Mojica, M. F.; Bonomo, R. A.; Fast, W., B1-Metallo-beta-Lactamases: Where do we stand? *Current drug targets* **2016**, *17* (9), 1029-1050.
55. Jaurin, B.; Grundstrom, T., ampC cephalosporinase of Escherichia coli K-12 has a different evolutionary origin from that of beta-lactamases of the penicillinase type. *Proc Natl Acad Sci U S A* **1981**, *78* (8), 4897-901.
56. Ouellette, M.; Bissonnette, L.; Roy, P. H., Precise insertion of antibiotic resistance determinants into Tn21-like transposons: nucleotide sequence of the OXA-1 beta-lactamase gene. *Proc Natl Acad Sci U S A* **1987**, *84* (21), 7378-82.
57. Galleni, M.; Lamotte-Brasseur, J.; Rossolini, G. M.; Spencer, J.; Dideberg, O.; Frere, J. M.; Metallo-beta-lactamases Working, G., Standard

numbering scheme for class B beta-lactamases. *Antimicrob Agents Chemother* **2001**, *45* (3), 660-3.

58. Karsisiotis, A. I.; Damblon, C. F.; Roberts, G. C. K., A variety of roles for versatile zinc in metallo-[small beta]-lactamases. *Metallomics* **2014**, *6* (7), 1181-1197.

59. Bebrone, C., Metallo-beta-lactamases (classification, activity, genetic organization, structure, zinc coordination) and their superfamily. *Biochem Pharmacol* **2007**, *74* (12), 1686-701.

60. Widmann, M.; Pleiss, J.; Oelschlaeger, P., Systematic analysis of metallo-beta-lactamases using an automated database. *Antimicrob Agents Chemother* **2012**, *56* (7), 3481-91.

61. Garau, G.; Di Guilmi, A. M.; Hall, B. G., Structure-based phylogeny of the metallo-beta-lactamases. *Antimicrob Agents Chemother* **2005**, *49* (7), 2778-84.

62. Hall, B. G.; Salipante, S. J.; Barlow, M., Independent origins of subgroup B1 + B2 and subgroup B3 metallo-beta-lactamases. *J Mol Evol* **2004**, *59* (1), 133-41.

63. Daiyasu, H.; Osaka, K.; Ishino, Y.; Toh, H., Expansion of the zinc metallo-hydrolase family of the beta-lactamase fold. *FEBS Lett* **2001**, *503* (1), 1-6.

64. Garau, G.; Bebrone, C.; Anne, C.; Galleni, M.; Frere, J. M.; Dideberg, O., A metallo-beta-lactamase enzyme in action: crystal structures of the monozinc carbapenemase CphA and its complex with biapenem. *J Mol Biol* **2005**, *345* (4), 785-95.
65. Garcia-Saez, I.; Mercuri, P. S.; Papamichael, C.; Kahn, R.; Frere, J. M.; Galleni, M.; Rossolini, G. M.; Dideberg, O., Three-dimensional structure of FEZ-1, a monomeric subclass B3 metallo-beta-lactamase from *Fluoribacter gormanii*, in native form and in complex with D-captopril. *J Mol Biol* **2003**, *325* (4), 651-60.
66. Ullah, J. H.; Walsh, T. R.; Taylor, I. A.; Emery, D. C.; Verma, C. S.; Gamblin, S. J.; Spencer, J., The crystal structure of the L1 metallo-beta-lactamase from *Stenotrophomonas maltophilia* at 1.7 Å resolution. *J Mol Biol* **1998**, *284* (1), 125-36.
67. Docquier, J. D.; Benvenuti, M.; Calderone, V.; Stoczko, M.; Menciassi, N.; Rossolini, G. M.; Mangani, S., High-resolution crystal structure of the subclass B3 metallo-beta-lactamase BJP-1: rational basis for substrate specificity and interaction with sulfonamides. *Antimicrob Agents Chemother* **2010**, *54* (10), 4343-51.
68. Leiros, H. K.; Borra, P. S.; Brandsdal, B. O.; Edvardsen, K. S.; Spencer, J.; Walsh, T. R.; Samuelsen, O., Crystal structure of the mobile metallo-beta-lactamase AIM-1 from *Pseudomonas aeruginosa*: insights into antibiotic

binding and the role of Gln157. *Antimicrob Agents Chemother* **2012**, *56* (8), 4341-53.

69. Moran-Barrio, J.; Lisa, M. N.; Larrieux, N.; Drusin, S. I.; Viale, A. M.; Moreno, D. M.; Buschiazzo, A.; Vila, A. J., Crystal Structure of the Metallo-beta-Lactamase GOB in the Periplasmic Dizinc Form Reveals an Unusual Metal Site. *Antimicrob Agents Chemother* **2016**, *60* (10), 6013-22.

70. Felici, A.; Amicosante, G., Kinetic analysis of extension of substrate specificity with *Xanthomonas maltophilia*, *Aeromonas hydrophila*, and *Bacillus cereus* metallo-beta-lactamases. *Antimicrob Agents Chemother* **1995**, *39* (1), 192-9.

71. Felici, A.; Amicosante, G.; Oratore, A.; Strom, R.; Ledent, P.; Joris, B.; Fanuel, L.; Frere, J. M., An overview of the kinetic parameters of class B beta-lactamases. *Biochem J* **1993**, *291* ( Pt 1), 151-5.

72. Walsh, T. R.; Gamblin, S.; Emery, D. C.; MacGowan, A. P.; Bennett, P. M., Enzyme kinetics and biochemical analysis of ImiS, the metallo-beta-lactamase from *Aeromonas sobria* 163a. *J Antimicrob Chemother* **1996**, *37* (3), 423-31.

73. Segatore, B.; Massidda, O.; Satta, G.; Setacci, D.; Amicosante, G., High specificity of *cphA*-encoded metallo-beta-lactamase from *Aeromonas hydrophila* AE036 for carbapenems and its contribution to beta-lactam resistance. *Antimicrob Agents Chemother* **1993**, *37* (6), 1324-8.



74. Poeylout-Palena, A. A.; Tomatis, P. E.; Karsisiotis, A. I.; Damblon, C.; Mata, E. G.; Vila, A. J., A minimalistic approach to identify substrate binding features in B1 Metallo-beta-lactamases. *Bioorg Med Chem Lett* **2007**, *17* (18), 5171-4.
75. Rasia, R. M.; Vila, A. J., Structural determinants of substrate binding to *Bacillus cereus* metallo-beta-lactamase. *J Biol Chem* **2004**, *279* (25), 26046-51.
76. Davies, R. B.; Abraham, E. P., Metal cofactor requirements of beta-lactamase II. *Biochem J* **1974**, *143* (1), 129-35.
77. Badarau, A.; Damblon, C.; Page, M. I., The activity of the dinuclear cobalt-beta-lactamase from *Bacillus cereus* in catalysing the hydrolysis of beta-lactams. *Biochem J* **2007**, *401* (1), 197-203.
78. Badarau, A.; Page, M. I., The variation of catalytic efficiency of *Bacillus cereus* metallo-beta-lactamase with different active site metal ions. *Biochemistry* **2006**, *45* (35), 10654-66.
79. Hu, Z.; Spadafora, L. J.; Hajdin, C. E.; Bennett, B.; Crowder, M. W., Structure and mechanism of copper- and nickel-substituted analogues of metallo-beta-lactamase L1. *Biochemistry* **2009**, *48* (13), 2981-9.
80. Concha, N. O.; Rasmussen, B. A.; Bush, K.; Herzberg, O., Crystal structures of the cadmium- and mercury-substituted metallo-beta-lactamase from *Bacteroides fragilis*. *Protein Sci* **1997**, *6* (12), 2671-6.

81. Gonzalez, J. M.; Buschiazzo, A.; Vila, A. J., Evidence of adaptability in metal coordination geometry and active-site loop conformation among B1 metallo-beta-lactamases. *Biochemistry* **2010**, *49* (36), 7930-8.
82. Garau, G.; Garcia-Saez, I.; Bebrone, C.; Anne, C.; Mercuri, P.; Galleni, M.; Frere, J. M.; Dideberg, O., Update of the standard numbering scheme for class B beta-lactamases. *Antimicrob Agents Chemother* **2004**, *48* (7), 2347-9.
83. Sousa, S. F.; Lopes, A. B.; Fernandes, P. A.; Ramos, M. J., The Zinc proteome: a tale of stability and functionality. *Dalton Trans* **2009**, (38), 7946-56.
84. Kim, Y.; Cunningham, M. A.; Mire, J.; Tesar, C.; Sacchettini, J.; Joachimiak, A., NDM-1, the ultimate promiscuous enzyme: substrate recognition and catalytic mechanism. *FASEB J* **2013**, *27* (5), 1917-27.
85. Murphy, T. A.; Catto, L. E.; Halford, S. E.; Hadfield, A. T.; Minor, W.; Walsh, T. R.; Spencer, J., Crystal structure of *Pseudomonas aeruginosa* SPM-1 provides insights into variable zinc affinity of metallo-beta-lactamases. *J Mol Biol* **2006**, *357* (3), 890-903.
86. Carfi, A.; Pares, S.; Duee, E.; Galleni, M.; Duez, C.; Frere, J. M.; Dideberg, O., The 3-D structure of a zinc metallo-beta-lactamase from *Bacillus cereus* reveals a new type of protein fold. *EMBO J* **1995**, *14* (20), 4914-21.
87. Kim, Y.; Tesar, C.; Mire, J.; Jedrzejczak, R.; Binkowski, A.; Babnigg, G.; Sacchettini, J.; Joachimiak, A., Structure of apo- and monometalated forms

of NDM-1--a highly potent carbapenem-hydrolyzing metallo-beta-lactamase. *PLoS One* **2011**, *6* (9), e24621.

88. Fast, W.; Wang, Z.; Benkovic, S. J., Familial mutations and zinc stoichiometry determine the rate-limiting step of nitrocefin hydrolysis by metallo-beta-lactamase from *Bacteroides fragilis*. *Biochemistry* **2001**, *40* (6), 1640-50.

89. de Seny, D.; Heinz, U.; Wommer, S.; Kiefer, M.; Meyer-Klaucke, W.; Galleni, M.; Frere, J. M.; Bauer, R.; Adolph, H. W., Metal ion binding and coordination geometry for wild type and mutants of metallo-beta -lactamase from *Bacillus cereus* 569/H/9 (BcII): a combined thermodynamic, kinetic, and spectroscopic approach. *J Biol Chem* **2001**, *276* (48), 45065-78.

90. Paul-Soto, R.; Bauer, R.; Frere, J. M.; Galleni, M.; Meyer-Klaucke, W.; Nolting, H.; Rossolini, G. M.; de Seny, D.; Hernandez-Valladares, M.; Zeppezauer, M.; Adolph, H. W., Mono- and binuclear Zn<sup>2+</sup>-beta-lactamase. Role of the conserved cysteine in the catalytic mechanism. *J Biol Chem* **1999**, *274* (19), 13242-9.

91. Rasia, R. M.; Vila, A. J., Exploring the role and the binding affinity of a second zinc equivalent in *B. cereus* metallo-beta-lactamase. *Biochemistry* **2002**, *41* (6), 1853-60.

92. Jacquin, O.; Balbeur, D.; Damblon, C.; Marchot, P.; De Pauw, E.; Roberts, G. C.; Frere, J. M.; Matagne, A., Positively cooperative binding of zinc ions to *Bacillus cereus* 569/H/9 beta-lactamase II suggests that the

binuclear enzyme is the only relevant form for catalysis. *J Mol Biol* **2009**, *392* (5), 1278-91.

93. Horsfall, L. E.; Izougarhane, Y.; Lassaux, P.; Selevsek, N.; Lienard, B. M.; Poirel, L.; Kupper, M. B.; Hoffmann, K. M.; Frere, J. M.; Galleni, M.; Bebrone, C., Broad antibiotic resistance profile of the subclass B3 metallo-beta-lactamase GOB-1, a di-zinc enzyme. *FEBS J* **2011**, *278* (8), 1252-63.

94. Moran-Barrio, J.; Gonzalez, J. M.; Lisa, M. N.; Costello, A. L.; Peraro, M. D.; Carloni, P.; Bennett, B.; Tierney, D. L.; Limansky, A. S.; Viale, A. M.; Vila, A. J., The metallo-beta-lactamase GOB is a mono-Zn(II) enzyme with a novel active site. *J Biol Chem* **2007**, *282* (25), 18286-93.

95. Fonseca, F.; Bromley, E. H.; Saavedra, M. J.; Correia, A.; Spencer, J., Crystal structure of *Serratia fonticola* Sfh-I: activation of the nucleophile in mono-zinc metallo-beta-lactamases. *J Mol Biol* **2011**, *411* (5), 951-9.

96. Hernandez Valladares, M.; Felici, A.; Weber, G.; Adolph, H. W.; Zeppezauer, M.; Rossolini, G. M.; Amicosante, G.; Frere, J. M.; Galleni, M., Zn(II) dependence of the *Aeromonas hydrophila* AE036 metallo-beta-lactamase activity and stability. *Biochemistry* **1997**, *36* (38), 11534-41.

97. Palzkill, T., Metallo-beta-lactamase structure and function. *Ann N Y Acad Sci* **2013**, *1277*, 91-104.

98. Crowder, M. W.; Spencer, J.; Vila, A. J., Metallo-beta-lactamases: novel weaponry for antibiotic resistance in bacteria. *Acc Chem Res* **2006**, *39* (10), 721-8.
99. Fink, A. L.; Page, M. I., Beta-Lactamases, ed. J.-M. Frère. Nova Science Publishers, Inc.: New York. **2011**.
100. Weston, J., Mode of action of bi- and trinuclear zinc hydrolases and their synthetic analogues. *Chem Rev* **2005**, *105* (6), 2151-74.
101. Kaminskaia, N. V.; He, C.; Lippard, S. J., Reactivity of mu-hydroxodizinc(II) centers in enzymatic catalysis through model studies. *Inorg Chem* **2000**, *39* (15), 3365-73.
102. Kaminskaia, N. V.; Spingler, B.; Lippard, S. J., Hydrolysis of  $\beta$ -Lactam Antibiotics Catalyzed by Dinuclear Zinc(II) Complexes: Functional Mimics of Metallo- $\beta$ -lactamases. *Journal of the American Chemical Society* **2000**, *122* (27), 6411-6422.
103. Kaminskaia, N. V.; Spingler, B.; Lippard, S. J., Intermediate in beta-lactam hydrolysis catalyzed by a dinuclear zinc(II) complex: relevance to the mechanism of metallo-beta-lactamase. *J Am Chem Soc* **2001**, *123* (27), 6555-63.
104. Page, M. I.; Badarau, A., The mechanisms of catalysis by metallo beta-lactamases. *Bioinorg Chem Appl* **2008**, 576297.

105. Carfi, A.; Duee, E.; Galleni, M.; Frere, J. M.; Dideberg, O., 1.85 Å resolution structure of the zinc (II) beta-lactamase from *Bacillus cereus*. *Acta Crystallogr D Biol Crystallogr* **1998**, *54* (Pt 3), 313-23.
106. Concha, N. O.; Rasmussen, B. A.; Bush, K.; Herzberg, O., Crystal structure of the wide-spectrum binuclear zinc beta-lactamase from *Bacteroides fragilis*. *Structure* **1996**, *4* (7), 823-36.
107. Fabiane, S. M.; Sohi, M. K.; Wan, T.; Payne, D. J.; Bateson, J. H.; Mitchell, T.; Sutton, B. J., Crystal structure of the zinc-dependent beta-lactamase from *Bacillus cereus* at 1.9 Å resolution: binuclear active site with features of a mononuclear enzyme. *Biochemistry* **1998**, *37* (36), 12404-11.
108. Wang, C.; Guo, H., Inhibitor binding by metallo-beta-lactamase IMP-1 from *Pseudomonas aeruginosa*: quantum mechanical/molecular mechanical simulations. *J Phys Chem B* **2007**, *111* (33), 9986-92.
109. Dal Peraro, M.; Vila, A. J.; Carloni, P.; Klein, M. L., Role of Zinc Content on the Catalytic Efficiency of B1 Metallo  $\beta$ -Lactamases. *Journal of the American Chemical Society* **2007**, *129* (10), 2808-2816.
110. Zheng, M.; Xu, D., New Delhi metallo-beta-lactamase I: substrate binding and catalytic mechanism. *J Phys Chem B* **2013**, *117* (39), 11596-607.
111. Xu, D.; Guo, H.; Cui, Q., Antibiotic deactivation by a dizinc beta-lactamase: mechanistic insights from QM/MM and DFT studies. *J Am Chem Soc* **2007**, *129* (35), 10814-22.

112. Zhu, K.; Lu, J.; Liang, Z.; Kong, X.; Ye, F.; Jin, L.; Geng, H.; Chen, Y.; Zheng, M.; Jiang, H.; Li, J. Q.; Luo, C., A quantum mechanics/molecular mechanics study on the hydrolysis mechanism of New Delhi metallo-beta-lactamase-1. *J Comput Aided Mol Des* **2013**, *27* (3), 247-56.
113. Spencer, J.; Clarke, A. R.; Walsh, T. R., Novel mechanism of hydrolysis of therapeutic beta-lactams by *Stenotrophomonas maltophilia* L1 metallo-beta-lactamase. *J Biol Chem* **2001**, *276* (36), 33638-44.
114. King, D. T.; Worrall, L. J.; Gruninger, R.; Strynadka, N. C. J., New Delhi Metallo- $\beta$ -Lactamase: Structural Insights into  $\beta$ -Lactam Recognition and Inhibition. *Journal of the American Chemical Society* **2012**, *134* (28), 11362-11365.
115. Wu, S.; Xu, D.; Guo, H., QM/MM studies of monozinc beta-lactamase CphA suggest that the crystal structure of an enzyme-intermediate complex represents a minor pathway. *J Am Chem Soc* **2010**, *132* (51), 17986-8.
116. Xu, D.; Xie, D.; Guo, H., Catalytic mechanism of class B2 metallo-beta-lactamase. *J Biol Chem* **2006**, *281* (13), 8740-7.
117. Xu, D.; Zhou, Y.; Xie, D.; Guo, H., Antibiotic binding to monozinc CphA beta-lactamase from *Aeromonas hydrophila*: quantum mechanical/molecular mechanical and density functional theory studies. *J Med Chem* **2005**, *48* (21), 6679-89.

118. Shakil, S.; Azhar, E. I.; Tabrez, S.; Kamal, M. A.; Jabir, N. R.; Abuzenadah, A. M.; Damanhour, G. A.; Alam, Q., New Delhi Metallo- $\beta$ -Lactamase (NDM-1): An Update. *Journal of Chemotherapy* **2011**, *23* (5), 263-265.
119. Zhang, H.; Hao, Q., Crystal structure of NDM-1 reveals a common beta-lactam hydrolysis mechanism. *FASEB J* **2011**, *25* (8), 2574-82.
120. Khan, A. U.; Ali, A.; Danishuddin; Srivastava, G.; Sharma, A., Potential inhibitors designed against NDM-1 type metallo- $\beta$ -lactamases: an attempt to enhance efficacies of antibiotics against multi-drug-resistant bacteria. *Scientific Reports* **2017**, *7* (1), 9207.
121. Chandar, B.; Poovitha, S.; Ilango, K.; MohanKumar, R.; Parani, M., Inhibition of New Delhi Metallo- $\beta$ -Lactamase 1 (NDM-1) Producing Escherichia coli IR-6 by Selected Plant Extracts and Their Synergistic Actions with Antibiotics. *Frontiers in Microbiology* **2017**, *8*, 1580.
122. Chiou, J.; Wan, S.; Chan, K. F.; So, P. K.; He, D.; Chan, E. W.; Chan, T. H.; Wong, K. Y.; Tao, J.; Chen, S., Ebselen as a potent covalent inhibitor of New Delhi metallo-beta-lactamase (NDM-1). *Chem Commun (Camb)* **2015**, *51* (46), 9543-6.
123. Groundwater, P. W.; Xu, S.; Lai, F.; Varadi, L.; Tan, J.; Perry, J. D.; Hibbs, D. E., New Delhi metallo-beta-lactamase-1: structure, inhibitors and detection of producers. *Future Med Chem* **2016**, *8* (9), 993-1012.



124. Tripathi, R.; Nair, N. N., Mechanism of Meropenem Hydrolysis by New Delhi Metallo  $\beta$ -Lactamase. *ACS Catalysis* **2015**, *5* (4), 2577-2586.
125. Thomas, P. W.; Spicer, T.; Cammarata, M.; Brodbelt, J. S.; Hodder, P.; Fast, W., An altered zinc-binding site confers resistance to a covalent inactivator of New Delhi metallo-beta-lactamase-1 (NDM-1) discovered by high-throughput screening. *Bioorg Med Chem* **2013**, *21* (11), 3138-46.
126. Chen, J.; Chen, H.; Zhu, T.; Zhou, D.; Zhang, F.; Lao, X.; Zheng, H., Asp120Asn mutation impairs the catalytic activity of NDM-1 metallo-beta-lactamase: experimental and computational study. *Phys Chem Chem Phys* **2014**, *16* (14), 6709-16.
127. Bebrone, C.; Anne, C.; De Vriendt, K.; Devreese, B.; Rossolini, G. M.; Van Beeumen, J.; Frere, J. M.; Galleni, M., Dramatic broadening of the substrate profile of the *Aeromonas hydrophila* CphA metallo-beta-lactamase by site-directed mutagenesis. *J Biol Chem* **2005**, *280* (31), 28195-202.
128. Guo, Y.; Wang, J.; Niu, G.; Shui, W.; Sun, Y.; Zhou, H.; Zhang, Y.; Yang, C.; Lou, Z.; Rao, Z., A structural view of the antibiotic degradation enzyme NDM-1 from a superbug. *Protein Cell* **2011**, *2* (5), 384-94.
129. Green, V. L.; Verma, A.; Owens, R. J.; Phillips, S. E.; Carr, S. B., Structure of New Delhi metallo-beta-lactamase 1 (NDM-1). *Acta Crystallogr Sect F Struct Biol Cryst Commun* **2011**, *67* (Pt 10), 1160-4.

130. Lisa, M. N.; Hemmingsen, L.; Vila, A. J., Catalytic role of the metal ion in the metallo-beta-lactamase GOB. *J Biol Chem* **2010**, 285 (7), 4570-7.
131. ICP-OES - General Instrumentation.  
<http://www.ru.nl/science/gi/facilities-activities/elemental-analysis/icp-oes/>  
(accessed May 21, 2018).
132. pET-28a-c(+) Vectors. <https://www.staff.ncl.ac.uk/p.dean/pET28.pdf>  
(accessed May 21, 2018).
133. Wang, F.; Cassidy, C.; Sacchettini, J. C., Crystal structure and activity studies of the Mycobacterium tuberculosis beta-lactamase reveal its critical role in resistance to beta-lactam antibiotics. *Antimicrob Agents Chemother* **2006**, 50 (8), 2762-71.
134. Marcoccia, F.; Bottoni, C.; Sabatini, A.; Colapietro, M.; Mercuri, P. S.; Galleni, M.; Kerff, F.; Matagne, A.; Celenza, G.; Amicosante, G.; Perilli, M., Kinetic Study of Laboratory Mutants of NDM-1 Metallo-beta-Lactamase and the Importance of an Isoleucine at Position 35. *Antimicrob Agents Chemother* **2016**, 60 (4), 2366-72.
135. MCAT Biochemistry Review. Chapter 2.3 Enzyme Kinetics.  
[http://schoolbag.info/chemistry/mcat\\_biochemistry/11.html](http://schoolbag.info/chemistry/mcat_biochemistry/11.html) (accessed May 23, 2018).
136. King, A. Michaelis-Menten kinetics.  
<http://slideplayer.com/slide/9396440/> (accessed May 23, 2018).

137. Eissenthal, R.; Danson, M. J.; Hough, D. W., Catalytic efficiency and  $k_{cat}/K_M$ : a useful comparator? *Trends in Biotechnology* **2007**, *25* (6), 247-249.
138. Khan, A. U.; Rehman, M. T., Role of Non-Active-Site Residue Trp-93 in the Function and Stability of New Delhi Metallo-beta-Lactamase 1. *Antimicrob Agents Chemother* **2016**, *60* (1), 356-60.
139. Lefurgy, S. T.; de Jong, R. M.; Cornish, V. W., Saturation mutagenesis of Asn152 reveals a substrate selectivity switch in P99 cephalosporinase. *Protein Science : A Publication of the Protein Society* **2007**, *16* (12), 2636-2646.
140. Jensen, F., *Introduction to computational chemistry*. Wiley, New York. 2001.
141. Berendsen, H. J. C., Bio-Molecular Dynamics Comes of Age. *Science* **1996**, *271* (5251), 954.
142. McCammon, J. A.; Gelin, B. R.; Karplus, M.; Wolynes, P. G., The hinge-bending mode in lysozyme. *Nature* **1976**, *262* (5566), 325-6.
143. Shaw, D. E.; Maragakis, P.; Lindorff-Larsen, K.; Piana, S.; Dror, R. O.; Eastwood, M. P.; Bank, J. A.; Jumper, J. M.; Salmon, J. K.; Shan, Y.; Wriggers, W., Atomic-level characterization of the structural dynamics of proteins. *Science* **2010**, *330* (6002), 341-6.
144. Groenhof, G., Introduction to QM/MM simulations. *Methods Mol Biol* **2013**, *924*, 43-66.

145. Allen, M. P., Introduction to Molecular Dynamics Simulation. *NIC Series* **2004**, 23, 1-28.
146. King, D.; Strynadka, N., Crystal structure of New Delhi metallo- $\beta$ -lactamase reveals molecular basis for antibiotic resistance. *Protein Science : A Publication of the Protein Society* **2011**, 20 (9), 1484-1491.
147. Li, P.; Merz, K. M., Jr., MCPB.py: A Python Based Metal Center Parameter Builder. *J Chem Inf Model* **2016**, 56 (4), 599-604.
148. Gaussian 16. <http://gaussian.com/gaussian16/> (accessed May 23, 2018).
149. Gaussian 16 Citation. <http://gaussian.com/citation/> (accessed May 23, 2018).
150. Gromacs Home Page. <http://www.gromacs.org/> (accessed May 23, 2018).
151. Coot Home Page. <https://www2.mrc-lmb.cam.ac.uk/personal/pemsley/coot/> (accessed June 25, 2018).
152. Jorgensen, W. L.; Chandrasekhar, J.; Madura, J. D.; Impey, R. W.; Klein, M. L., Comparison of simple potential functions for simulating liquid water. *The Journal of Chemical Physics* **1983**, 79 (2), 926-935.
153. VMD Home Page. <http://www.ks.uiuc.edu/Research/vmd/> (accessed June 25, 2018).

154. Jeffrey, G. A., An introduction to hydrogen bonding. *Oxford University Press* **1997**, 12-14.
155. Wang, R.; Lai, T. P.; Gao, P.; Zhang, H.; Ho, P. L.; Woo, P. C.; Ma, G.; Kao, R. Y.; Li, H.; Sun, H., Bismuth antimicrobial drugs serve as broad-spectrum metallo-beta-lactamase inhibitors. *Nat Commun* **2018**, 9 (1), 439.